TRANSIENT THERMAL ANALYSIS AND EXPERIMENTAL INVESTIGATIONS OF FRICTION STIR WELDING ON SIMILAR AND DISSIMILAR MATERIALS

Thesis submitted to
Indian Institute of Technology Guwahati
for the award of the degree

of

Doctor of Philosophy

by

Anil Kumar Deepati

Under the Supervision

of

Dr. Pankaj Biswas

DEPARTMENT OF MECHANICAL ENGINEERING
INDIAN INSTITUTE OF TECHNOLOGY GUWAHATI
FEBRUARY-2015

Department of Mechanical Engineering
Indian Institute of Technology Guwahati
Guwahati- 781039
INDIA

CERTIFICATE

This is to certify that the thesis entitled **Transient Thermal analysis and Experimental Investigations of Friction Stir Welding on Similar and Dissimilar Materials,** submitted by **Mr. Anil Kumar Deepati** to Indian Institute of Technology Guwahati, is a record of bonafide research work under my supervision and is worthy of consideration for the award of the degree of Doctor of Philosophy of the Institute.

Dr. Pankaj Biswas

Associate Professor
Department of Mechanical Engineering,
Indian Institute of Technology Guwahati,
Guwahati-781039
INDIA

Date: 20-02-2015

Acknowledgements

I start this by thanking **God Almighty** for giving me health and patience throughout this duration. I believe without divine will not even a leaf can move in this world. This work has been done, became possible only because of His wish and mercy.

I express my sincere gratitude and appreciation to my supervisor, **Dr. Pankaj Biswas,** Associate professor, Department of Mechanical Engineering, IITGuwahati, for his valuable advices, expert guidance, patience, encouragement and for all the support he has given me form the day one and throughout the PhD. Regardless of his work load, He always found time to discuss with me, which is a very difficult thing to do. I feel privileged for having the opportunity to work with them.

I sincerely appreciate **Prof. Anoop K. Dass, Prof. D. Chakraborty and Prof. P. Mahanta**, the present and former Heads of the department, for extending all necessary facilities of the department. I must take this opportunity to express my gratitude to the members of my doctoral committee **Prof. P.S Robi, Dr. Swarup Bag and Dr. S.K Majumder** for their valuable suggestions and encouragements during the period of my research work. Thanks to all the faculty members of the department for not only their technical suggestions at times but also their friendly interactions that create an enjoyable working environment in the department.

This is further aided by an amazingly helpful staff. Special mention should be made to Mr. NK Das, Mr. Chetri, Mr. Medhi, Mr. Amjad, Mr. Kaklary and to all the staff at the central workshop, IITG for their helping hands in experimental work. And also many thanks to Mr. Sanjib, technical staff of strength of materials lab, Mr. Ahmed, staff of materials science lab, CIF staff and TA's of SEM and FESEM. I like to acknowledge my friends Muthu, Shiva, Sateesh, Srikanth, and Yadiah. I express my special thanks to members my group Biplab, Arpan, Arun, Bhadra and Himanshu.

Last but not least, I express my gratitude to my **Parents**, family members and my wife's family members for their cooperation and encouragements. I express my sincere thanks to my wife **Spandana** for her love and patience which was always a source of strength to me.

Anil Kumar Deepati,
IIT Guwahati. India.

Abstract

The purpose of the present work is to evaluate the optimal conditions of Friction Stir Welding for joining of both similar and dissimilar materials. For welding of this kind of materials by FSW process the most important and influencing operating parameters which include tool rotational speed, traverse speed, tool dimensions and the tool plunge force etc. A slight variation in these parameters significantly effects the heat generation between tool and work piece which influence the weld quality. Hence the present study focused on the effect of operating parameters and tool geometries on weld quality for welding of 6mm and 12mm thick similar alluminium alloys and also for 6mm thick dissimilar alloys (i.e. AA1100-AA5083 and Al-Cu). Initially this work started with finding out the effective shoulder diameter for welding of 6mm thick alluminium plate. This study focused on the effect of tool plunging force and tool shoulder size on heat generation of FSW by using 3-D finite element (FE) transient thermal analysis. It was noticed that both plunging force and shoulder diameter have considerable effect on FSW process. Suitable correlations were made between the ratio of tool pin to shoulder diameter vs. peak temperature and tool plunging force vs. peak temperature. The present developed FE model results were well matched with experimental results. The same FE model was extended for analyzing the thermal history of FSW on dissimilar alloys (i.e. Al-Cu). It was seen that the peak temperature varies non-uniformly about the center of weld line at two dissimilar metal plates. The computed results were compared with experimental results to understand the influence of process parameters on the heat generation and weld quality.

Further study was the experimental investigation to find out the effective tool pin geometry for better weld quality of 6mm thick alluminium alloys. The observations form this investigation revealed that the tools with trapezoidal and tapered cylindrical pin profile provides the optimal results. The outcomes of these above three studies provides the optimal tool shoulder diameter, tool plunging force and desirable tool pin geometry for welding of 6mm thick alluminium plates. Using the same tool geometries and other parameters achieved from the previous analysis, FSW of thick alluminium plates was performed to verify their feasibility in welding of thicker plates. It was also noticed that the same tool geometries with proportional dimensions produces the defect free welds for thick plates also. It was also found that for thicker plate the higher tool rpm with lower welding speed results in finer grain

structure which leads to higher strength as well as higher ductility of welded joints. The tensile strength of the welds was found to be almost similar to that of base metal. This study was also focused on the tool dwell time effect on tensile property and quality of joints. Dwell time has a very significant effect closer to the starting position of welding. And it was also observed that at very low and high dwell time the ductility of welded joints reduces significantly.

Furthermore, the study was extended to experimental investigations of FSW on aluminium and copper alloy plates and FSW of dissimilar alluminium alloys plates. The study on FSW of alluminium and copper includes the investigation of weld quality by microstructural investigation, and mechanical properties study. Microstructural investigations were performed by using optical microscope for micro and macro structure examination and further it was analyzed by using the FESEM to understand the material mixing phenomena. It was predicted that the sound welds with defect-free joint can be produced by arranging Aluminium on advancing side with sufficient probe offset to Al side.

Finally, the study FSW of dissimilar alluminium alloys particularly focused on the optimization of process parameters and found that the most influencing and highly contributing parameters was the tool rotational speed and followed by the tool traversing speed. The mechanical investigation includes tensile and micro hardness properties study for all the cases.

Key words:

FSW, Transient thermal analysis, 3-D Finite Element Analysis, Taguchi DOE, Grey Taguchi method, Mechanical and microstructural study, FESEM, Dissimilar Alloys, AA1100, AA5083, Cu-Alloy, Dwell time, Tool rotational speed, Tool traverse speed, Tool shoulder diameters, Plunging force.

List of Symbols

R=	Shoulder radius
r_p=	Pin radius
r_{pt}=	Conical Pin radius at tip
r_{pb}=	Conical Pin radius at base
l=	Pin height
ω=	Speed of the tool
P_n=	Plunging force
v=	Tool velocity
S_{ys}^{*}=	The yield strength of the material at 80% of the melting point temperature
τ^{*}=	The shear strength of the material at 80% of its melting point temperature
s=	Slant length of conical pin
h=	Conical pin height
h_2=	Tool depression in welding area
μ=	Frictional co-efficient between the tool and workpiece
F=	Frictional force for heat generation on shoulder
F_p=	Force acting on pin
Q_{S1}=	Heat generation due to vertical pressure in shoulder
Q_{S2}=	Heat generation in shoulder due to travelling of tool shoulder
A_{sp}=	The side surface area of tool pin
h_f=	Convection coefficient
c=	Specific heat
K=	Thermal conductivity
q_p=	Distribution of heat flux over the pin-plate interface
q'''=	Heat Generation
ρ =	Density of plate material
$\{L\}$=	Vector Operator
$\{q\}$=	heat flux vector
∇=	Represents grad operator
$[D]$=	conductivity matrix
$\{n\}$=	Unit outward normal vector

S_2= Area of all the surface except welding zone

S_1= surface of welding zone

Vol = Volume of the element

δT = Allowable virtual temperature

T= Temperature

$\{N\}$= Element shape function

$[C_e^t]$= Element specific heat matrix

$[K_e^{tb}]$= Element diffusion conductivity matrix

$[K_e^{tc}]$= Element convection surface conductivity matrix

$\{Q_e^f\}$= Element convection surface heat flow vector

Abbreviations

1018MS	1018 Mild Steel
3-D FE	Three Dimensional Finite Element
AA1100	Alluminium Alloy 1100
AA5083	Alluminium Alloy 5083
BM	Base Material
DOE	Design of Experiments
E	Experiment
EDX	Energy-Dispersive X-ray
FE	Finite Element
FEM	Finite Element Method
FESEM	Field Emission Scanning Microscope
FSW	Friction Stir Welding
HAZ	Heat Affected Zone
HV	Vickers Hardness
LHT	Left Helix Threaded
NZ	Nugget Zone
PCBN	Poly Crystalline Cubic Boron Nitride
PD	Pin/Probe Diameter
PL	Pin Length
PFZ	Precipitate Free Zone
RHT	Right Helix Threaded
rpm	Rotations Per Minute
SS	Stainless Steel
SD	Shoulder Diameter
SEM	Scanning Electron Microscope
SZ	Stirred Zone
TP	Tool Pin
TEM	Transmission Electron Microscope
TRS	Tool Rotational Speed
TMAZ	Thermo-Mechanical Affected Zone
TWI	The Welding Institute

UTS	Ultimate Tensile Strength
VHN	Vickers Hardness Number
WS	Welding Speed
WZ	Weld Zone

List of Figures

Figure. No.		Page. No.
1.1	Types of welding processes based on phases……....	1
1.2	Variants of friction stir technology……..	2
1.3	Friction stir welding process……	3
2.1	Year wise publications on FSW …….....	7
2.2	Tri-flute pin FSW tool fabricated at SMU [21] …….....	9
2.3	WorlTM and MXTM Triflute tools developed by TWI, UK. [22]……..	9
2.4	Flared-TrifluteTM tools developed by The Welding Institute (TWI), UK. (Thomas et al. [23]) (a) Neutral flutes, (b) left flutes, and (c) right hand flutes…….....…….....	10
2.5	Patterns of various tool shoulder surface developed by The Welding Institute (TWI), UK. [22]……....	10
2.6	(a) Tool with a ‘pyramid’ in the (b) diagram of friction welding: 1, the plating; 2, the tool with the ‘pyramid’; and 3, the web [45]……	12
2.7	Macrograph showing various microstructural zones welded by conical pin tool…….....…….....	15
2.8	Precipitate microstructures in the grain interior and along grain boundaries in: (a) base metal, (b) HAZ, (c) TMAZ near HAZ, and (d) TMAZ near nugget zone (FSW 7050Al-T651, tool rotation rate: 350 rpm, traverse speed: 15 mm/min) (Su *et al*. [10])…….....	16
2.9	SEM images of AZ31 in different regions (a) BM; (b) HAZ; (c) Interface of TMAZ/SZ; (d) SZ in Mg side; (e) SZ in Al side; (f) Intercalated microstructure [66]…….....…….....	17
2.10	Microstructures showing different regions (a) fine equiaxed grains in stir zone of aluminum near Al/Cu interface, (b) elongated aluminum grains in the TMAZ of advancing side [67]……....	18
2.11	Cross-sectional macrograph of FSW lap Al–Cu joint: dash lines represent exact locations of hardness lines [68]……....	18
2.12	Macroscopic overviews of the FSW joint cross sections at constant tool rotational speed of 1180rpm and welding speeds of (a) 30, (b) 60, (c) 95, (d) 118, and (e)190 mm/min [67]……....	21

2.13	Schematic of FSW Al–Cu lap joints when Al plates were fixed on (a) advancing side (AS), (b) retreating side (RS) and (c) tensile shear specimen [68]……..……..	23
2.14	Comparison of experimental and FEM values [106]: (A) vertical force and temperature, (B) torque and (C) welding force…….....	26
2.15	Right side showing temperature evolution compared with experiment on pin, shoulder and root on the left Tracer visualization, simulation (left) experiment (right)[107]…….....…….....	27
2.16	Strain rate fields for different friction coefficient [108]……..	28
2.17	Partition of the welding zone for the definition of the elementary velocity fields and boundaries of the model [110] …….....	28
2.18	Material properties of (a) Al 6061-T6 used in model [117] and (b) CPM 1V tool steel used in model [118]…….....	29
2.19	Comparison of the modeled and the measured temperature history for workpiece. [113] …….....…….....	30
2.20	Tool geometries are shown above (a) Tapered pin, (b) Inverse tapered pin, (c) Convex shoulder, (d) Concave shoulder, (e) triangular pin with concave shoulder [129]…….....…….....	33
2.21	Computed temperature field [139]…….....	35
3.1	Flat cylindrical shoulder and cylindrical probe…….....	36
3.2	Tool shoulder small elementary area…….....	37
3.3	Force acting on tool shoulder due to travelling of FSW tool……...	38
3.4	Force acting on tool probe due to travelling of FSW tool……	39
3.5	Schematic diagram of flat cylindrical shoulder and conical pin……..	41
3.6	Probe small elemental area…….....…….....	42
3.7	Small elemental triangle…….....…….....	42
3.8	Heat source model for Cu-Al dissimilar FSW…….....	45
3.9	Meshed model…….....…….....	50
3.10	FSW Experimental setup…….....…….....	52
3.11	Data acquisition system for temperature measurement……	53
3.12	Hydraulic universal tensile testing machine…….....	55
3.13	Tensile sample dimensions (ASTM E-8 standard)…….....	55
3.14	Tensile samples…….....…….....	55
3.15	Vickers micro hardness testing machine…….....	56
3.16	Procedure for microstructure analysis…….....	57
3.17	(a) Sectioning machine (b) Mounting press (c) Polishing machine ……	58

3.18	Optical microscope (Make: Zeiss 4.2)…….....	59
3.19	Field emission scanning electron microscope (FESEM)…….	60
4.1	FE Model and meshing view……	62
4.2	Temperature distribution from center of weld line to away from weld line…	62
4.3	Quasi-static temperature distributions along center of weld line…….	63
4.4	Isothermal patterns for a particular time step during welding for 6mm pin….	63
4.5	Details of tool geometry for cylindrical and conical probe……..	64
4.6	Peak temperature distributions along plate breadth perpendicular to weld lin	65
4.7	Comparision of peak temperature distribution with distance perpendicular to the weld line…….....…….....	65
4.8	Tool geometry used…….....…….....	66
4.9	Temperature contour for 12mm shoulder diameter……..	67
4.10	Temperature contour for 24mm shoulder diameter…….	67
4.11	Thermal contours 20mm shoulder diameter…….....……	68
4.12	Thermal contours with 24mm shoulder diameter…….....…	68
4.13	Temperature distributions at centre of weld line…….....…	69
4.14	Temperature distributions at 16mm away from centre of weld line…….....	69
4.15	Peak temperature distribution perpendicular to the centre of weld line……....	70
4.16	Shoulder diameters vs. maximum temperature…….....…	70
4.17	Shoulder diameter and pin diameter ratio vs. maximum temperature…….	71
4.18	Numerical and experimental temperature distribution at 5mm and 20mm away from weld centre line of 18mm shoulder tool…….	72
4.19	Numerical and experimental temperature distribution for welding with 20mm shoulder tool…….....…….....	72
4.20	Time vs. Temperature distribution at center of weld line……	73
4.21	Peak temperature distribution perpendicular to the centre of weld line for various plunging forces…….....…	73
4.22	Numerical and experimental peak temperature at distance 5 mm and 21mm away from weld line…….....…….....	74
4.23	Numerical and experimental temperature vs. plunging force……..	75
4.24	Cu-Al FSW process…….....…	76
4.25	Cu-Al FSW plate…….....…….....	76
4.26	Temperature contour for traverse speed (ts) = 120 mm/min, Rotational speed (rs) = 1000 rpm and plunging force (p) = 4000 N……	77
4.27	Temperature iso-contour for traverse speed (t_s) = 120 mm/min, rotational	

	speed (r_s) = 1000 rpm and plunging force (p) = 4000 N……..	77
4.28	Cross-sectional temperature contour for traverse speed (t_s) = 120 mm/min, rotational speed (r_s) = 1000 rpm and plunging force (p) = 4000 N……	78
4.29	Peak temperature distributions at distance perpendicular to the centre of the weld line 1……....	78
4.30	Peak temperature distributions at distance perpendicular to the centre of the weld line 2……..…….....	79
4.31	Plot of peak temperature versus Pr_s / t_s ratio [N rad/mm] for copper……..	80
4.32	Plot of peak temperature versus Pr_s / t_s ratio [N rad/mm] for aluminium……	80
4.33	Comparisons of FE model and experimental weldment……..	81
5.1	Different FSW tool geometries…….....	85
5.2	Fabricated FSW tools……..…….....	85
5.3	Trapezoidal pin tool 1000rpm 80 mm/min feed……...	87
5.4	Trapezoidal pin tool 1000rpm112 mm/min feed.....	87
5.5	Hardness at different zones for varying weld speed, at 1000 rpm……..	86
5.6	Hardness at different zones for varying tool rpm, at 112mm/min……....	88
5.7	Vickers Hardness at different zones for varying FSW tool pin geometries….	89
5.8	Tensile test samples……..…….....	89
5.9	Effect of variation of tool pin geometries on engineering stress-strain characteristics of the test specimens……	90
5.10	Effect of tool rpm and welding speed on engineering stress-strain characteristics of the test specimens…….....	91
5.11	Effect of the ratio of tool rpm to tool traverse speed on maximum load…….	92
5.12	Variation of elongation of test specimens with the ratio of tool rpm to tool traverse speed……..……...	93
5.13	Different FSW tool geometries (all dimensions are in ‘mm’)…….	94
5.14	Designed and developed FSW tools…….....	95
5.15	Detail dimension of tensile test specimen…….....	95
5.16	Some of the tested tensile specimens of FSW Joints of good quality……..	97
5.17	Some of the tested tensile specimens of FSW Joints of bad quality……	97
5.18	Load vs. displacement for Trapezoidal probe geometry……..	98
5.19	Load vs. displacement for tapered cylindrical probe geometry……...	98
5.20	Nominal stress vs. Nominal strain for Trapezoidal probe geometry……	99
5.21	Nominal stress vs. Nominal strain for tapered cylindrical probe geometry….	99
5.22	Position of tensile test specimen…….....	100
5.23	Effect of dwell time on tensile properties of FSW weld samples……	100

5.24	Macrographs (a) Improper mixing of material (b) Wormhole due to high dwell time……..…….....	101
5.25	Trapezoidal pin with tool rotational speed 2000rpm and welding speed 40 mm/min…….....…….....	101
5.26	Tapered cylindrical pin with tool rotational speed 2000rpm and welding speed 40 mm/min…….....	102
5.27	Vickers Hardness at different zones of weld samples……..	103
6.1	FSW set up…….....…….....	104
6.2	Fabricated Tools…….....…….....	105
6.3	Hardness values for the samples welded by right helix threaded tool (RHT)..	107
6.4	Hardness values for the samples welded by left helix threaded tool (LHT)…	107
6.5	Stress vs. elongation plots for the base materials……..	108
6.6	Stress vs. elongation plots for the specimens welded by RHT tool…….	109
6.7	Stress vs. elongation plots for the specimens welded by LHT tool……..	109
6.8	Macrograph of Cu-Al FSW Joint shows various zones……...	111
6.9	Micro structures at various zones of Al-Cu joint…….	112
6.10	Copper and aluminum grain refinement at Nugget zone……..	112
6.11	(a) Good weld (b) Tunnel defect (c) Void…….....…….....	113
6.12	Microstructure at different areas in the nugget zone of Cu-Al FSW joint…...	113
6.13	Elemental plotting by FESEM-EDX…….....…….....	114
6.14	FESEM-EDX compositional analyses on FSW of Cu-Al (at Nugget portion)	115
6.15	Fabricated FSW tools…….....…….....	116
6.16	Tensile test samples…….....…….....	118
6.17	Main effect plots for overall Grey relational grade……..	122
6.18	FESEM analysis of fractograph of FSW samples no 6……	123

List of Tables

Table. No.		Page. No.
1.1	Industrial applications of FSW……..	4
2.1	Temperature-dependent material properties for Al 6061-T6 [110]……	29
3.1	Temperature dependent thermal material properties of aluminum …..	51
3.2	Temperature dependent coefficient of friction for aluminum and steel combination…….....	51
3.3	Thermo mechanical properties of Cu……	52
3.4	Chemical Etchants used for Alluminium and copper [148]……..	58
4.1	FSW process parameters……..……	64
4.2	Peak temperatures for different geometries……..	65
4.3	Process parameter and shoulder diameters……...	66
4.2	Process parameter ……..……..	70
4.3	Process parameters versus maximum temperature……...	79
5.1	Composition of SS310 by percentage…….....	84
5.2	Physical properties of SS310……...……	84
5.3	Names of the tools used……...……	85
5.4	Process parameters for 6mm thick aluminum plates……	86
5.5	Variation of average grain size with tool geometry……..	88
5.6	Variation of average grain size with FSW process parameters……	88
5.7	Welding process parameters for trapezoidal probe geometry……...	96
5.8	Welding process parameters for tapered cylindrical probe geometry……..	96
6.1	Design of experiments……..	106
6.2	Results of mechanical and weld zone in thickness direction……..	110
6.3	Process parameters and their limits……..	117
6.4	Taguchi's L16 orthogonal array design……...	117
6.5	Mechanical properties of AA1100 and AA5083……	118
6.6	Experimental data……	118
6.7	Normalization of output data (Grey relational generation)……	120
6.8	Evaluation of Δ0i for each of the responses……...	120
6.9	Grey relational coefficients of each performance characteristics…….	121
6.10	Grey relational grades……..	122
6.11	Analysis of variance using adjusted SS for tests……	123

Contents

- **Title page** Page. No
- **Certificate**
- **Acknowledgements**
- **Abstract** **i**
- **List of symbols** **iii**
- **List of abbreviations** **v**
- **List of figures** **vii**
- **List of tables** **xii**
- **Contents** **xiii**

Chapter 1 Introduction

1.1 Back ground of welding..... 1
1.2 Classification of welding techniques..... 1
1.3 Motivation..... 2
1.4 Introduction to FSW..... 3
1.4.1 Industrial applications of FSW..... 4
1.5 Research objectives..... 5
1.6 Thesis structure..... 6
1.7 Target application..... 6

Chapter 2 Literature Review

2.1 Introduction..... 7
2.2 Operating parameters and their effect on weld quality..... 7
2.2.1 Summary..... 13
2.3 Mechanical and microstructural properties study..... 13
2.3.1 Summary..... 19
2.4 FSW of dissimilar materials..... 19
2.4.1 FSW of dissimilar alluminium alloys..... 20
2.4.2 FSW of alluminium to other alloys..... 21
2.4.3 Summary..... 24
2.5 Numerical and analytical study..... 25

2.5.1 Summary……..... 35

Chapter 3 Methodology

3.1 Introduction……. 36
3.2 Transient thermal Analysis……..…… 36
3.2.1 Heat generation at cylindrical tool shoulder and cylindrical tool pin. 36
3.2.1.1 Heat generation at cylindrical shoulder..... 37
3.2.1.2 Heat generation at cylindrical probe..... 39
3.2.2 Heat generation at cylindrical tool shoulder with conical tool pin..... 40
3.2.3 Heat Source Model……. 44
3.2.3.1 Heat source model for similar material..... 44
3.2.3.2 Heat source model for dissimilar material..... 44
3.2.4 Three-dimensional finite element model.....……..... 45
3.2.4.1 Initial condition..... 47
3.2.4.2 First boundary condition..... 47
3.2.4.3 Second boundary condition..... 47
3.2.4.4 Derivation of heat flow matrices..... 48
3.2.4.5 FE model..... 50
3.3 Experimental setup and procedures..... 52
3.3.1 Design of experiments..... 53
3.4 Mechanical and Microstructural properties study…..... 54
3.4.1 Tensile test……..…… 54
3.4.2 Micro hardness……..……..... 55
3.4.2.1 Sample preparation for hardness test..... 56
3.4.3 Microstructural study..... 57
3.4.4 Compositional and fractograph analysis……..... 59
3.5 Summary……. 60

Chapter 4 Transient thermal analysis

4.1 Introduction…… 61
4.2 Results and Discussions……..... 61
4.2.1 Effect of tool pin geometries……..……..... 63
4.2.2 Effect of tool shoulder diameter and tool plunging force…….. 66
4.2.2.1 Effect of tool shoulder diameter……..... 66
4.2.2.2 Effect of tool plunging force……..... 73
4.2.1 Summary..... 75
4.3 Numerical studies on thermal history of FSW on Dissimilar alloys…. 76

4.3.1 Summary..... 81

Chapter 5 Experimental Results

5.1 Introduction..... 83
5.2 FSW of aluminum alloy with varying tool geometry and process parameters..... 83
5.2.1 Metallographic examination..... 86
5.2.2 Vickers micro hardness..... 88
5.2.3 Tensile strength..... 89
5.2.4 Summary..... 93
5.3 Friction stir welding of thick aluminum alloy plates..... 94
5.3.1 Tensile properties..... 95
5.3.2 Effect of dwell time on mechanical properties..... 99
5.3.3 Microstructure..... 101
5.3.4 Microhardness..... 102
5.35 Summary..... 103

Chapter 6 FSW of dissimilar materials

6.1 Introduction..... 104
6.2 FSW of alluminium and copper alloy plates..... 104
6.2.1 Micro hardness..... 106
6.2.2 Tensile strength..... 102
6.2.3 Metallographic study..... 111
6.2.4 Elemental scanning 114
6.2.5 Summary..... 115
6.3 Investigation of FSW on dissimilar alluminium alloys..... 116
6.3.1 Introduction..... 116
6.3.2 Optimisation of FSW on AA1100-AA5083..... 119
6.3.3 Summary..... 124

Chapter 7 Summary and conclusions

7.1 Summary..... 125
7.2 Conclusions 126
7.3 Scope for Future Research..... 127
References 129
Author's Resume/Publications 140

Chapter 1
Introduction

1.1 Background of welding

In general, welding is described as the joining of two materials by coalescence produced by application of with or without external heating/pressure. It joins various metals/alloys with the help of different welding processes in which heat is supplied either electrically or by a gas torch. This coalescence can be achieved by melting the two metal pieces together as in case of fusion welding or heating up to plastic state to form a metallic bond across the interface i.e. solid state welding. Solid state joining is one of the oldest joining technique which was used by blacksmith for making different iron tools about 3500 years ago [1]. Joining of metal pieces was started more than 2000 years back. In the late 1800's welding emerged as a manufacturing process and this has undergone many inventions and discoveries [2]. Blacksmiths of the middle Ages welded various types of iron tools by hammering. The welding methods remained more or less unchanged until the dawn of the 19th century. Several inventions and improvements of welding techniques were takes numerously place so far.

1.2 Classification of welding techniques

The demand of metals leads to its huge production and establishing of its processing procedures. Welding plays a vital role in processing and fabrication of metals structures which is the reason for its development. Different types of welding techniques have been established and used for various applications. Classification of welding processes according to the phase of metal at weld zone is shown in Figure 1.1

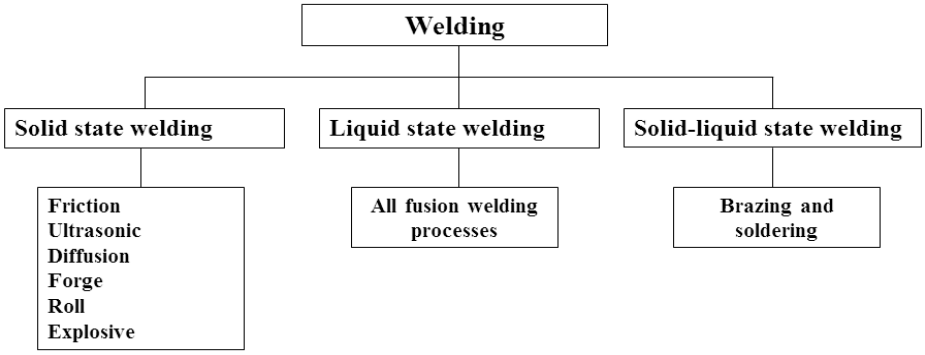

Figure 1.1 Types of welding processes based on phases

Amongst solid state welding, Friction welding plays a vital role in joining metals. This process is used for the applications where the base metal characteristics must remain unaffected at weld nugget. Based on this technique many other processing techniques have been developed which is shown in the Figure 1.2.

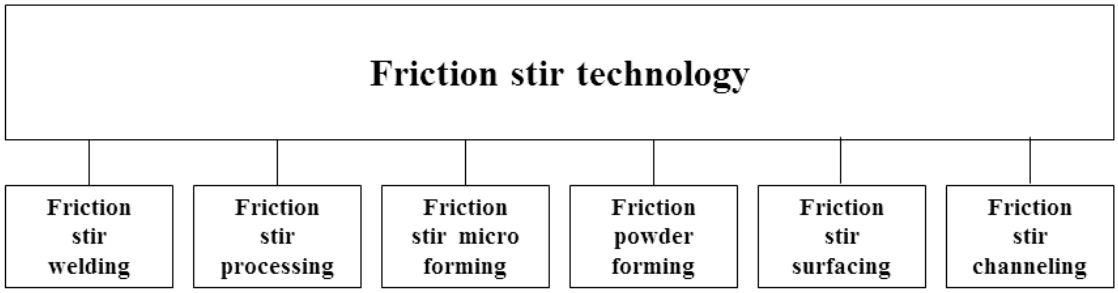

Figure 1.2 Variants of friction stir technology

1.3 Motivation

Friction stir welding (FSW) is one of the variant of friction stir technology which got roots from the friction welding method. This process has ability to produce welds of high quality without melting the material and eliminates almost all the defects seen in the conventional welding processes. This process contains many advantages with minimal limitations and it has been rapidly establishing as a choice for manufacturing light weight transport structures such as ships, trains and aeroplanes. The main detrimental effects of arc welding i.e. distortion and residual stresses are due to the rapid heating beyond the melting temperature and cooling of the joints. These detrimental effects are minimized in FSW, as the heat generated is not severe enough. Furthermore no special preparation of the sample is required during the FSW process. FSW of aluminum alloys offers the advantages of low heat input, low distortion, therefore, low residual stresses and higher mechanical properties compared to conventional fusion welding methods. The interesting aspect of FSW is an unchanged material property throughout the weld zone means it doesn't require any filler material at the joint.

In the present study, Friction stir welding has been considered as an area of research interest. In this investigation, FSW of similar, dissimilar materials and its characteristics and & analysis have been carried out.

1.4 Introduction to Friction Stir welding

Friction stir welding (FSW) is a unique joining technique; its uniqueness in welding metals indicates the usage of frictional heat generated by the contact of rotating tool and the workpiece. This technique comes under the solid state welding processes as the joint occurs without melting of the material. In principle, FSW generates weld by means of a hard revolving non consumable welding tool softens/plasticizes the workpiece locally, through the heat generated by friction and plastic work, and thus allows the tool to stir the joint surfaces. Finally, by means of both the tool stirring and tool traversing actions the weldment produces. The typical FSW process can be clearly understand by the following steps/stages as shown in Figure 1.3.

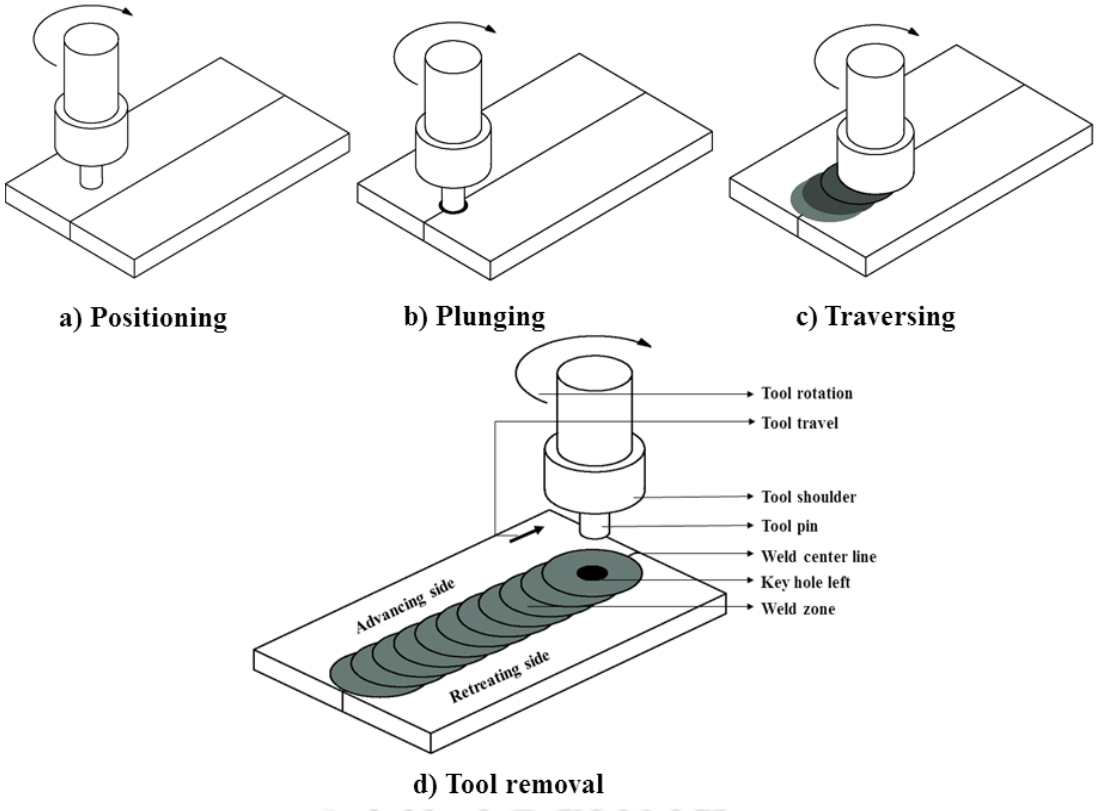

Figure1.3 Friction stir welding process

Prior to the FSW, the workpieces must be rigidly tightened in order to withstand the forces of the tool. The tool should be positioned with the centre line of the plates to be joined as shown in Figure 1.3a. The tool pin is plunged into the work piece until its shoulder touches the work piece as shown in Figure 1.3b. The rotating tool is allowed to remain constantly stirring in the position until it acquires the required temperature (i.e. about 80% of base materials melting point temperature). Figure 1.3c, Then it proceeds over the weld line by the given traversing motion as shown in Figure 1.3d. The final stage of this process is the tool removal which is

shown in Figure 1.3d. The working principle and operational conditions of FSW are very simple and adequate as compared to conventional welding techniques. This technique also possesses a skill to weld a wide variety of joints like butt, lap, corner, spot, T- joints etc. Generally FSW but joints exhibit around 65-100% joint efficiencies. In this present investigation, FSW butt joints were done for both similar and dissimilar materials.

This process can be considered as an environmental and operator friendly as this doesn't produce any noise, flame and toxic fumes. As there is no fusion/material melting this process eliminates almost all the limitations of conventional welding techniques like, weld plate distortions, porosity in the weld zone and shrinkage etc. Therefore this process functions as a promising technique for welding of non-ferrous, lightweight materials like aluminium, magnesium alloys, etc. And it is widely applicable in various industries like aerospace, ship building, automobile etc.

1.4.1 Industrial applications of FSW

Many industries have adopted this process for fulfilling the difficulties of welding alluminium alloys and other light weight metals since 1991. This process has been rewarding the following industries for joining of lightweight materials [3] as shown in Table 1.1. Few of its important industrial applications have been tabulated below. Table 1.1 shows the industrial applications of FSW.

Table 1.1 Industrial applications of FSW

Industry	Material	Part	Reference
Aerospace	Alluminium(AA7075)	Rocket Fuel tanks, Space shuttle external fuel tank, Toe nails of cargo aircraft, T-joints and lap joints of commercial air crafts	[3,4,5]
Shipbuilding	Alluminium(AA5083)	Food Freezer panels for preservation, Oil rig panels for bulk heads and decks, Hull of an ocean viewer, Honey comb panels, Corrosion resistant panels	

		Deck panels for civil and naval ships	[3, 4]
Railway	(AA1100,AA5083)	Roof panels for rolling stocks and floor panels	[3]
Automotive	Alluminium(AA6061)	Tailors blanks for door, roof panels	[3,6,7]

1.5 Research objectives

Based on the research gaps found in the previously published literatures, the objectives of the present work have been decided. These objectives have been categorised into two sub group's i.e. a) Experimental investigation and b) Numerical analysis.

a) Experimental investigation

i) Development of a set of simple and ease in manufacture of FSW tool geometries to achieve a better weld quality for joining both similar and dissimilar materials.

ii) Studies on effect of weld parameters (tool transverse speed, tool rotational speed, tool pin geometries, tool shoulder and pin dimensions, tool plunging force) on weld quality of similar materials.

iii) Studies on effect of weld parameters (tool transverse speed, tool rotational speed, tool pin geometries, tool shoulder and pin dimensions, tool plunging force) on weld quality of dissimilar materials.

iv) Investigations of experimental feasibility on FSW of thick sections

b) Numerical analysis

v) Development of three dimensional finite element model for conducting the transient thermal analysis on FSW of similar and dissimilar materials.

vi) Study the effect of welding process parameters (welding transverse speed, tool rotational speed, tool plunging force) on thermal history on FSW of similar and dissimilar materials.

vii) Study the effect of tool shoulder diameter on thermal history on FSW of similar and dissimilar materials.

1.6 Thesis structure

The contents in this thesis focus on the study of both numerical and experimental work associated to FSW of similar and dissimilar materials. It covers the influence of various FSW operating parameters on weld qualities and thermal histories. The principal intention of this work is to develop a set of FSW tools which are simple in geometry and ease in fabrication for welding of both similar and dissimilar metals. Development of three dimensional FE-model to predict the process parameters effect on thermal history.

The content of this thesis is divided into seven chapters and they are as follows:

- ***Chapter 1*** provides a brief background and general introduction to Friction stir welding and its applications.
- ***Chapter 2*** has been devoted fully to a brief review on numerical and experimental investigations of FSW associated to the objectives of the present thesis.
- ***Chapter 3*** covers the methodologies followed in pre and post experimental work. And here, methodologies applied in numerical modelling have also elaborated.
- ***Chapter 4*** presents results of numerical analysis on several FSW process parameters and tool geometries have been reported. And validations of numerical investigations with experimental results have been focussed here.
- ***Chapter 5*** completely deals with experimental investigations on FSW of both similar materials as stated in research objectives.
- ***Chapter 6*** has been dedicated to the experimental investigations on FSW of dissimilar materials.
- ***Chapter 7*** summarises the entire work of this thesis in a concise form. The summary is followed by the conclusions of the present research and the scope of future work in this particular area. The thesis ends with a complete list of references.

1.7 Target application

The applications of the outcomes produced from the present study can be implemented in the industries mentioned in Section 1.4.1. However the present work can also be helpful in the domestic and small scale industries. Prior to the experimentation, one can forecast the various effects involved in this process using the developed FE model in the present work. The outcome of this study helps various manufacturing industries whose motto is to weld dissimilar metals by FSW process.

Chapter 2
Literature review

2.1 Introduction

Friction stir welding is an emerging technology of solid state joining process invented by Thomas WM and his group [8] in 1991 and got patented. This technique was recognised by the scientific community soon after its invention. By the year 2013 this publishing rate has been tremendously increased. The average research journals published on FSW from the year 2005-2014 is nearly about 280 journals per a year. Figure 2.1 represents the graph of publications per year on FSW. The reason for this huge attention on this process is its ability to weld almost all non weldable alluminium alloys like AA5083, AA7075 etc. This chapter focusses on the literature review of following topics, i.e. 2.2 Operating parameters and their effect on weld quality, 2.3 Mechanical and microstructural properties study, 2.4 FSW of dissimilar materials, 2.5 Numerical and analytical study on FSW.

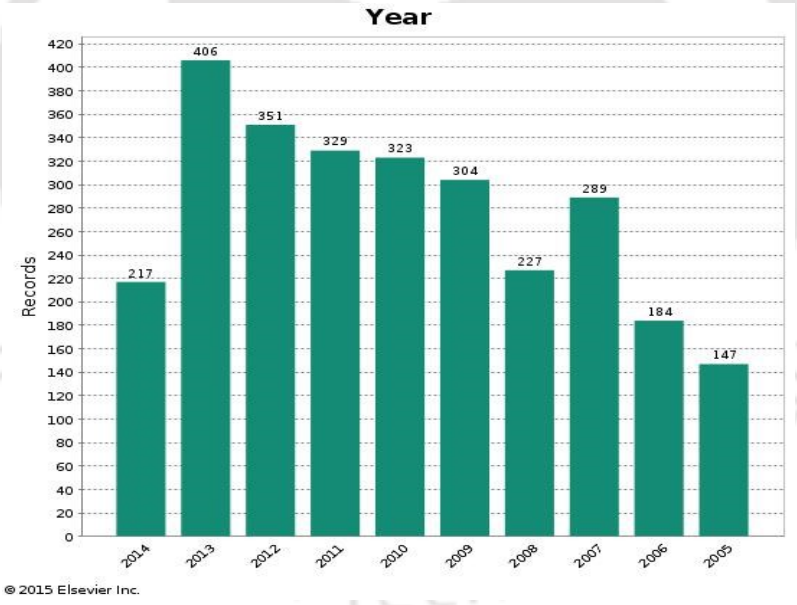

Figure 2.1 Year wise publications on FSW (Picture from INSPEC- ©Elsevier Inc)

2.2 Operating parameters and their effect on weld quality

Both tool geometries and process parameters have significant effect on final weld quality in FSW. The main process parameters of FSW are rotational speed of the tool, tool traverse speed, and vertical pressure on the plates during welding, Rajakumar *et al*. [9]. However, the tool geometry which involves the geometry of pin profile and shoulder has an important

characteristic which may affect the weld quality, Su *et al*. [10]. The FSW tool is the heart of this welding process. Dawes & Thomas [11] described the tool development approach taken at The Welding Institute (TWI) and outlined the tool design aspects of the scroll shoulder concept. FSW tool shoulder diameter has a significant effect on generating heat required for the welding. Whereas the pin helps to mix, extrude the material around it and final formation of joint. Researchers have developed various tool geometries up until now, and they have mentioned these developed tools are specifically for welding of various alloys, few of them have been mentioned here.

Narayanan & Balasubramanian [12] fabricated a FSW tool using high carbon steel for welding RDE-40 aluminium alloy. They applied Taguchi approach to determine the most influential control factors which will yields better tensile strength. Saeid *et al*. [13] used a tool of WC material for welding 2205 duplex stainless steel by FSW process, the tool dimensions are SD16, PD5, and PL1.5. They analysed the effect of the welding speed on the microstructure and mechanical properties of the stir zone (SZ). Cam *et al.* [14] fabricated a conical tool using HSS whose diameter is 4:3 for welding Al-5086. Their results suggest that both strength and ductility performances and they also stated it can be increased by optimizing the tool penetration depth. Lorrain *et al*. [15] joined 7020-T6 rolled sheets of 4 mm thickness by using a tool made of HCS material whose dimensions are SD13, PD5, PL3 and found material flow with unthreaded pin was the same features as material flow using classical threaded pins.

Guerra *et al.* [16] used the tool of D2 Tool Steel with dimensions 19SD, 6.3PD, 5.8PL, RHT for welding Al 6061 and studied the material flow using the high purity copper foil of 0.1mm. They noticed that the material undergoes a helical motion within the rotational zone and descends in the downward direction of the threads on the nib and rises on the outer part of the rotational zone. Lienert *et al*. [17] used Molybdenum and Tungsten-based alloys, for making FSW tool whose dimensions are, SD19, PL6.22, to weld 1018MS sheets and studied the deformation and wear of the tool dimensions and its effects on the weld quality.

Yutaka *et al.* [18] studied on preparation a tool of material PCBN (polycrystalline cubic boron nitride) of dimensions 25SD, 3.2PL, 3F, for processing 304L SS, 6.4mm thick by using Friction stir processing technique. They examined the recrystallization phenomenon by orientation imaging microscopy. Charit & Mishra [19] have developed a FSW tool with a cobalt-base alloy for welding Al–Zn–Mg–Sc alloy and found that an ultrafine grained alloy

exhibited super plasticity. Barcellona *et al*. [20] manufactured a FSW tool with the H13 steel material, of dimensions PD3, PL2.88, for welding AA2024-T4 of 3mm thickness sheets. Localized softening in the HAZ is observed and they also observed that the joint strength was about 60% of the UTS of the parent material. And they also noticed that by the post-welding heat treatment improves its mechanical characteristics.

Some other complex tool pin geometries and tool shoulder surfaces have been introduced by the TWI and others as well as shown below. Figure 2.2 shows the trifluted pin profiles, Figure 2.3 Worl and MX Tri-flute tools, Figure 2.4 shows Flared Tri-flute tools and Figure 2.5 represents the various shoulder surfaces.

Figure 2.2 Tri-flute pin FSW tool fabricated at SMU [21]

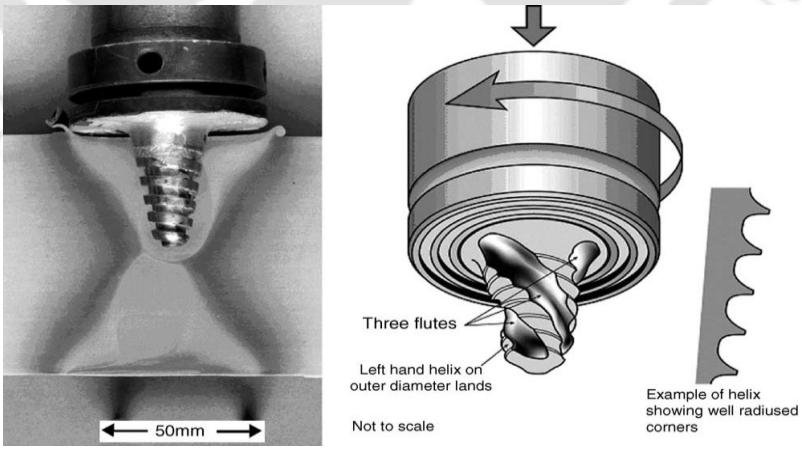

Figure 2.3 Worl^{TM} and MX^{TM} Triflute tools developed by The Welding Institute (TWI), UK. [22]

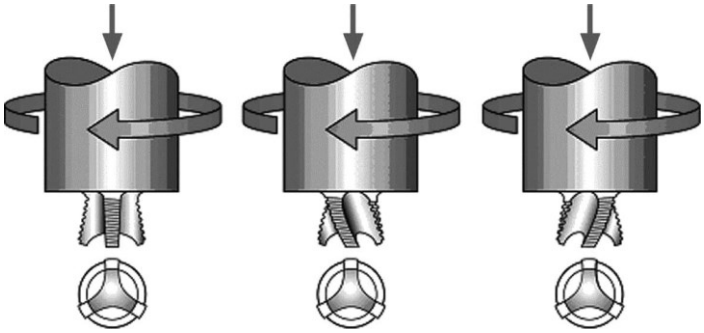

Figure 2.4 Flared-Triflute™ tools developed by The Welding Institute (TWI), UK. [23]
(a) Neutral flutes, (b) left flutes, and (c) right hand flutes

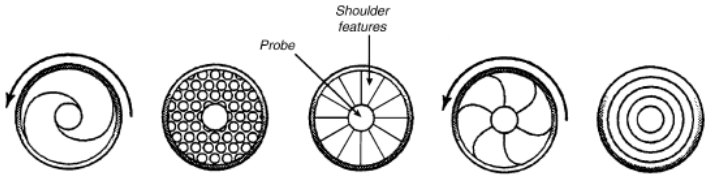

Figure 2.5 Patterns of various tool shoulder surface developed by The Welding Institute (TWI), UK. [22]

Yuqing *et al.* [24] has used four different tools with the pin eccentricity of 0.1 mm, 0.2 mm, 0.3 mm and 0.4 mm were designed to friction stir weld 10 mm thick AA7075-O plate. They studied the effect of pin eccentricity on microstructure, secondary phase particles transformation and mechanical properties of the joints. Their results show that the nugget area increases initially and then decreases with increasing the pin eccentricity. They also stated that the joints produced by the pin with 0.2 mm eccentricity perform the highest tensile strength and elongation, which is attributed to better interfaces, finer grains and more dispersive secondary phase particles.

Rabby & Reynolds [25] correlated different types of tools and various process parameters. They focused on parametric effects of pin features on material flow and friction stir weldability of two different aluminum alloys. They have done a series of bead on plate friction stir welds on two different aluminum alloys (AA 7050 and AA6061) with cylindrical tool pin having four thread pitches (1.02 mm, 1.41 mm, 2.12 mm & 3.18 mm) including smooth unthreaded pin attached to an unvarying single scrolled shoulder geometry. Welds were performed under set of process parameters. They have observed that thread forms are benefitted for improving tool performance and reducing in several forces on tool. They have also observed elimination of wormhole defects in the weld nugget. Their huge macroscopic investigation reveals that the tool pins having intermediate thread pitches (1.41mm and 2.12

mm) perform better than either extreme over the range of attempted parameters. Biswas *et al*. [26] studied the FSW of aluminum alloy by varying the tool geometries.

More studies on tool geometries have reported recently [27-30]. They show that as the geometrical difficulty increases the wear and tear of the tool increases which may produce defective welds. A worn-out threaded or fluted tool again turns as a cylindrical pin tools. Partial worn FSW tool pin generates voids in the welds due to improper material mixing. Typical pin geometries may often experience the problem of tool pin breakage which has to undergo re-machining leads to increase the tool manufacturing cost. Hence, it is always preferable to consider the simple and regular tool geometries in manufacturing concern.

The joint quality of FSW weldment is also affected by heat generation between tool and workpiece interface. This heat generation and material flow at the interface has a high impact on the process parameters viz., tool rotation speed, tool travel speed, plunging force, and dwell time etc. It is very important to choose a proper rotational speed and welding speed to obtain effective joints. While there has been several studies focused on the effect of variation of rotation and welding speeds on the resulting microstructures for aluminum alloys, limited reporting was found on the effects of variation of tool geometries [31-34].
Some authors analyzed the influence of the tool rotation speed (Sato *et al.* [35]), tool traverse speed (Lee *et al.* [36], Simar *et al.* [37]) and both parameters simultaneously [31-34] on the microstructure and mechanical properties of 6XXX and 5XXX aluminum alloys by considering the same tool geometry. Sato *et al.* [35] studied the effect of different tool rotation speeds on AA 6063, T5 and T4. They observed that different rotational speeds did not result in significant differences in the hardness profile in FSW welds, except for the width of the softened region in the weld of AA 6063-T5. Lee *et al*. [36] studied the microstructural change related to the hardness profile of friction stir welded, age hardenable AA 6005. They suggested that frictional heat and plastic flow during friction stir welding created fine and equiaxed grains in the stir zone and elongated, recovered grains in the thermomechanically affected zone (TMAZ).

The FSW process parameters and tool geometry play a major role in deciding the joint strength [9, 42]. Rajakumar *et al*. [9] made an attempt to establish an empirical relationship between the FSW process of AA7075 alloy and tool parameters (tool rotational speed, welding speed, axial force, shoulder diameter, pin diameter, and tool material hardness) and the tensile strength of the joint. Soundararajan *et al.* [43] were carried out for joining similar

and dissimilar metals using a high-speed rotating tool under various rotational speeds and traverse speeds and for different tool penetration depths. They discussed the detection and analysis of the acoustic emission (AE) signals to investigate the possibility of applying the AE technique for the in-process monitoring of the friction-stir-welding process.

Aota & Ikeuchi [44] used a probe-less FSW tool for lap welding of 6mm alluminium plate. They designed and fabricated the new tool shapes which have a dome shape at the top. In this process, the rotating tool was plunged into the aluminium plate. They have welded the specimen on these following parameters i.e. 20 mm/s welding speed and 18000 rpm of tool rotation speed. They observed that the weld quality was better if they kept plunge depth at 0.1mm.

Shtrikman *et al.* [45] joined a T-joint using a specially designed and fabricated tool which is shown in Figure 2.6. They reported that their tool and the process parameters have significant effect on weld quality based on their microstructural results. They also observed some defects occurred due to lesser tool plunge depths. They stated that the proposed tool design gives the better weld for alluminium alloys.

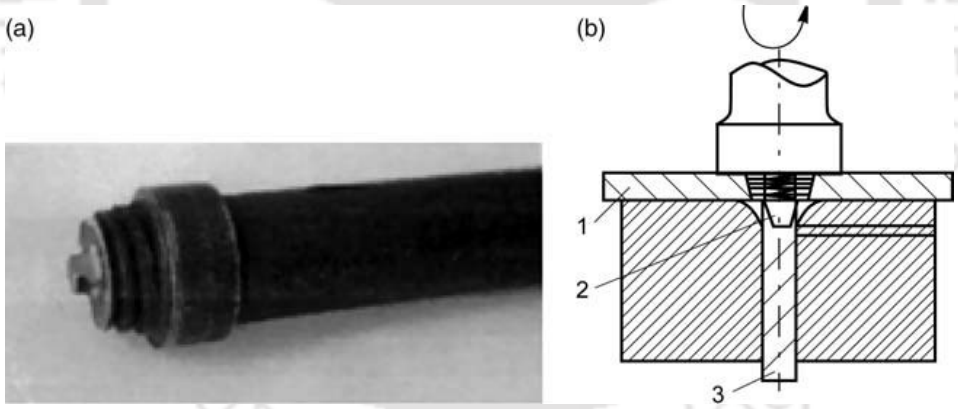

Figure 2.6 (a) Tool with a 'pyramid' in the (b) diagram of friction welding: 1, the plating; 2, the tool with the 'pyramid'; and 3, the web [45].

Kumar *et al.* [46] conducted few FSW experiments to study systematically and analyse the intrinsic mechanisms governing the formation of the weld and to effectively utilize the analysis to establish a logical basis for design of the tool. Based on their experimental results they proposed an optimal mechanism for the selection of pin diameter and tool shoulder diameter for successful welds.

2.2.1 Summary

FSW process parameters such as rotational speed, dwell time, longitudinal speed/traverse speed, axial force/plunging force significantly influence the weld quality [49]. The design of the tool like, probe shape and size, shoulder diameter, shoulder surface plays major role in acquiring the best weld joint properties [80]. Literature on effect of tool geometry and process parameters on FSW welds reveals that, as the geometrical difficulty increases the wear and tear of the tool increases which may produce defective welds. A worn-out threaded or fluted tool again turns as a cylindrical pin tools and a partial worn FSW tool pin generates voids/tunnels in the welds due to improper material mixing. Critical design in tool pin geometries may often experience the problem of tool pin breakage which has to undergo re-machining, that leads to increase in the tool manufacturing cost. Hence, it is always preferable to consider the simple and regular tool geometries in considering the tool life, weld zone symmetry and also in tool manufacturing concern. The available literatures correlating the process parameter and the various pin geometries effect on weld quality are limited. Hence, some contributions have been prerequisite based on these issues for both similar and dissimilar material welding which promotes this process enhancement.

2.3 Mechanical and Microstructural properties study

The process parameters of FSW have significant effects on mechanical and microstructural properties of FSW weldments. A number of studies have been reported on this for FSW of various materials. FSW results in significant microstructural evolution within and around the stirred zone, i.e., nugget zone, TMAZ, and HAZ. This leads to substantial change in post weld mechanical properties of the welded material. In the following sections, typical mechanical properties, such as: strength, ductility, fatigue, and microstructural changes are briefly reviewed.

Cavaliere *et al*. [47] studied the effect of processing parameters on the mechanical and microstructural properties of dissimilar AA6082–AA2024 joints. They varied the advancing speeds of the tool as 80 and 115 mm/min and by varying the alloy positioned on the advancing side of the tool. Kept rotating speed fixed at 1600 RPM, and welded perpendicularly to the rolling direction for both the alloys. Micro hardness (HV) and tensile tests performed at room temperature were used to evaluate the mechanical properties of the joints. The mechanical tests were performed on the joints previously subjected to annealing at

2500C for 1h. For the fatigue tests, a resonant electromechanical testing machine was employed under constant loading control up to 250 Hz sine wave loading. To analyse the microstructural evolution of the material, the welds' cross-sections were observed optically and SEM observations were made on the fracture surfaces. The forces acting on the plates in the case of the higher strength material (AA2024) positioned on the advancing side of the tool resulted higher with respect to the corresponding welds with the softer material (AA6082) positioned in the advancing side.

Taban & Kaluc [48] conducted the comparative study of conventional fusion welding processes like; MIG, TIG and solid state process friction stir welding (FSW) were applied to 6.45 mm thick plates of 5086-H32 aluminium alloy. They evaluated their weldments by performing microstructural examinations including light optical microscope (LOM) and transmission electron microscope (TEM) and EDX analysis as well as hardness measurements. Mechanical testing was done by means of tensile and bend tests. Fracture surfaces were examined by LOM and scanning electron microscope (SEM) and concluded that properties obtained, by double pass friction stir welded joints of 5086-H32 aluminium alloy have superior properties than that of MIG and TIG welded joints.

Peel *et al*. [49] reported the results of microstructural, mechanical property and residual stress investigations of four aluminium AA5083 friction stir welds produced under varying conditions. Found that the weld properties were dominated by the thermal input rather than the mechanical deformation by the tool. According to their results they stated that due to the recrystallization results in the weld zone having considerably lower hardness and yield stress than the parent AA5083. During tensile testing, almost all the plastic flow occurs within the recrystallized weld zone. Lee *et al*. [50] observed the improvement of mechanical properties at the weld zone of FSW A356 alloys, welded at various welding speeds. The BM shows the hypoeutectic Al-Si dendrite structure. The microstructure of the SZ is very different from that of the BM. They observed that hardness of the weld zone was more uniformly distributed than that of the BM because some defects are remarkably reduced and the eutectic Si particles are dispersed over the SZ.

Due to the immense plastic deformation of the material at nugget zone experiences very high temperature which results in the development of texture and recrystallization [51, 52]. Material flow and micro structural changes obtained by the severe churning action of the FSW tool results the grain coarsening at thermomechanical and grain refinement at nugget

zone was reported in these articles [53, 54, 55, 56, 57, 58]. These microstructural studies of grains and precipitates consists of three distinct zones, i.e. i) nugget/stirred zone, ii) thermo-mechanically affected zone (TMAZ), and iii) heat-affected zone (HAZ) which is shown in Figure 2.7.

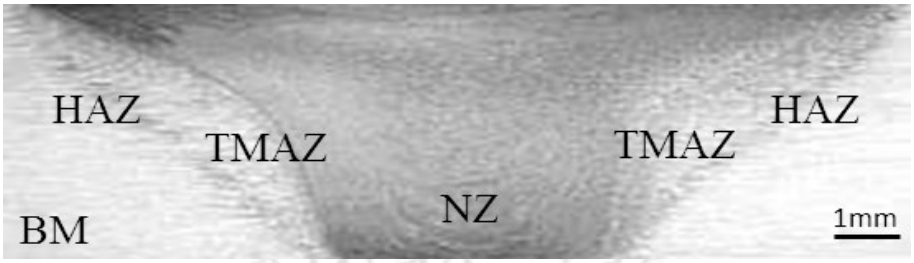

Figure 2.7 Macrograph showing various microstructural zones welded by conical pin tool

The microstructural changes in various zones have significant effect on post weld mechanical properties. Therefore, the microstructural evolution during FSW was studied by a number of investigators. In the weld nugget, generation of a recrystallized fine-grained microstructure was due to extensive plastic deformation and frictional heating during FSW. This region is usually referred to as nugget zone (or weld nugget) or dynamically recrystallized zone (DXZ). Rhodes *et al.* [59] & Liu *et al.* [60] stated that the interior of the recrystallized grains, usually there is low dislocation density. However, some researchers reported that the small recrystallized grains of the nugget zone comprise high density of sub-boundaries [61, 62, 63, 64], sub-grains, and dislocations. The interface between the recrystallized nugget zone and the parent metal is relatively diffuse on the retreating side of the tool, but quite sharp on the advancing side of the tool.

Depending on the process parameter, tool geometry, temperature of workpiece, and thermal conductivity of the material, various shapes of nugget zone have been observed. Basically, nugget zone can be classified into two types, basin-shaped nugget that widens near the upper surface and an elliptical nugget. Sato *et al.* [61] reported the formation of basin-shaped nugget on friction stir welding of 6063Al-T5 plate. They suggested that the upper surface experiences extreme deformation and frictional heating by contact with a cylindrical-tool shoulder during FSW, thereby resulting in generation of basin-shaped nugget zone. Rhodes *et al*. [59] & Mahoney *et al*. [55] reported elliptical nugget zone in the weld of 7075Al-T651. Another report stated that lower tool rotation rate of 300–500 rpm resulted in generation of basin-shaped nugget zone, whereas elliptical nugget zone was observed by FSP at higher tool

rotation of greater than 700 rpm [58]. This specifies that the same tool geometry produces different nugget shapes by changing processing parameters.

Zhao & Reynolds, [65] reported the relationship between nugget size and pin size. He reported that the nugget zone was slightly larger than the pin diameter, except at the bottom of the weld where the pin tapered to a hemispherical termination. He also stated that as the pin diameter increases, the nugget acquires a more rounded shape. It is well accepted that the dynamic recrystallization during FSW results in generation of fine and equiaxed grains in the nugget zone [49-54]. FSW parameters, tool geometry, temperature of the workpiece, vertical pressure, material properties and cooling rate of weld at nugget exert significant influence on the size of the recrystallized grains.

In FSW process thermo-mechanically affected zone (TMAZ) produced between the parent material and the nugget zone. The TMAZ experiences both temperature and deformation during FSW. The TMAZ is characterized by a highly deformed structure. The presence of precipitates in the grain interior at different zones is shown in Figure 2.8 reported by (Su *et al*. [10]).

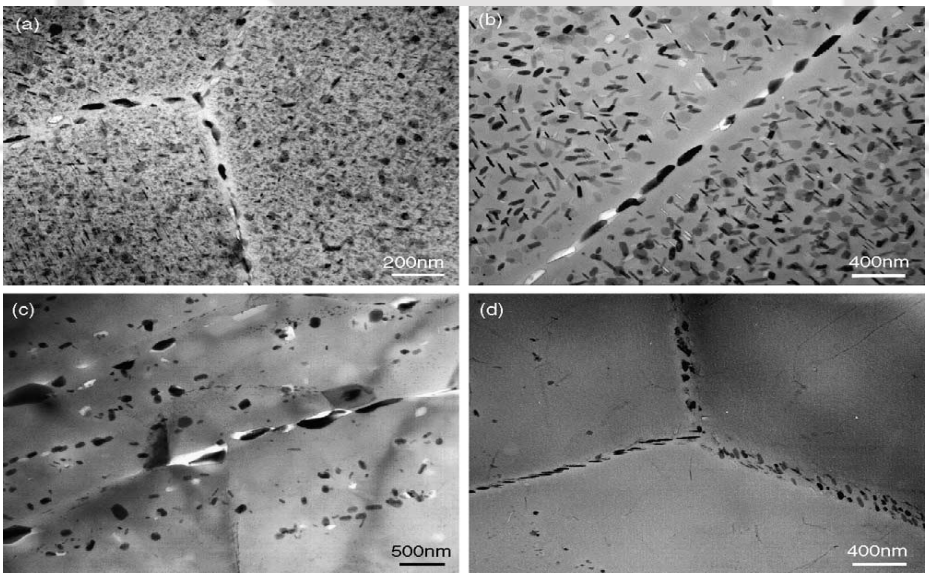

Figure 2.8 Precipitate microstructures in the grain interior and along grain boundaries in: (a) base metal, (b) HAZ, (c) TMAZ near HAZ, and (d) TMAZ near nugget zone (FSW 7050Al-T651, tool rotation rate: 350 rpm, traverse speed: 15 mm/min)[10]

The parent metal elongated grains were deformed in an upward flowing pattern around the nugget zone. Although the TMAZ underwent plastic deformation, recrystallization did not occur in this zone due to insufficient deformation strain. Sato *et al*. [61] revealed that the

grains in the TMAZ usually contain a high density of sub-boundaries. Heat effected zone (HAZ) can be observed beyond the TMAZ. This zone experiences a thermal cycle, but does not undergo any plastic deformation.

Mahoney *et al*. [55] defined the HAZ as a zone experiencing a temperature rise above 250^0C for a heat-treatable aluminium alloy. The HAZ retains the same grain structure as the parent material. However, the thermal exposure above 250^0C exerts a significant effect on the precipitate structure. Jata *et al*. [63] investigated the effect of friction stir welding on microstructure of 7050Al-T7451 aluminium alloy. They reported that while FSW process has relatively little effect on the size of the sub-grains in the HAZ, it results in coarsening of the strengthening precipitates and the precipitate-free zone (PFZ) increases by a factor of 5. Similar observation was also made by Su *et al*. [9] using a TEM examination on FSW 7050Al-T651 as shown in Figure 2.9b.

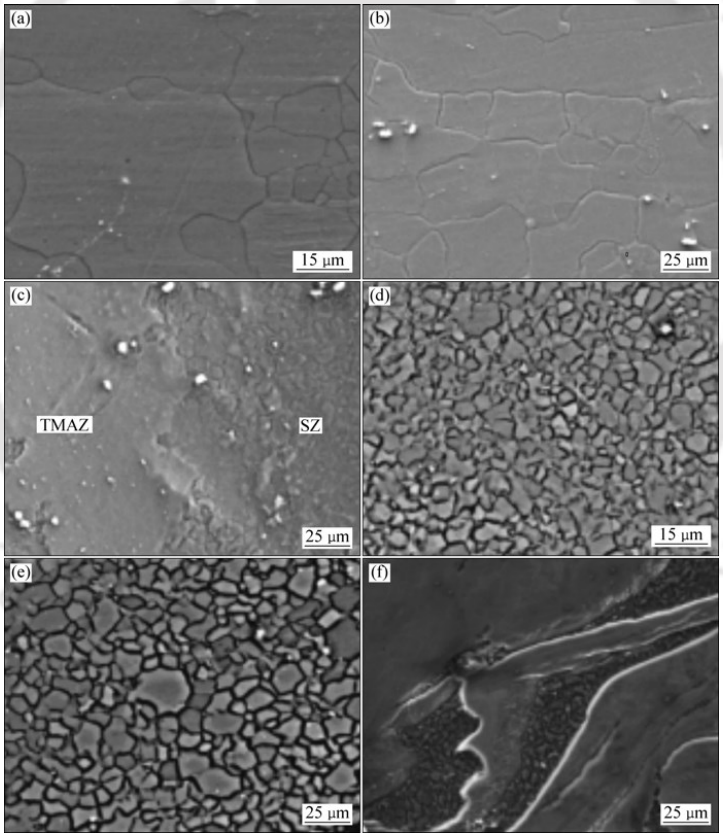

Figure 2.9 SEM images of AZ31 in different regions (a) BM; (b) HAZ; (c) Interface of TMAZ/SZ; (d) SZ inMg side; (e) SZ in Al side; (f) Intercalated microstructure [66]

Yong *et al*. [66] joined dissimilar materials 5052 Al alloy and AZ31 Mg alloy of thickness 6 mm by FSW process and noticed that sound welds were obtained at rotation speed of 600 rpm and welding speed of 40 mm/min. They noticed that the stir zone was significantly

redefined compared to the base material. They conducted SEM analysis for evaluating the changes in the weld zones. Figure 2.9 represents their micro structural changes in their specimens. Saeid *et al.* [67] welded a lap joint of dissimilar materials i.e. copper and alluminium and performed the micro structural studies and noticed that the fine equiaxed grains in stir zone and an elongated alluminium grains in at TMAZ advancing side of alluminum plate were reported as shown in Figure 2.10. The copper particles with irregular shape and inhomogeneous distribution were observed in the aluminum dark area.

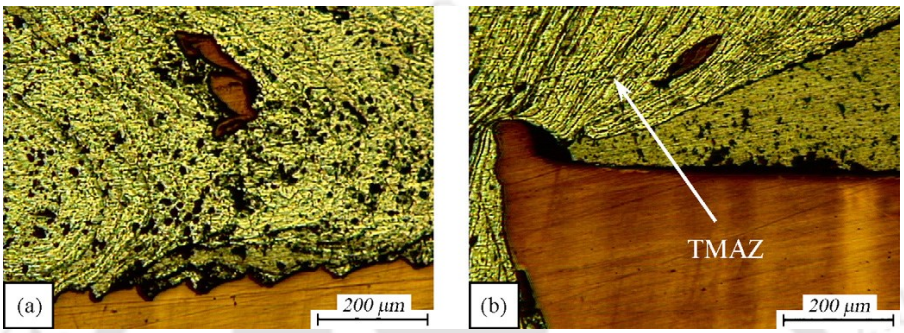

Figure 2.10 Microstructures showing different regions (a) fine equiaxed grains in stir zone of aluminum near Al/Cu interface, (b) elongated aluminum grains in the TMAZ of advancing side [67].

Xue *et al.* [68] joined two dissimilar copper alluminum alloys by two lapping modes and studied microstructural changes achieved in the nugget zones, as shown in Figure 2.11. They noticed that the nugget zone consisted of two distinctly different parts, defined as NZ-1 and NZ-2 for the upper and lower parts respectively.

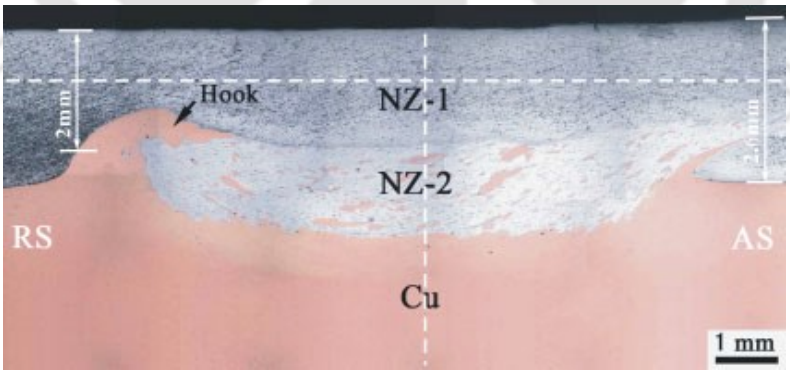

Figure 2.11 Cross-sectional macrograph of FSW lap Al–Cu joint: dash lines represent exact locations of hardness lines [68]

They also conducted the EDS analysis for confirming the material mixing phenomenon and stated that the NZ-1 was pure Al material according to the EDS results from SEM, and the NZ-2 exhibited a composite structure consisting of Al matrix and Cu particles.

Miara & Pietras., [69] joined two dissimilar alluminium castings i.e. EN AC-43200 (AK9) and EN AC-45000 (AK64) by FSW process. They tested the joint quality by visual inspection, mechanical testing, weldment structure analysis and hardness tests. Their results shows good weldability of aluminium casting alloys by the FSW method. They reported that the best mechanical properties of the joints were achieved with 900 rpm of tool rotational speeds. Gachi *et al.* [70] measured residual stresses across the weld by ultrasonic method. Thereafter, the microstructure phenomenon and microhardness measurements were investigated both in parent metal and in the joint. The results show a higher residual stresses in the heat-affected zone. Small compressive residual stresses were detected in the parent metal adjacent to the heat-affected zone and the nugget zone. Lakshminarayanan & Balasubramanian [71] presented the comparative evaluation of microstructural features and mechanical properties of electron beam welded (high energy density fusion welding) and friction stir welded (FSW) (solid-state welding) on 409M grade ferritic stainless steel joints. Welds were tested by using optical microscopy, microhardness testing, transverse tensile, and impact tests were performed. They observed coarser ferrite grains in the base material were changed to finer grains consisting duplex structure of ferrite and martensite due to the rapid cooling rate and high strain induced by severe plastic deformation caused by frictional stirring.

2.3.1 Summary

It is evident that microstructural visualization of different zones and defects occurring by FSW process are very important. By varying the processing parameter and tool geometry, variations in the microstructure can be observed there by the mechanical properties can be achieved. As aluminum behaves in a different manner than most of the other materials, it is possible to get significant plastic strain without recrystallization in this region, and there is a distinct boundary between the recrystallized zone and the deformed zones of the TMAZ. But, while joining the dissimilar metals by this process the absence of this distinct boundary between nugget region and TMAZ. Hence it is very important to study the different zones occurring and the boundaries between these zones in dissimilar FSW process.

2.4 FSW of dissimilar materials

FSW is a successful technology for welding of similar combination of light materials and it has been serving in various industrial applications. Joining of dissimilar materials is another

latest objective in scientific community, in particular high strength alloys to low strength materials. This section focusses on the published literatures of FSW on dissimilar materials. This section has been sub divided into two subtopics i.e. 2.4.1) FSW of dissimilar alluminium alloys. 2.4.2) FSW of aluminium to other alloys.

2.4.1 FSW of dissimilar alluminium alloys

Few studies are reported on FSW of dissimilar alluminium alloys. Topic *et al.* [72] reported on FSW of dissimilar alluminium alloys AA1050 to AA6016 and they concentrated on measuring the weld quality by the micro structural examination and hardness measurements. Tehyo *et al.* [73] worked on joining of dissimilar combination metals i.e. AA6061 to a semisolid metal 356 and reported the tensile and hardness properties of the welds. Chao *et al.* [74] similar publications are reported on mechanical and microstructural study of FSW on dissimilar alluminium alloys i.e. AA2024-t3 and AA7075-t7351. Moreira *et al.* [75] reported some mechanical results on dissimilar alloy combination AA6061-T6 with AA6082-T6. Their work included microstructure examination, micro hardness, tensile and bending tests of all joints and found that in tensile tests the dissimilar joint displayed intermediate properties. They stated that the lowest hardness values were obtained in the AA6082-T6 alloy plate side where rupture occurred, and in the nugget all type of joints present similar values.

Koilraj *et al.* [76] carried out friction stir welding of AA2219-T87 and AA5083-H321 plates and optimized the process parameters using Taguchi L16 orthogonal design of experiments. The parameters taken into consideration are the rotational speed, transverse speed, tool geometry and ratio between tool shoulder diameter (D) and pin diameter (d). The obtained optimum levels of the rotational speed, transverse speed, and D/d ratio were 700 rpm, 15 mm/min and 3 respectively. The cylindrical threaded pin tool profile was found to be the best. Among all the parameters D/d ratio contributes 60% to the overall contribution. Zadpoor *et al.* [77] observed the global and local mechanical properties and FSW weld microstructure for two aluminum alloys, namely, 2024-T3 and 7075-T6. They found a WN with strongly heterogeneous texture varying both through the thickness and around the weld line. Large intermetallic particles were observed in the HAZ and WN. The yield strength and plasticity parameters drastically vary around the weld centreline. The fracture mechanism of FSW joints was found to match the definition of quasi-cleavage fracture.

Hantrais *et al.* [78] prepared dissimilar FSW joint of 20mm thick 2050-T3 Al–Cu–Li alloy/7449-TAF Al–Mg–Zn–Cu alloy. They have used triflute threaded pin tools for welding

these dissimilar material combinations. They concluded that the high thickness decreases the joint efficiency factor with respect to base material. They also found an increase in the required energy per unit length mainly due to the decrease in the advancing speed, and an increase in the in-plane force opposite to the advance. DaSilva *et al.* [79] carried out a stop action technique to study the mechanical properties, microstructural features and material flow of dissimilar AA2024-T3 and AA7075-T6 aluminium alloys. In this technique the FSW machine was switched off immediately stopping both translation and spindle drives. They placed the 7075-T6 Al alloy in the advancing side and other one in retreating side. They concluded that for the 1000 rpm FSW condition the weld efficiency in terms of tensile strength is approximately 96%. A sharp transition from HAZ/TMAZ to SZ was observed in the advancing side. The minimum hardness value of the samples was found in the HAZ at the retreating side. They also observed that the tool pin plays an important role in the material flow and mixing pattern.

2.4.2 FSW of alluminium to other alloys

Saeid *et al*. [67] welded lap joints of 1060 aluminium alloy and commercially pure copper by FSW and the effect of welding speed on interface morphology, microstructure, and joint strength was investigated. Figure 2.12 shows their macrographs of welded sample cross-section wise for various welding speeds.

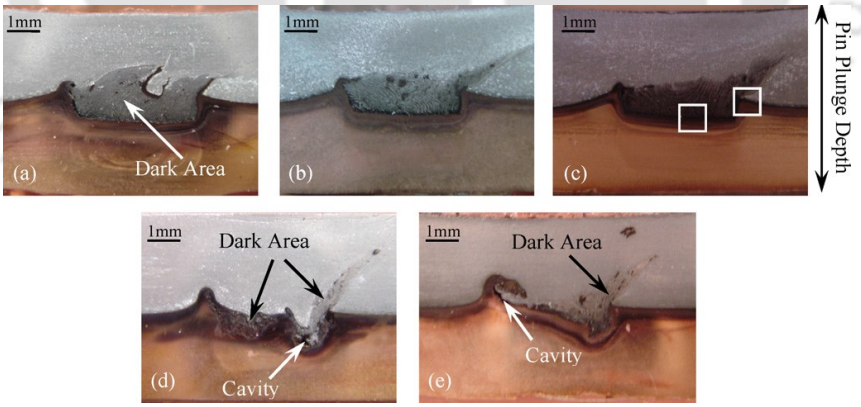

Figure 2.12 Macroscopic overviews of the FSW joint cross sections at constant tool rotational speed of 1180rpm and welding speeds of (a) 30, (b) 60, (c) 95, (d) 118, and (e)190 mm/min [67]

Their experimental results revealed that in the aluminum close to the Al/Cu interface, a dark area was formed. They found that intermetallic compounds of Al_4Cu_9 and Al_2Cu, and some micro-cracks were detected at that dark area and they have concluded that the frequency of such micro cracks decreased with the increasing welding speed.

Galvao *et al*. [80] analysed the influence of the shoulder geometry on the formation and distribution of brittle structures during friction stir welding of aluminium and copper. Their welds were produced using two different FSW tools i.e. i) scrolled and ii) conical shoulder tool. They observed that, different tools with same welding parameters produce different intermetallic pieces in the weld nugget zone. They reported that the scrolled tool helps the formation of a mixing region almost exclusively composed of $CuAl_2$, and the conical tool gave rise to the formation of aluminium, copper, $CuAl_2$ and Cu_9Al_4 mixture, with higher heterogeneity and lower intermetallic components.

Xiawei *et al*. [81] joined pure copper with 1350 aluminum alloy sheet of 3mm thickness by keeping tool pin-off set through FSW process. They obtained sound welds with the parameters of rotational speed of 1000 rpm and a welding speed of 80 mm/min. They also observed a unique and complicated microstructure at nugget zone, and they stated that vortex-like pattern and lamella structure was found. They reported that there is no intermetallic compounds were found in the nugget and the ultimate tensile strength and elongation of the dissimilar welds are 152 MPa and 6.3%, respectively. Wei *et al*. [82] welded a lap joint of two dissimilar high strength to low strength alloys i.e. aluminum 1060 and titanium alloy Ti–6Al–4V by friction stir welding. A cutting pin of rotary burr made of tungsten carbide was employed for this experimental study. They observed the microstructures of the joining interface using scanning electron microscopy and they analysed the joint strength by a tensile shear test. Their microstructures analysis showed that a visible swirl-like mixed region existed at the interface. In that region, the Al metal, Ti metal and the mixed layer formed. They reported that their welded samples got 100% ultimate tensile shear strength of 1060Al.

Xue *et al*. [68] joined a lap-weld of dissimilar material combination of 3mm aluminium and copper sheets using a larger pin of 8 mm in diameter by clamping the plates as shown in Figure 2.13. They observed many Cu particles consisting of pure Cu and intermetallic compound layers were generated at the lower part of the nugget zone, which formed a composite structure with increased hardness. They stated that the lower rotational speed resulted in a decrease in annealing softening in the heat affected zone (HAZ), and a larger diameter pin increased the Al–Cu bonding area.

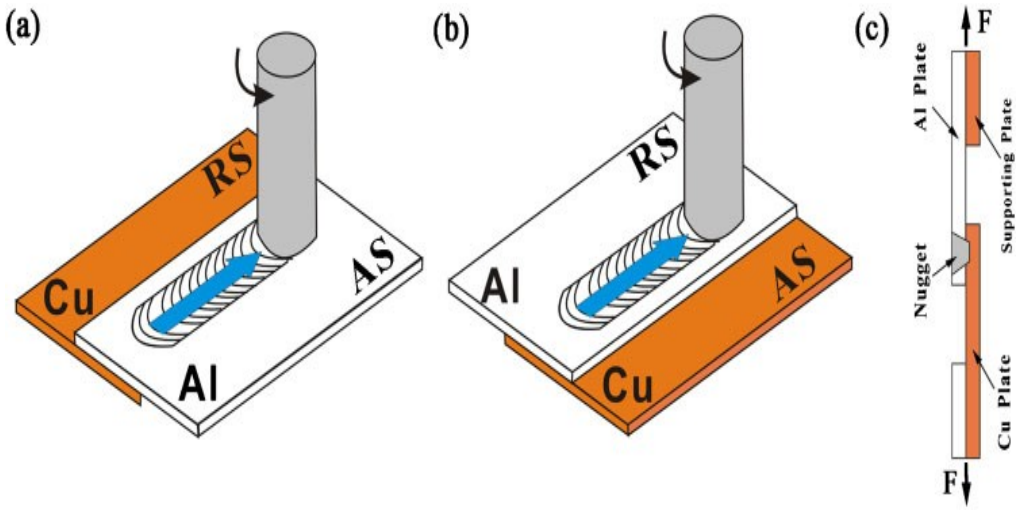

Figure 2.13 Schematic of FSW Al–Cu lap joints when Al plates were fixed on (a) advancing side (AS), (b) retreating side (RS) and (c) tensile shear specimen [68]

Shojaeefard *et al*. [83] joined a lap joint of Al-Mg and CuZn34 alloys by keeping the aluminum alloy sheet on the CuZn34. They characterized the mechanical properties of each welded samples using shear tests, scanning electron microscopy and X-ray diffraction. And an artificial neural network model was also developed to simulate the correlation between the Friction Stir Lap Welding (FSLW) parameters and mechanical properties. They have also performed a sensitivity analysis which is to investigate the effect of each input parameter on the output in terms of magnitude and direction. Shtrikman *et al*. [84] 2004 studied the feasibility of producing high-quality welded joints in 1201 AMg6 and 1201 +AMg6 alloys using friction welding method. Okamura & Aota [85] checked the possibility of joining a variety of dissimilar materials combinations by FSW process. They welded Al to magnesium, Al to copper, Al-steel and stated that the tool should be offsetted more towards the alluminium side for getting proper welds.

Studies on material flow paths were studied by few researchers using some techniques like inserting some copper powders/steel balls in the faying surfaces of the two metal plates to be joined [86 - 88]. In a dissimilar friction stir weld, the weaker component dictates the performance of the joint, where failure happens in the region of the greatest strength reduction related to annealing phenomena [89]. Chen & Lin [90] studied on FSW of AA6061 aluminum alloy and SS400 low carbon steel; they stated that the best quality of dissimilar joints is produced by the combination of the tool rotation speed 550 rpm and transverse speed 0.9 mm/sec. The impact value of the dissimilar metals joints is about 90% of base material AA6061 aluminum alloy. Dissimilar alloys welding i.e., for Cu-Al were reported by few authors [91-93]. Few authors reported that the welding of this combination Cu-Al is very

difficult. The reason for the difficulty in welding this type of combination is formation of intermetallic component phases [94, 95] which is harder in nature.

Movahedi *et al.* [96] prepared friction stir lap welded joints of Al-5083 and St-12 alloy sheets at different travel (7– 23 cm/min) and rotation (750–1125 rev/min) speeds of the welding tool. They observed that the weld zone defects reduced with decreasing tool travel speed from 23 to 7 cm/min. The joint strength improved by decreasing the travel and increasing the tool rpm. The reaction layer formation increases the strength of the joint interface, which shifts the fracture location from the interface to the swirl layered structure. Barlas & Ozsarac [97] investigated the effects of FSW) parameters (tool rotation speed, tool tilt angle, and tool rotation direction) on the macrostructure, microstructure and mechanical properties of AlMg3 aluminum Alloy (Al 5754) joints. They obtained the best results at a tool rpm of 1100, tool tilt angle of 2º when the tool was rotated in counter clockwise direction. This joint showed the tensile strength of 86% as compared with the base metal. Four zones such as unaffected base metal, heat-affected zone having coarse grains, thermo-mechanically affected zone consisting of plastically deformed and elongated grains, and recrystallized weld nugget zone were found out. Their weld nugget zones showed the highest hardness value of approximately 82 HV.

Many efforts were reported in FSW of similar metals and dissimilar aluminum alloys. But there is much requirement to advance this process in dissimilar alloys i.e Al-Cu, Al-Mg, Al-Fe etc. The applications of this type of dissimilar metals joints were reported by Kahl & Osikowicz [98].

2.4.3 Summary

Literature portrays that work was explored on several features of tool geometries, microstructural studies, simulation studies and process optimization in friction stir welding of similar metals. Many researchers have reported on FSW of dissimilar aluminum alloys using various tool geometries [142-146] but joining alluminium with other metals such as Al-Cu or Al-Steel is of much important in engineering and design aspect. This combination of welds are difficult to produce as it gives some defects like formation of brittle intermetallic compounds, thermal cracks, worm hole defect, etc. Some other researchers also contributed on welding alluminium to copper and steel [68, 92, 99]. However, using FSW process in this type of combination is not fully explored and still there are some issues to be clarified. Huge

variation in the melting point temperatures and thermal conductivity of Al/Cu is one of the reasons for its poor weld quality. So it is very important to study the heat generation and temperature distribution for friction stir welding of dissimilar materials with experimental validations.

2.5 Numerical and analytical study

The analytical study and numerical simulation is important method for the understanding the mechanisms of FSW process. It allows observing insights of the welding characteristics both qualitative and quantitative without performing costly experiments. The numerical methods (in particular FEM) are more flexible in treating complex geometries and boundary conditions, against their analytical counterparts. The FSW simulation typically involves studies of the transient temperature and its dependence on the rotation and advancing speed, residual stresses in the work-piece, etc. This simulation is a complex task since it involves the interaction of thermal, mechanical and metallurgical phenomena. A brief description on the contributions of numerical and analytical methods on FSW has been presented here.

Assidi *et al.* [99] used Arbitrary Lagrangian Eulerian (ALE), formulation in a 3D numerical simulation in FORGE3 F.E software using Notron's and coulomb's model to accurately compute the contact and frictional surface between the plate and the tool, moreover, temperature and forces were determined experimentally which is highly sensitive to small variation of friction and achieved best calibration with coulomb's model using μ is 0.3. Kim *et al.* [100] utilized FVM code in STAR-CCM + (based on Eulerian formulation) to study the temperature histories at different welding parameters of AA5083-H18 taking full sticking condition and found satisfactory results. Feulvarch *et al.* [101] proposed a simple and robust moving mesh technique for finite element simulation of friction stir welding in which the material flow and heat transfer analysis were achieved with all kinds of tool pin geometry.

Song & Kovacevic [102] introduced a moving coordinate in a transient 3D heat transfer analysis with the help of a mathematical model and suitable boundary condition and studied the thermal history of Al 6061- T6 friction stir weld. Chen & Kovacevic [103] analyzed a 3-D model for different process parameter of friction stir welding of Aluminium Alloy 6061-T6 in a commercial Finite Element package ANSYS considering sliding condition only.

Buffa *et al.* [104] predicted the residual stresses distribution with a 3D elasto plastic model Finite element model in DEFORM-3D™. AA6060-T4 aluminum alloy was used to perform a

butt joint of two 300X100 mm^2 sheets, 4mm in thickness with a conical tool at 500 rpm and 325 mm/min rotational and advancing velocity respectively. Trimble *et al,* [105] computed the forces required for a smooth and threaded pin tool for AA2024-T3 plates in DEFORM-3D™ software using a single block with tetrahedral element for three stages plunge, dwell and translation. They compared the results with the experiment and concluded that the FEM results predicted slightly larger forces and lower temperatures.

Chiumenti *et al.* [106] computed the friction stir welding process for a coupled thermo-mechanical analysis with ALE (Arbitrary Lagrangian Eulerian) adaptive mesh technique using a triflute pin design. They applied momentum and mass conservation equations for mechanical problems and for thermal analysis energy balance equations were required and for a rigid visco-elastic behavior strain rate effect were considered. Figure 2.14(a) (b) (c) shows the experimental and FE numerical data for Force, Torque and welding force which was reported by Chiumenti *et al.* [106].

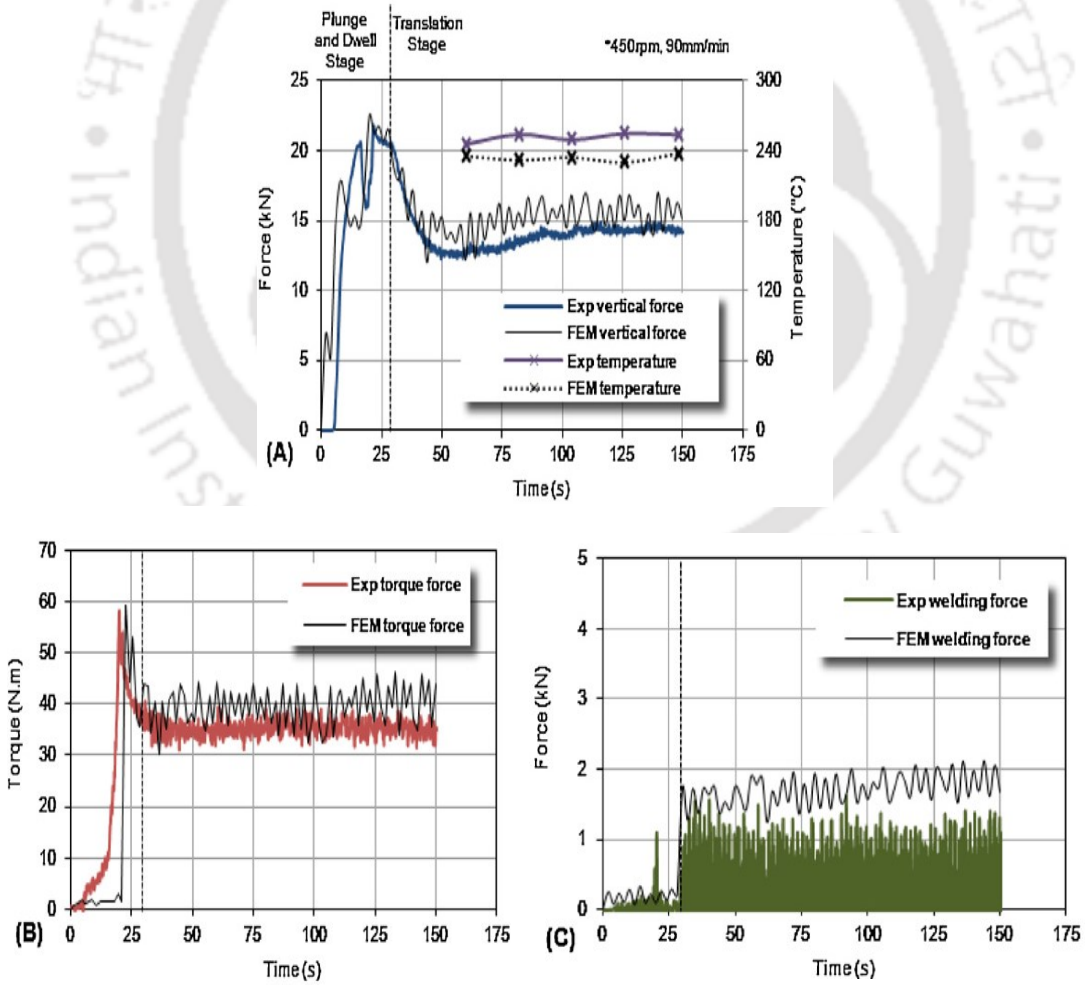

Figure 2.14 Comparison of experimental and FEM values [106]: (A) vertical force and temperature, (B) torque and (C) welding force

Dialami *et al.* [107] numerically simulated a thermo-mechanically coupled model of Friction stir welding of AL6061 workpiece with same backing plate and used a steel tool for generating heat during the process. They divided the mesh into three main parts i.e. pin, HAZ and plate with Lagrangian, ALE and Eularian mesh generation respectively with the help of connecting nodes. To find out the material flow experimentally Marker Insert Technique (MIT) was used and numerically Particle Tracer (PT) method was used. 8mm and 6.35mm are the pin dimensions with 25.4mm pin diameter while welding speed and rotational speeds were taken 3.39mm/s and 650rpm respectively. Figure 2.15 represents the experimental and numerical temperature distribution curve and the result of MIT.

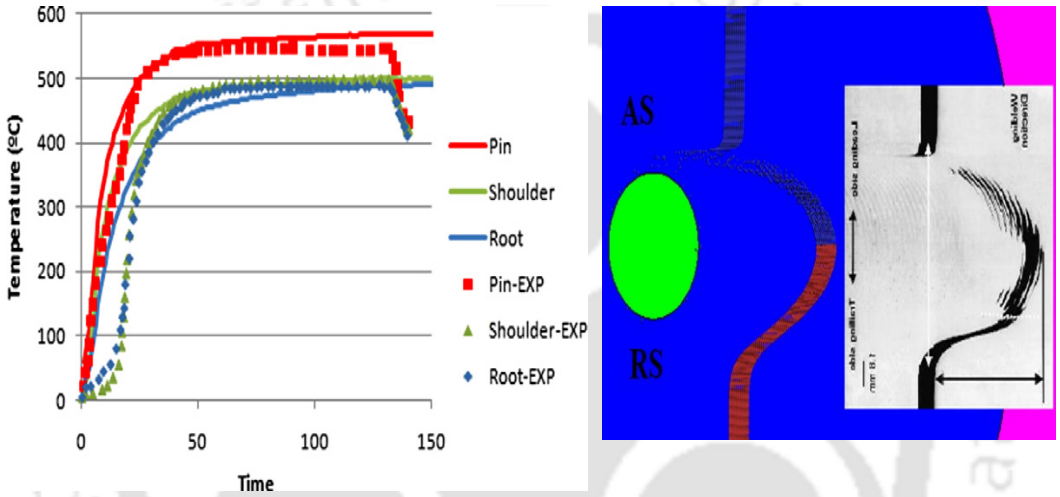

Figure 2.15 Right side showing temperature evolution compared with experiment on pin, shoulder and root on the left Tracer visualization, simulation (left) experiment (right)[107]

An attempt was made by Gemme *et al.* [108] to model and study the dwell phase of friction stir welding and analyzed the effect of material behavior, heat transfer and the contact condition at the tool/workpiece interface as shown in Figure 2.16. For the analysis the material was considered as visco-plastic and Norton Hoff law was implemented. The finite element model used in this work was developed using the FORGE3® code. The experiment was performed on 7075-T6 aluminium plate of 2 mm thick with pin diameter, shoulder diameter and pin length 3.15 mm, 9.52 mm and 1.26 mm respectively at the rpm of 600, 900 and 1200. Vilaca *et al.* [109] used *i*STIR* model to analyze the friction stir welding of similar and dissimilar materials. They determine the thermal histories in 2D and 3D model and studied the heat flow by conduction mechanism inside the plate domain. The calculated values were then verified with the experimental ones.

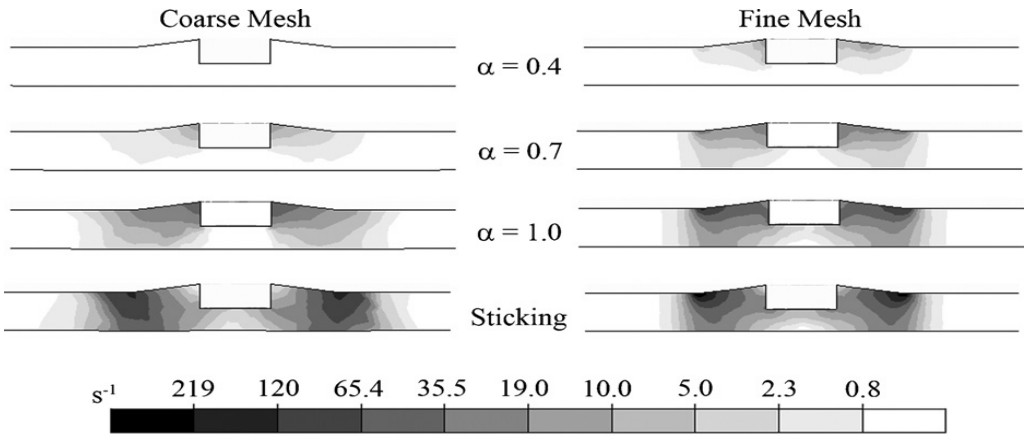

Figure 2.16 Strain rate fields for different friction coefficient [108]

Zhang *et al.* [110] performed 3D modeling in conventional Finite Element Package ABAQUS in order to study the material flow around the tool by varying the axial load 10-100 MPa. As shown in Figure 2.17 the welding zone is divided into three parts defined as the flow arm zone (1) for the torsion velocity field, the stirring zone (2) for the "vortex like" velocity field, and the rest of the sheet (3). The analysis was performed for 100, 400, 800 mm/min translational speed and results obtained were verified with the experimental data. The analysis was also performed by changing the translational speed from 2 to 10 mm/s and rotational speed from 390 to 690 rpm. The material used was Al 6061-T6 plate 100x30x3mm^3 with temperature dependent material properties as shown in Table 2.1. Figure2.19 represents the material properties of (a) Al 6061-T6 used in their model [118]. The tool shoulder radius was 7.5mm while the pin radius was 3mm and the ALE adaptive mesh generation technique is being used in the model. The properties considered were nonlinear based on temperature.

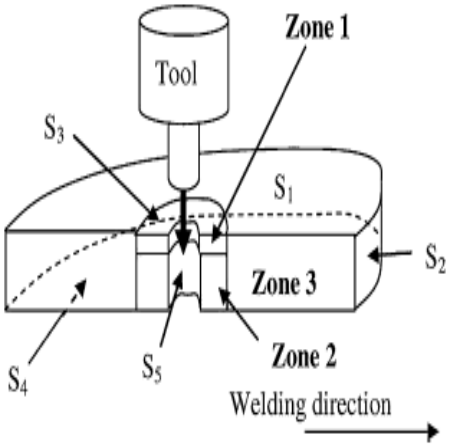

Figure 2.17 Partition of the welding zone for the definition of the elementary velocity fields and boundaries of the model [110]

Table 2.1 Temperature-dependent material properties for Al 6061-T6 [110]

T(◦C)	E(GPa)	σu(MPa)	ν Poisons ratio
25	66.94	278.12	0.33
100	63.21	260.68	0.334
148.89	61.32	251.24	0.335
204.44	56.8	221.01	0.336
260	51.15	152.26	0.338
315.56	47.17	73.87	0.36
371.11	43.51	36.84	0.4
426.67	28.77	21.58	0.41
482.22	20.2	10.49	0.42

Jacquin *et al.* [111] worked on a 3D thermo-mechanical model based on the model proposed by Heurtier *et al*. [112] based on Eularian approach. In that model partial sliding and partial sticking was considered. In thermal or mechanical modeling the boundary condition is very important for the model. Soundararajan *et al.* [113] modeled a 3D model in ANSYS package with adaptive boundary condition; earlier proposed model used constant boundary condition in their model. They studied the thermal history at 344 rpm and 133 mm/min speed. The material used was 6061-T6 Al alloy plates with a dimension of 200x50x6.4 mm^3. The nonlinear temperature dependent thermal material properties were used as shown in Figure 2.18. Figure 2.19 shows the comparison of Time vs Temperature curves for experimental and numerical model.

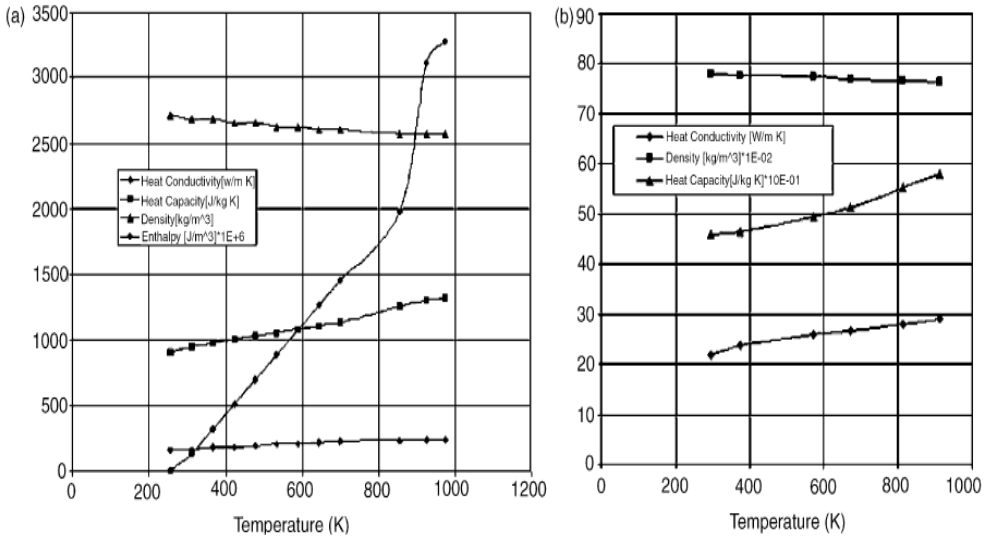

Figure 2.18 Material properties of (a) Al 6061-T6 used in model [117]

and (b) CPM 1V tool steel used in model [118]

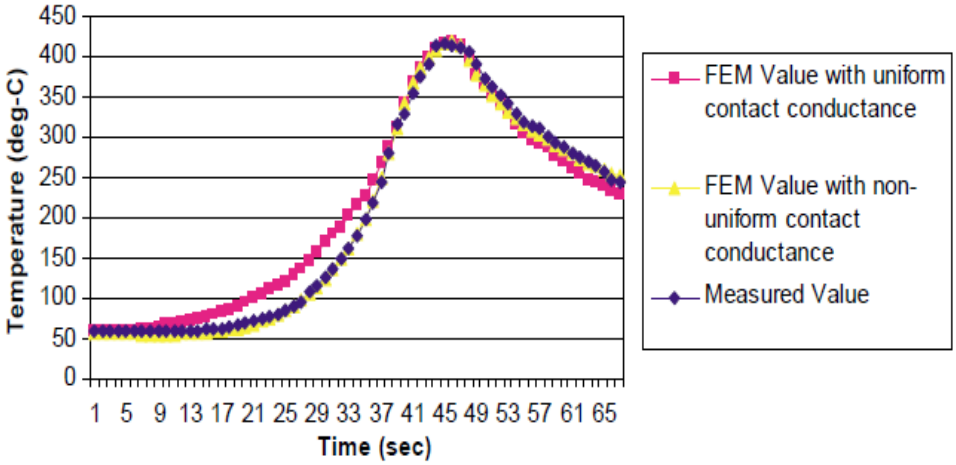

Figure 2.19 Comparison of the modeled and the measured temperature history for workpiece. [113]

Geiger *et al.* [114] used a complete new Friction stir Knead welding technique with a pin less tool for the welding of 1 mm Aluminum and steel plates. They simulated their model in ABACUS and performed the experiment. Hamilton *et al.* [115] made another attempt for a thermal model based on the Jonson-Cook plasticity model. In this model they incorporated the heat generation due to plastic deformation of the material. According to them at lower energy welding the heat generation due to plastic deformation dominates. The model was performed for the tool rotational speeds of 225, 250, 300 and 400 rpm. Vilaca *et al.* [116] used an inverse engineering approach by using the analytical thermal code iSTIR to establish the correlation between the parameter of friction stir welding and the properties of the resulting joints.

Hamilton *et al.,* [119] used a new energy based slip factor in thermal modeling of friction stir welding. T_{total} is the total torque (J) and average power was calculated as shown in equation (2.1).

$$P_{avg} = T_{total}\omega \qquad 2.1$$

where 'ω' is the rotational velocity of FSW tool.

Energy per unit length is calculated by dividing P_{avg} by the welding velocity which is shown in equation (2.2)

$$E_l = \frac{P_{avg}}{v_w} = T_{total}\frac{\omega}{v_w} \qquad 2.2$$

Therefore slip factor they have calculated was shown in equation (2.3)

$$\delta_E = exp\left(-\frac{(E_l)_{eff}}{(E_l)_{max}}\right) \quad 2.3$$

On the basis of this slip factor they modeled a thermal model which was able to predict the maximum temperature for a wide range of energy models.

Aval *et al.* [120] studied the dissimilar alloys of aluminum i.e. AA6061-T6 and AA5086-O. They first used a 3D finite element model in ABAQUS to predict the temperature profile and followed by the experiment. They studied the mechanical properties and the microstructure in the affected zone. Some of the results are shown below. Zhu & Chao [121] studied the variations of transient temperature and residual stresses in friction stir welding of 304L stainless steel plates with the help of three-dimensional nonlinear thermal and thermo-mechanical simulations are performed for the FSW process using the finite element analysis code—WELDSIM. They considered two different rotational speeds i.e. 300 and 500 rpm and found temperature profile at various distance from the weld line.

Heurtier *et al.* [122] presented a three-dimensional thermo-mechanical model of Friction Stir Welding based on velocity fields classically used in fluid mechanics. The velocity potential function was taken as shown in equation (2.4).

$$\varphi = V\left(x + \frac{a^2 x}{x^2+y^2}\right) \quad (2.4)$$

The material used in this study was a 10mm thick AA2024 T351 plate. They varied the velocity ratio R (rad/mm) i.e. tool rotation velocity (rad/min) to translational velocity (mm/min) and predicted the temperature and micro hardness profile. Mandal and Williamson [123] utilized the thermomechanical hot channel approach and modeled the three moving point heat sources where heat input from were taken from laser, plasma and tool. The material used for welding was taken as steel and the temperature achieved by the tool was 1100º C. Williamson & Abdel-Salam [124] presented the significance of the third region present in friction stir welding i.e. stir induced plastic flow region (SIPFR) and analyzed the heat generation due to the plastic deformation in this region. Buffa *et al.* [125] studied the continuous dynamic recrystallization phenomena and predicted the grain size in the weld region. They used the two analytical approaches for the FE modeling in package DEFORM-3D^{TM}. The first model was implemented by the authors and used for AA6082-T6 alloys [126]

$$D_{CDRX} = C_1 \varepsilon^k \dot{\varepsilon}^j D_0^h exp\left(-\frac{Q}{RT}\right) \quad (2.5)$$

Where D_{CDRX} is the average grain size due to the continuous dynamic recrystallization phenomena, ε the equivalent plastic strain, $\dot{\varepsilon}$ the strain rate, D_0 the initial grain size, Q the material continuous recrystallization activation energy, R the gas constant, T the absolute temperature and C_1, k, j and h are the material constants. The second model takes into account the Zener-Hollomon parameter and a few material constants [127]

$$D_{CDRX} = \frac{1}{a+b\ln(Z)} \tag{2.6}$$

where a = 3.63, b =−1.62, $Z = \dot{\varepsilon}\, Q/RT$, and Q the gas constant and finally compared with the experimental results.

Zhang & Zhang [128] studied the effect of process parameters in Friction Stir Welding and they found that the maximum temperature can be increased by increasing the rotating speed, which require increase in power input but with increase in rotating speed the welding flash also increases. They also observed that the material on retreating side did not enter into advancing side but the advancing side material entered into the retreating side and the material on top surface pile up at the border of the wake. They observed that in order to increase the stirring effect, the rotational speed should be increased and the welding speed should be decreased. They also found that the longitudinal residual stress is much higher than the transverse stresses and the simultaneous increase in rotating and translating speed leads to increase of residual stress.

Hirasawa *et al.* [129] analyzed the effect of tool geometry on the plastic flow and material mixing during friction stir spot welding using the particle method approach. The pin geometries evaluated include tapered pin, inverse tapered pin, triangular pin, convex shoulder, and concave shoulder which is shown in Figure 2.20.

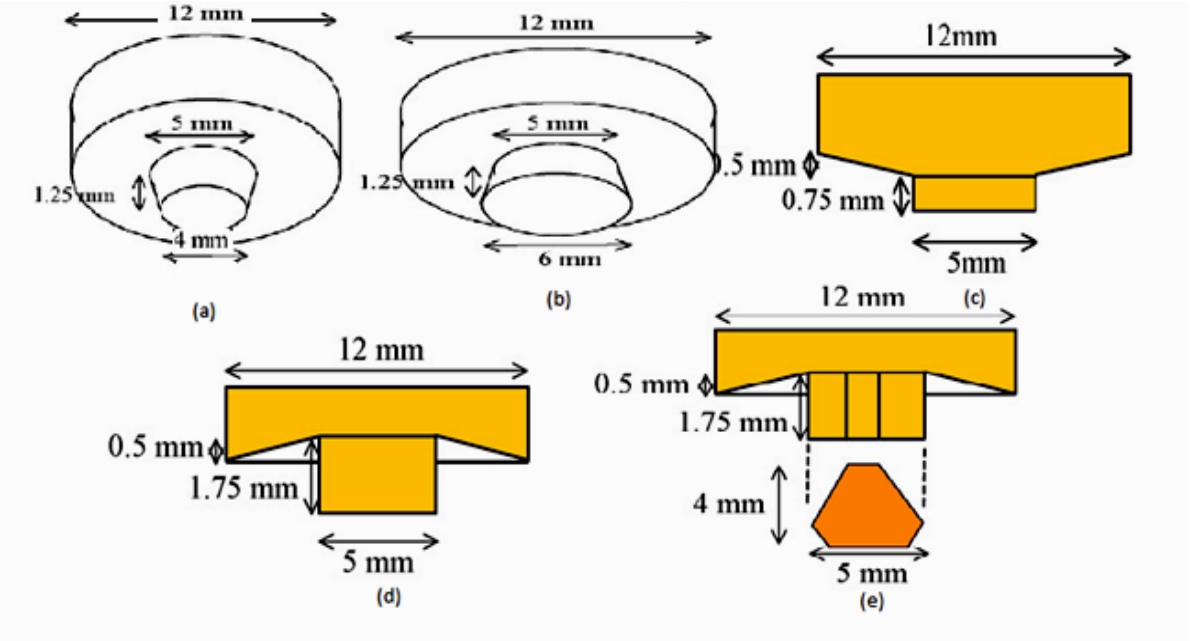

Figure 2.20 Tool geometries are shown above (a) Tapered pin, (b) Inverse tapered pin, (c) Convex shoulder, (d) Concave shoulder, (e) triangular pin with concave shoulder [129]

After investigating the above mentioned geometries, they concluded triangular pin with a concave shoulder is the preferred tool geometry for friction stir spot welding.

Hilgert *et al.* [130] implemented three thermal 3D models for bobbin tool friction stir welding in Comsol and Matlab which involve thermal pseudo-mechanical heat sources. They implemented the arbitrary lagrangian and eularian approach and finally validated with the experimental results. They described the method which needs to be implemented and the essential boundary conditions. Hattel *et al.* [131] made a first attempt to couple an in-situ thermo-mechanical weld simulation for the friction stir welding, with a post-welding micro-mechanics based damage model for structural analysis. They used a step wise approach in this model and first model a thermo-mechanical model to predict the thermal stresses and then move to the damage model for post welding failure analysis then they coupled those two models and found the results.

Zhang Hong *et al.* [132] used a temperature-dependent elastic visco-plastic model for the simulation of friction stir welding process. The non-elastic response of the rate-dependent material in the large deformation problems was calculated by using the closest point algorithm. The generalization of the classic von-Mises criterion for the rate dependent material can be expressed as [133] shown in equation 2.7.

$$f = \bar{\sigma} - \sigma_0(T) - \eta(\bar{\varepsilon}^p)^n(\dot{\bar{\varepsilon}}^p)^m = 0 \tag{2.7}$$

where σ_o is the initial yield stress, *m* is the viscosity exponent, *n* is the strain hardening exponent, and η is the viscosity coefficient. They analyzed the material flow and calculated the circumferential, radial and radial stress distribution around the pin with different viscosity coefficient.

Chuan-song *et al.* [134] studied the plastic material flow by embedding the copper sheets as marker material in the weld path 2024 aluminium alloy plates. A three-dimensional model was developed to conduct the numerical simulation of the temperature profile and plastic material flow in friction stir welding. Mendez *et al.* [135] coupled the plastic deformation and the heat transfer and derived the expressions for thickness of shear layer, maximum temperature in the process, volumetric heat generation. They also derived the expression for torque, maximum shear rate, heat input. The expressions obtained were found consistent with the experimental results. The formulation obtained was modeled inspired by Prandtl's boundary layer theory.

Schmidt & Hattel [136] worked on thermal modeling of friction stir welding with temperature dependent yield stress. The heat generation was calculated analytically with the sets of equations where the material phases taken into consideration and obtained the temperature profile of the friction stir welding. Boldsaikhan *et al.* [137] utilized a non-destructive method to find out the quality of weld and to detect the wormhole defects. They analyzed the feedback forces from the frequency spectra and proposed an algorithm and validated it with the experiment.

Lawrjaniec *et al.* [138] worked on mechanical characteristics of the various macrographic zones were empirically determined and they also conducted thermo-mechanical simulations without factoring in the tool or the material flow. Deloison *et al.* [139] reported the results of numerical modelling of two welding processes i.e. Friction Stir (FSW) and Laser Beam Welding (LBW). Figure 2.21 indicates temperature contour of their numerical model. For FSW, they predicted the residual stresses using a simplified approach. For LBW, they developed a methodology to predict distortions and residual stresses of welded fuselage panels.

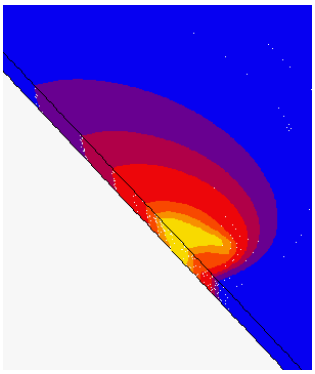

Figure 2.21 Computed temperature field [139]

Arora *et al.* [140] proposed an approximate analytical technique for the calculation of three-dimensional material flow during FSW by considering the motion of an incompressible fluid induced by a solid rotating disk. They tested the accuracy of the calculations for the three alloys. They noticed and proposed a relation between the hardness of the thermomechanically affected zone and the chemical composition of the aluminum alloy. Sinclair *et al.* [141] they checked the feasibility and the final weld quality of FSW by introducing the additional heating source in front of FSW tool. For this experimentation they used a Trivex tool to weld aluminum alloy (AA 6061). They heated the workpiece unto initial material temperatures up to 300C. Macrograph cross-sections of the welds revealed a slight increase in material flow with increasing temperatures. They reported that the preheating results up to reduction in the axial force of 43%.

2.5.1 Summary

Few numerical studies have also reported on material mixing of FSW on similar alluminium alloys. Above mentioned investigators indicates that the heat generation and the resulting thermal history of FSW process greatly influenced by tool rotational speed and very less extent by the tool traverse speed. In the published literature, there is less information available on the effect of tool geometry including tool pin on thermal profile, and the effect of tool plunging force on thermal profile has not clearly reported.

Therefore, it is very necessary to conduct numerical study on the influence of tool geometries particularly shoulder size and pin size effects on thermal history for both similar and dissimilar materials. And the effect of tool plunging force on thermal history of FSW is also essential for understanding of this process for its further development.

Chapter 3
Methodology

3.1 Introduction

This chapter deals with the complete information of detailed procedures followed during both experimental investigation and numerical analysis. It also elaborates sequentially the procedures applied during pre and post-welding operations. It contains three important sub-sections i.e. 3.2 Transient thermal analysis, 3.3 Experimental setup and procedures and 3.4 Mechanical and microstructural properties study.

3.2 Transient thermal analysis

In FSW, friction is the major source for heat generation amongst tool and the workpiece; this is because of the interaction of rotating tool to workpiece and due to traversing action of the tool along the butted weld line. It is very essential to understand the process of heat generation in this technique for achieving the better results. The thermal modelling of FSW helps to get a clear idea of the process and its parameters for achieving the best welds. A complete description about heat generation in FSW has been given below in four sub sections i.e. 3.2.1) Heat generation at cylindrical tool shoulder with cylindrical tool pin, 3.2.2) Heat generation at cylindrical tool shoulder with conical tool pin. 3.2.3) Heat source model and 3.2.4) Three dimensional finite element model.

3.2.1 Heat generation at cylindrical tool shoulder and cylindrical tool pin

A cylindrical tool with flat shoulder surface whose radius is R, radius of its probe is r_p and height of the probe is *l* as shown in Figure. 3.1.

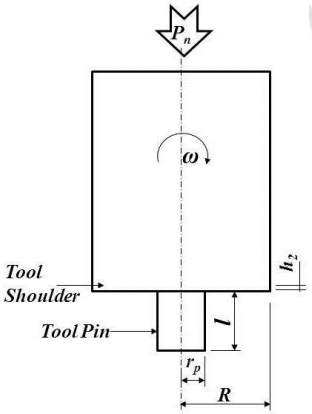

Figure 3.1 Flat cylindrical shoulder and cylindrical probe

It is considered that the P_n is the tool plunging force with an angular speed of ω, and tool shoulder impression on workpiece of h_2 as a result of this pressure the entire heat generation was calculated.

3.2.1.1 Heat generation at cylindrical shoulder

There are two mechanisms of heat generations have been observed in tool shoulder surface i.e.

a) Heat generation due to vertical pressure

b) Heat generation due to traveling of shoulder

a) Heat generation due to vertical pressure

Considered an elemental ring of thickness 'δr' and it is 'r' distance away from the center of tool shoulder surface as shown in Figure 3.2. Therefore the area of the elemental ring can be represented as,

$$A = 2\pi r \delta r \qquad 3.1$$

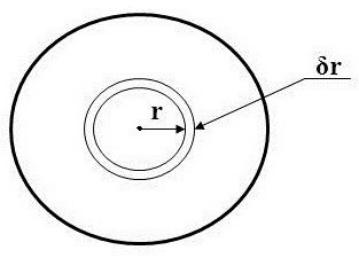

Figure 3.2 Tool shoulder small elementary area

So, the normal force acting due to this elemental ring is shown in equation (3.2),

$$\delta N = P.2\pi \mathrm{r}\delta \mathrm{r} \qquad 3.2$$

Let 'μ' is the co-efficient of friction between tool-workpiece interfaces, then the frictional force on this elemental ring can be represented as shown in equation (3.3)

$$\delta F = 2\mu P\pi \mathrm{r}\delta \mathrm{r} \qquad 3.3$$

Therefore, the heat generation due to elemental ring is shown in equation (3.4),

$$\delta Q_{s1} = 2\mu P\pi \mathrm{r}\delta \mathrm{r}.\omega \mathrm{r} \qquad 3.4$$

Now, integrating both sides of equation (3.4) the heat generation due to vertical pressure in tool shoulder has obtained, which is shown in equation (3.5), i.e.

$$Q_{S1} = \frac{2}{3}\pi\mu\omega P\ (R^3 - r_p^3) \qquad 3.5$$

b) Heat generation due to travelling of tool shoulder

Considered that tool shoulder is moving with a velocity of v, and the yield strength of the workpiece at 80% of its melting temperature is S_{ys}^{*}. Considered the tool shoulders impression in welding area is 'h_2' as shown in Figure 3.3. Only half of the curved surface area is responsible for heat generation during the travelling of probe.

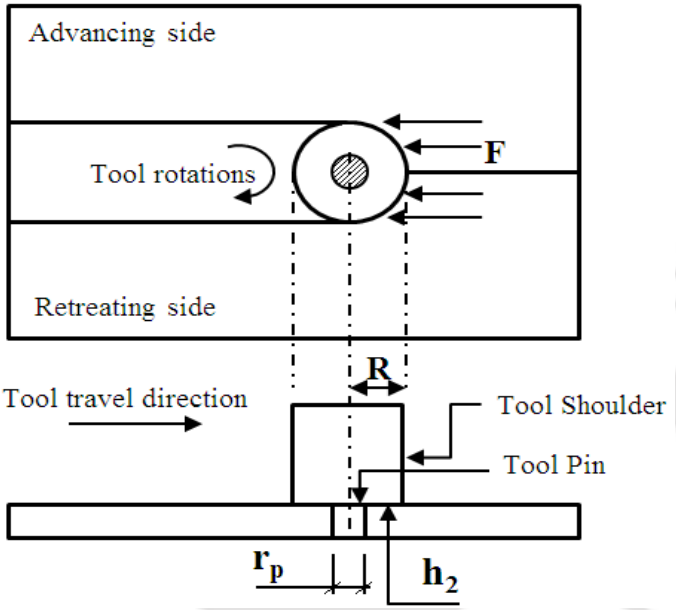

Figure 3.3 Force acting on tool shoulder due to travelling of FSW tool

The contact area of the tool shoulder to the workpiece as shown in equation (3.6)

$$A = \pi R h_2 \tag{3.6}$$

The frictional force for heat generation can be signified as shown in equation (3.7),

$$F = \mu\pi S_{ys}^{*} R h_2 \tag{3.7}$$

So, the heat generation in shoulder due to travelling of tool shoulder is shown in equation (3.8),

$$Q_{s2} = \mu\pi S_{ys}^{*} R h_2 v \tag{3.8}$$

Therefore, the total heat generation in shoulder of FSW tool is shown in equation (3.9),

$$Q_s = Q_{s1} + Q_{s2}$$

$$Q_s = \frac{2}{3}\pi\mu\omega P\left(R^3 - r_p^3\right) + \mu\pi S_{ys}^{*} R h_2 v \tag{3.9}$$

3.2.1.2 Heat generation in cylindrical probe

There are two important parts of probe which is responsible for heat generation i.e. a) Probe tip surface and b) Probe side surface. The details of heat generation both on probe tip and side surface are described below.

a) Heat generation due to vertical pressure at probe tip

Heat generation due to vertical pressure at probe tip is shown in equation (3.10) which is similar to equation (3.5),

$$Q_1 = \frac{2}{3}\pi\mu\omega P r_p^3 \qquad 3.10$$

b) Heat generation due to the rotational movement of the probe

Let τ be the shear strength of the workpiece and τ^* be the shear strength of the material at 80% of its melting point temperature. Therefore force acting on the probe on its surface is shown in equation (3.11),

$$F_p = \mu\tau^*.2\pi r_p l \qquad 3.11$$

So the heat generation through the curved surface area is shown in equation (3.12),

$$Q_2 = 2\mu\pi\tau^*\omega r_p^2 l \qquad 3.12$$

c) Heat generations due to travelling of the probe

Considered that probe is moving with a velocity of v, and the yield strength of the workpiece at 80% of its melting temperature is S_{ys}^*. Figure 3.4 represents the notations considered.

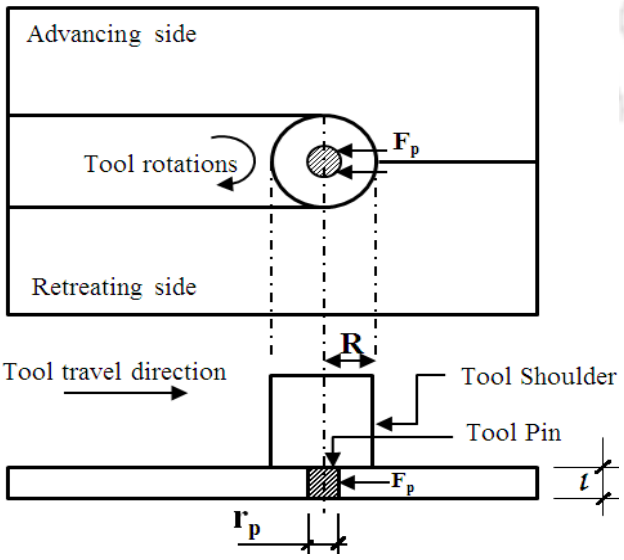

Figure 3.4 Force acting on tool probe due to travelling of FSW tool

Only half of the curved surface area is responsible for heat generation during the travelling of probe.

i.e. $$A = \pi r_p l \quad (3.13)$$

The force acting on the probe due to travelling on workpiece is shown in equation (3.14),

$$F_p = \mu S_{ys}^* \pi r_p l \quad (3.14)$$

Therefore heat generation due to travelling of the probe is shown in equation (3.15),

$$Q_3 = \mu S_{ys}^* \pi r_p l v \quad (3.15)$$

The total heat generation at the probe can be calculated by adding equations (3.10), (3.12) and (3.15).

i.e. $$Q_p = Q_1 + Q_2 + Q_3$$

$$Q_p = \frac{2}{3}\pi\mu\omega P r_p^3 + 2\mu\pi\tau^*\omega r_p^2 l + \mu S_{ys}^* \pi r_p l v \quad (3.16)$$

Therefore total heat generation in flat cylindrical shoulder with cylindrical probe is obtained by adding equations (3.9) and (3.16) which is shown in equation (3.17)

i.e. $$Q = Q_s + Q_p$$

$$Q = \frac{2}{3}\pi\mu\omega P\left(R^3 - r_p^3\right) + \mu\pi S_{ys}^* R h_1 v + \frac{2}{3}\pi\mu\omega P r_p^3 + 2\mu\pi\tau^*\omega r_p^2 l + \mu S_{ys}^* \pi r_p l v \quad (3.17)$$

3.2.2 Heat generation at cylindrical tool shoulder with conical tool pin

A cylindrical tool with flat shoulder surface whose radius is R, radius of its conical probe at base is r_{pb} at probe tip is r_{pt} and height of the probe is h as shown in Figure 3.5. It is considered that the P_n is the tool plunging force with an angular speed of ω, as a result of this pressure the entire heat generation was calculated.

As explained earlier (equation 3.9) the total heat generation in a flat cylindrical shoulder is given in equation (3.18)

$$Q_s = \frac{2}{3}\pi\mu\omega P\left(R^3 - r_{Pb}{}^3\right) + \mu\pi S_{ys}^* R h_1 V \quad (3.18)$$

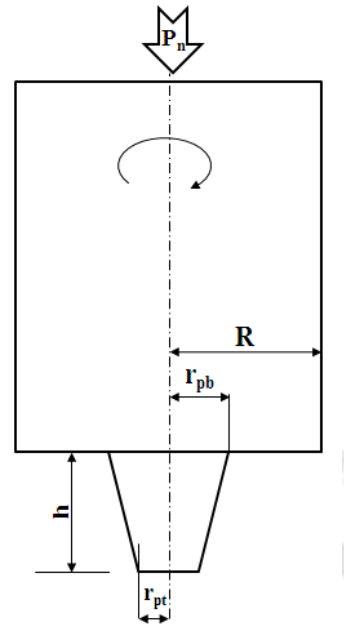

Fig 3.5 Schematic diagram of flat cylindrical shoulder and conical probe

There are two important parts of Probe which is responsible for heat generation as explained earlier (section 3.2.1.1) i.e.

a) At probe tip surface and
b) At probe side surface

The details of heat generation both on probe tip and side surface are described below.

a) Heat generation due to probe tip

Similar to equation (3.10),

$$Q_1 = \frac{2}{3}\pi\mu\omega P\,(r_{Pt}{}^3) \qquad 3.19$$

b) Heat generation due to rotational movement of the probe

Taking elemental area (as shown in Figure 3.6 and Figure 3.7) on the curved surface area of the probe at a distance "r" from the centre and thickness is δr and slant thickness δs.

$$\cos\theta = \frac{(r_{pb}-r_{pt})}{s} \qquad 3.20$$

Where'*s*' is the slant length, taking an elemental area of heat generation,

$$\delta A = 2\pi r \delta s \qquad 3.21$$

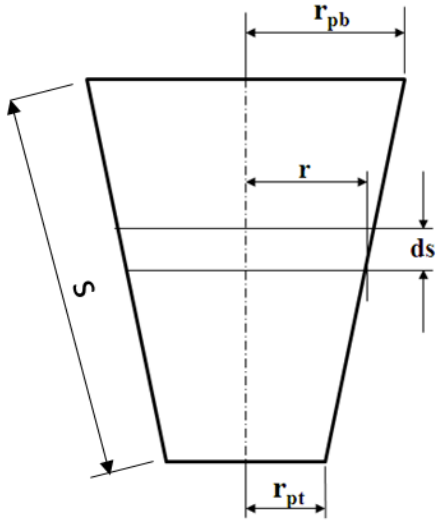

Figure 3.6 Probe small elemental area

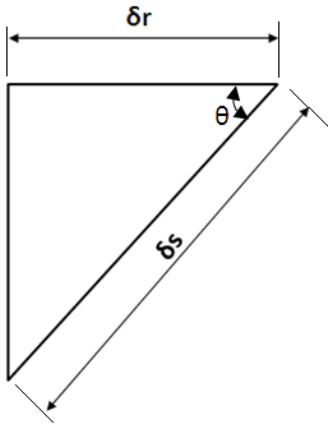

Figure 3.7 Small elemental triangle

Let τ^* be the shear strength of the workpiece at 80% of its melting point temperature.

Frictional heat generation,

$$\delta F_p = \mu \tau^* . 2\pi r \delta s \qquad 3.22$$

Heat generation,

$$\delta Q_2 = 2\mu\omega\tau^*\pi r^2 \delta s \qquad 3.23$$

From Figure 3.5,

$$\cos\theta = \frac{\delta r}{\delta s}$$

$$\delta s = \frac{\delta r}{\cos\theta} \qquad 3.24$$

Whereas,

$$s = \sqrt{(r_{Pb} - r_{Pt})^2 + h^2} \qquad 3.25$$

From equation (3.24) & (3.23)

$$\delta Q_2 = 2\frac{\mu\pi\omega}{\cos\theta}\tau^* r^2 \delta r$$

Integrating both sides,

$$Q_2 = 2\frac{\mu\pi\omega}{\cos\theta}\tau^* \int_{r_{Pt}}^{r_{Pb}} r^2 \delta r$$

$$Q_2 = \frac{2}{3}\frac{\mu\pi\omega}{\cos\theta}\tau^*({r_{Pb}}^3 - {r_{Pt}}^3)$$

Using equations (3.21) & (3.25)

$$Q_2 = \frac{2}{3}\pi\mu\omega\tau^*({r_{Pb}}^2 + r_{Pb}r_{Pt} + {r_{Pt}}^2)\sqrt{(r_{Pb} - r_{Pt})^2 + h^2} \quad (3.26)$$

c) Heat generation due to travelling of the probe

Considered that the probe is moving with a velocity of v, taking yield strength of the workpiece at 80% of its melting temperature S^*_{ys}. In this heat generation we only consider half of the curved surface area which is responsible for heat generation during the travelling of workpiece.

$$\delta A = \pi r \delta s \quad (3.27)$$

Therefore, force acting on the probe due to travelling of workpiece.

$$\delta F_p = \mu S^*_{ys}\pi r \delta s \quad (3.28)$$

Heat generation,

$$\delta Q_3 = \mu S^*_{ys}\pi r \delta s v \quad (3.29)$$

From equation (3.24)

$$\delta Q_3 = \mu S^*_{ys}\pi r \frac{\delta r}{\cos\theta} v$$

Integrating both sides

$$Q_3 = \mu S^*_{ys}\frac{\pi}{\cos\theta} v \int_{r_{Pt}}^{r_{Pb}} r\delta r$$

$$Q_3 = \mu S^*_{ys}\frac{\pi}{2\cos\theta} v({r_{Pb}}^2 - {r_{Pt}}^2)$$

Now using equations (3.20) & (3.25)

We get,

$$Q_3 = \frac{\mu}{2}\pi S^*_{ys} v(r_{Pb} + r_{Pt})\sqrt{(r_{Pb} - r_{Pt})^2 + h^2} \quad (3.30)$$

So, the total heat generation in probe is shown in equation (3.31)

$$Q_p = Q_1 + Q_2 + Q_3$$

$$Q_p = \frac{2}{3}\pi\mu\omega P\,(R^3 - r_{Pt}{}^3) + \left\{\frac{2}{3}\pi\mu\omega\tau^*(r_{Pb}{}^2 + r_{Pb}r_{Pt} + r_{Pt}{}^2) + \frac{\mu}{2}\pi S_{ys}^* V(r_{Pb} + r_{Pt})\right\}\sqrt{(r_{Pb} - r_{Pt})^2 + r^2} \quad (3.31)$$

Therefore total heat generation in flat cylindrical shoulder with conical probe is shown in equation (3.32)

$$Q = Q_s + Q_p$$

i.e.

$$Q = \frac{2}{3}\pi\mu\omega P\,(R^3 - r_{Pt}{}^3) + \mu\pi S_{ys}^* R h_1 V + \frac{2}{3}\pi\mu\omega P\,(R^3 - r_{Pt}{}^3) + \left\{\frac{2}{3}\pi\mu\omega\tau^*(r_{Pb}{}^2 + r_{Pb}r_{Pt} + r_{Pt}{}^2) + \frac{\mu}{2}\pi S_{ys}^* V(r_{Pb} + r_{Pt})\right\}\sqrt{(r_{Pb} - r_{Pt})^2 + h^2} \quad (3.32)$$

3.2.3 Heat source model

3.2.3.1 Heat source model for similar material

The modeling of heat source was considered based on the following assumptions,

i) The heat input is linearly proportional to the distance from the center of the tool.

ii) The plunging force applied to the plate surface by the tool creates a uniform pressure over the shoulder surface.

The distribution of heat flux [147] over the plate surface due to tool shoulder is given as,

$$q(r) = \frac{3Q_1 r}{2\pi R^3} \qquad \text{for } r_p \le r \le R \quad (3.33)$$

The distribution of heat flux over the pin-plate interface due to tool pin side surface is given as,

$$q_p = \frac{Q_p}{(A)_{ps}} \quad (3.34)$$

Where, $(A)_{ps}$ is the side surface area of tool pin.

3.2.3.2 Heat source model for dissimilar material

In this study the modeling of heat source was considered based on the same assumptions mentioned earlier in section 3.2.3.1. In this study heat flux was calculated based on the friction between Cu-plate & steel FSW tool and Al-plate & steel tool. The heat due to friction

between Cu-plate & steel-FSW tool was applied in Cu-plate side. And the heat due to friction between Al-plate & steel-FSW tool was applied in Al-plate side as shown in Figure 3.8.

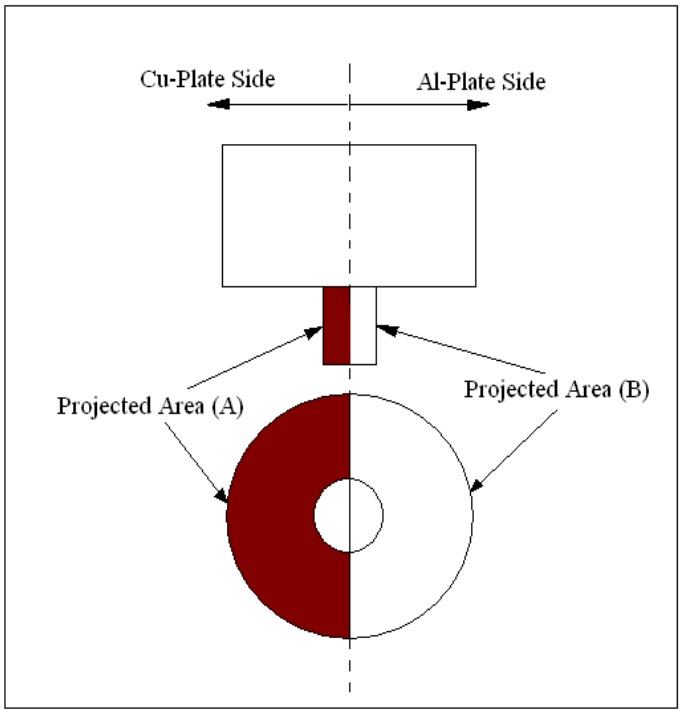

Figure 3.8 Heat source model for Cu-Al dissimilar FSW

The distribution of heat flux on the surface of the plate due to tool shoulder is used as mentioned above in equation 3.33 and equation 3.34 respectively.

3.2.4 Three-dimensional finite element model

A three dimensional finite element transient thermal model was developed in the present work to analyze the heat transfer and temperature distribution in a FSW process. In the thermal model the actual conditions were accommodated as far as possible. The following assumptions were made in developing the present thermal model of a FSW process.

1. All the thermal properties were considered as function of temperature.
2. Linear Newtonian convection cooling was considered on all the surfaces.
3. Heat generation was considered as a load.

The governing differential equation is:

$$\frac{\partial}{\partial x}\left[K\frac{\partial T}{\partial x}\right]+\frac{\partial}{\partial y}\left[K\frac{\partial T}{\partial y}\right]+\frac{\partial}{\partial z}\left[K\frac{\partial T}{\partial z}\right]+q'''=\rho C\frac{\partial T}{\partial t} \qquad (3.35)$$

Where,

$q''' =$ Heat Generation

ρ = density of plate material,

c = Specific heat and

K = Thermal conductivity.

Equation (3.35) can be written as:

$$\rho c \frac{\partial T}{\partial t} = -\{L\}^T\{q\} \quad (3.36)$$

Where,

$\{L\} = \begin{Bmatrix} \frac{\partial}{\partial x} \\ \frac{\partial}{\partial y} \\ \frac{\partial}{\partial z} \end{Bmatrix}$ = Vector Operator

$\{q\}$=heat flux vector

$\{L\}^T\{q\} = \nabla . \{q\}$ and

$\{L\}T = \nabla T$

Where,

∇ Represents grad operator

Fourier's law is used to relate the heat flux vector to the thermal gradient

$\{q\} = -[D]\{L\}T$ Where,

$[D] = \begin{bmatrix} K & 0 & 0 \\ 0 & K & 0 \\ 0 & 0 & K \end{bmatrix}$=conductivity matrix.

Equation (3.36) can be written as:

$$\rho c \frac{\partial T}{\partial t} = \{L\}^T([D]\{L\}T) \quad (3.37)$$

The following boundary conditions were applied in this FE model

3.2.4.1 Initial condition

A specified initial temperature for the FSW that covers all the elements of the specimen:

$T=T_{\alpha}$ for t=0 (3.38)

Where T_{α} is the ambient temperature.

To develop second and third boundary conditions the energy balance was considered at the work surface as shown in equations 3.39 and 3.41

Heat supply = Heat loss.

3.2.4.2 First boundary condition

A specific heat flows acting over surface S_1

$$Q_n = -q_{sup} \quad (3.39)$$

The quantity q_n represents the component of the conduction heat flux vector normal to the work surface. The quantity q_{sup} represents the heat flux supplied to the work surface in $\frac{W}{m^2}$.

$$q_n = \{q\}^T\{n\} \quad (3.40)$$

On the surface S_1 for t >0

Where,

$\{n\}$= unit outward normal vector.

S_1 is the surface of welding only.

3.2.4.3 Second boundary condition:

Considering heat loss (q_{conv}) due to convection over surface S_2 (Newton's law of cooling):
$q_n = q_{conv}$

or

$$\{q\}^T\{n\} = h_f(T - T_{\alpha}) \quad (3.41)$$

On surface S_2 for t > 0.

Where S_2 is the area of all the surface except welding zone i.e. S_1

Pre-multiplying equation (3.37) by a virtual change in temperature, integrating over the volume of the element, combining with equations (3.40) and (3.41), and with some algebraic manipulation

We get:

$$\int_{vol}\left(\rho c\delta T\left(\frac{\partial T}{\partial t}\right)+\{L\}^{T}(\delta T)([D]\{L\}T)\right)d(vol)=\int_{S_1}\delta T q_{sup}\,d(S_1)+\int_{S_2}\delta T h_f(T_\alpha T)d(S_2) \quad (3.42)$$

Where,

Vol = volume of the element

δT = an allowable virtual temperature $(=\delta T(x,y,z,t))$

3.2.4.4 Derivation of heat flow matrices

As stated before, the variable T is allowed to vary both in space and time. This dependency is expressed as:

$$T=\{N\}^{T}\{T_e\} \quad (3.43)$$

Where, $T=T(x,y,z,t)$= Temperature

$\{N\}=\{N(x,y,z)\}=$ element shape function

$\{T_e\}=\{T_e(t)\}$= nodal temperature vector.

The time derivatives of equation (3.43) may be written as:

$$\dot{T}=\frac{\partial T}{\partial t}=\{N\}^{T}\{T_e\} \quad (3.44)$$

δT has the same form as T:

$$\delta T=\{\delta T_e\}^{T}\{N\} \quad (3.45)$$

The combination of $\{L\}T$ is written as: $\{L\}T=[B]\{T_e\}$

Where $$[B]=\{L\}\{N\}^{T} \quad (3.46)$$

The variation statement of equation (3.42) can be combined with equations (3.43), (3.44), (3.45) & (3.46) to yield:

$$\int_{vol} \rho c \{\delta T_e\}^T \{N\}\{N\}^T \{\dot{T}_e\} d(vol) + \int_{vol} \{\delta T_e\}^T \{B\}^T [D][B]\{T_e\} d(vol)$$
$$= \int_{S_1} \{\delta T_e\}^T \{N\} q_{sup} d(S_1) + \int_{S_2} \{\delta T_e\}^T \{N\} h_f (T_\alpha - \{N\}^T \{T_e\}) d(S_2)$$

(3.47)

The density ρ is assumed to remain constant and specific heat c may vary over the element. Finally,$\{T_e\}$, $\{\dot{T}_e\}$ and $\{\delta T_e\}$ are nodal quantities and do not vary over the element, so that they also may be taken out from the integrals. Now, since all quantities are pre-multiplied by $\{\delta T_e\}$ this term may also be dropped from the resulting equation. Thus equation (3.47) may be reduced to:

$$\int_{vol} c \{N\}\{N\}^T d(vol)\{\dot{T}_e\} + \int_{vol} \{B\}^T [D][B] d(vol)\{T_e\}$$
$$= \int_{S_1} \{N\} q_{sup} d(S_1) + \int_{S_2} T_\alpha \{N\} h_f d(S_2) - \int_{S_2} h_f \{N\}\{N\}^T \{T_e\} d(S_2)$$

(3.48)

Equation (3.46) can be rewritten as: $[C_e^t]\{\dot{T}_e\} + ([K_e^{tb}] + [K_e^{tc}])\{T_e\} = \{Q_e^f\} + \{Q_e^c\}$

(3.49)

Where,

$[C_e^t] = \rho \int_{vol} c \{N\}\{N\}^T d(vol) =$ element specific heat matrix

$[K_e^{tb}] = [B]^T [D][B] d(vol) =$ element diffusion conductivity matrix

$[\mathrm{K_e^{tc}}] = \int_{S_2} \mathrm{h_f [N][N]^T d(S_2)} =$ element convection surface conductivity matrix

$\{Q_e^f\} = \int_{S_1} \{N\} q_{sup} d(S_1) =$ element heat flow vector for surface S1

$\{Q_e^c\} = \int_{S_2} T_\alpha \{N\} h_f d(S_2) =$ element convection surface heat flow vector.

The element specific heat matrix $[C_e^t]$ is evaluated from the specific heat of the material. In phase change problems, sharp change in the value of specific heat at the melting temperature

has been observed, which is not considered in this case, because generally the FSW process carried out bellow melting temperature. The solution is obtained using ANSYS FE package.

3.2.4.5 FE model

In order to reduce the computation time the meshing of the model was done as shown in Figure 3.9. A fine mesh was generated at the welding zone where as a coarser mesh was generated away to it. A continuous increment in mesh size is given from the weld centre to the end of the plate.

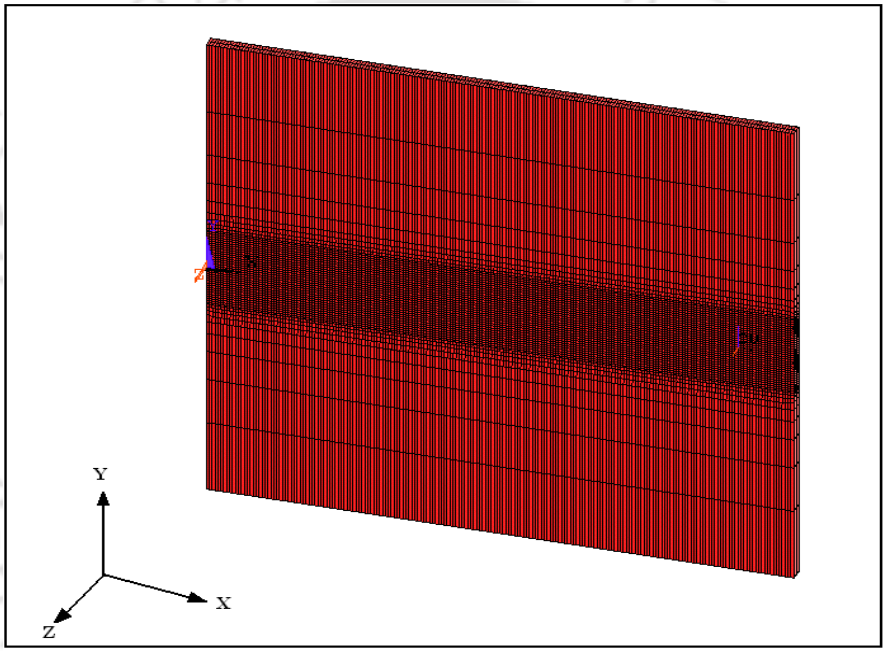

Figure 3.9 Meshed model

Constant convection co-efficient, 30 W/m^2°C was used for aluminum and in the analysis. The temperature dependent thermal properties and coefficient of friction of aluminum & steel combination [147, 151], are given in Table 3.1 and Table 3.2 respectively. The melting temperature of this aluminum alloy was taken as 660 ^{0}C. The temperature dependent material properties of copper were used in the modelling of dissimilar Cu-Al FSW analysis [152]. Table 3.3 shows the thermal properties of copper.

Table 3.1 Temperature dependent thermal material properties of aluminum alloy.

Temperature °C	Thermal Conductivity W/m°C	Heat Capacity J/Kg°C
37.8	162	945
93.3	177	978
148.9	184	1004
204.4	192	1028
260.0	201	1052
315.6	207	1078
371.1	217	1104
426.7	223	1133

Table 3.2 Temperature dependent coefficient of friction for aluminum and steel combination. Chao et al. (1998)

Temperature (°C)	Friction Coefficient (μ)
22	0.11
160	0.11
200	0.26
400	0.35
580	0.47

Table 3.3 Thermo mechanical properties of Cu

Properties	Copper
Specific heat (J/kgK)	385
Density (g/cm^3)	8.91
Thermal conductivity at 20^{0}C	397
Melting point (^{0}C)	1083
Coefficient of friction with steel	0.36

3.3 Experimental setup and procedures

A vertical milling machine with 7.5hp motor capacity was modified and used to carry out the FSW experiments. This machine has tool rotational speed range from 50 to 1500 rpm and table speeds range is from 22 to 555 mm/min. Figure 3.10 shows the experimental setup and Figure 3.11 is the data acquisition system (make: Agilent-34970A) which was used to record the temperature data.

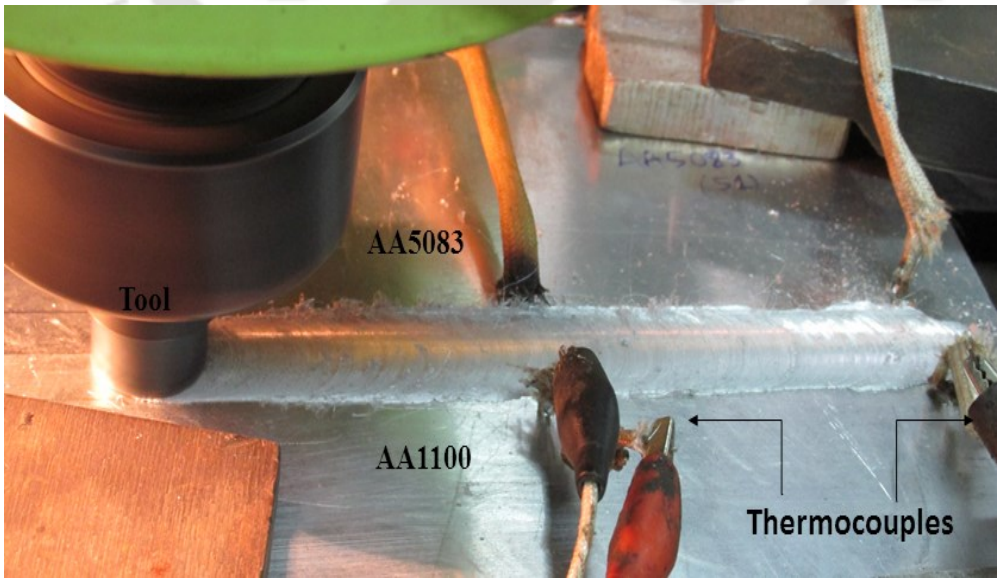

Figure 3.10 FSW Experimental setup

Figure 3.11 Data acquisition system for temperature measurement

Here, K-type thermocouple of 1mm diameter was used for measuring the temperature of the workpieces. These thermocouples were fixed 14mm and 16mm away to the center of the weld line at top side of the plate on both the specimens. The tool was mounted and tightened in the vertical arbor using a suitable collates. The edges of the test pieces were machined to obtain a perfect square butt. The workpieces are tightly fixed on a backing plate of stainless steel and are clamped to the horizontal bed with zero root-gap. The butt line was aligned with the center line of FSW tool. The clamping of the test pieces was done such that the movement of the plates was totally restricted under both plunging and translational forces of the FSW tool. The tool rpm and translational speed of the bed were set prior to each run of welding. After plunging the rotating tool at the plate butt and visually ensuring full contact of the tool shoulder with the plate surface, the bed movement was switched on.

3.3.1 Design of Experiments

Design of experiments (DOE) which was developed by Dr. Genichi Taguchi is an important tool for designing engineering or manufacturing processes. DOE involves identifying the right inputs and parameter levels quantitatively for achieving an acceptable and desirable output. Taguchi method is a well-planned systematic approach to determine the best possible combination of inputs for obtaining the desired output.

This method is based on orthogonal arrays experiment to predict the optimal process parameters. Orthogonal array offers a set of coordinated (least possible experimental paths) experiments and Taguchi's signal-to-noise ratios (S/N ratio), which are logarithmic functions of desired outputs assist as objective functions for optimization. This procedure helps to examine the output data and to predict the optimal results. The S/N ratio is the ratio of the mean (signal) to the standard deviation (noise). The standard S/N ratios generally used are as: Nominal is best (NB), lower the better (LB) and higher the better (HB). The optimal setting is the parameter combination, which has the highest S/N ratio. Taguchi's orthogonal arrays are highly fractional orthogonal designs. These designs can be used to estimate main effects using only a few experimental runs.

In the present study the design of experiments were performed based on the following three important steps, (i) Identification of important process parameters and variables (ii) Fixing the upper and lower limits of parameters and variables (iii) and developing the design matrix. In the section 6.2 and section 6.3 the mixed level design L16 was chosen for experimental study.

3.4 Mechanical and microstructural properties study

The weld quality of the weldments were examined by different mechanical testing and microstructural study which involves tension test, weld hardness test, microstructural studies, factographical studies, compositional studies and elemental scan tests.

3.4.1 Tensile test

All the tensile tests were performed on universal tensile testing machine (make Instron-8801) which has a maximum load capacity of about 100 kN. The objective of this test was to check the strength of the welded samples (i.e. the study of nominal stress vs. strain characteristics curves). The cross head displacement was set to 1mm/min for all the tests. The test specimens were taken perpendicular to the weld direction, sectioned and machined according to the ASTM E-8 standards. Figure 3.12 shows the Tensile testing machine and Figure 3.13 show the dimensions of tensile test specimens according to ASTM – E8 standards. Figure 3.14 represents the prepared tensile test samples.

Figure 3.12 Hydraulic universal tensile testing machine (Make: Instron 8801)

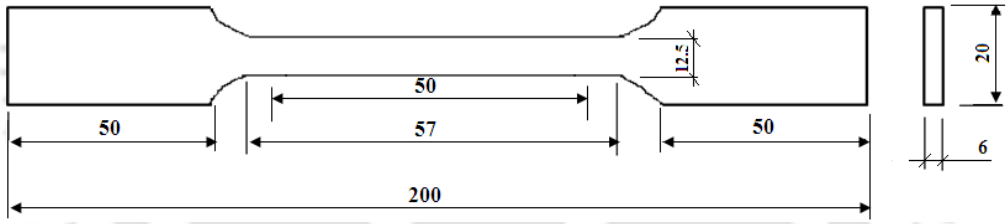

Figure 3.13 Tensile sample dimensions (ASTM E-8 standard)

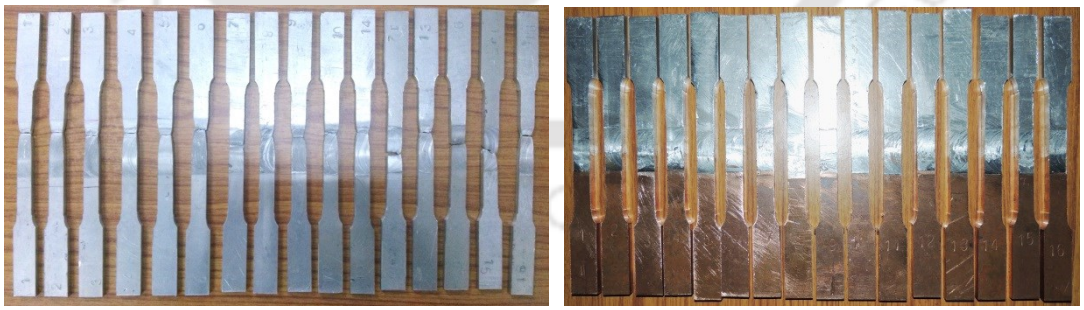

Figure 3.14 Tensile samples

3.4.2 Micro hardness test

In Vickers hardness test a diamond indenter indents into the test material, which gives an indentation in the form of a right pyramid of a square base which has an angle of 136 degrees between its opposite faces. In this present study the indentation was subjected to a load of

500gf. The full load is generally applied about 10 to 15 seconds. Figure 3.15 shows the micro hardness testing machine.

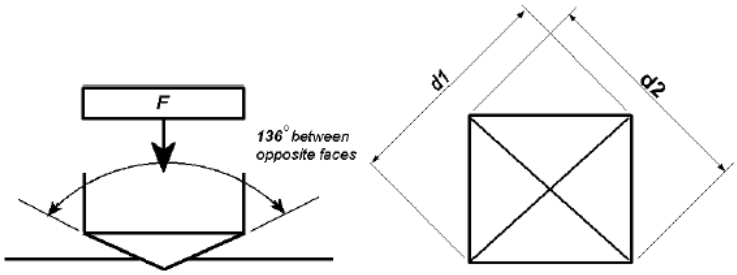

$$HV = \frac{2F\ sin\frac{136}{2}}{d^2} = 1.854\frac{F}{d^2}$$

Where F= Load in Kgf and d= arthemetic mean of two diagonals d_1 and d_2.

Figure 3.15 Vickers micro hardness testing machine

The two diagonals of the indenter make an indentation on the sample surface by the load removal. Before doing the above procedure the samples were made dimple free by polished using 300- 600 grit polishing papers. By using a microscope the area of the indentation surface was calculated. The Vickers hardness is the quotient obtained by dividing the gf load by the square mm area of indentation.

3.4.2.1 Sample preparation for hardness test

Samples were taken perpendicular to the weld which was a piece of cross section between two tensile test samples. These samples were sectioned in rectangular shape including weld bead and a small portion of base material. Further these samples were grounded with polishing papers of 300 and 400 grit size to make a flatten surface and to remove an uneven

portions. The polished samples were kept in the anvil of micro hardness testing machine. Automatic Vickers micro hardness tester (make: Buehler) was used to measure the hardness at different weld zones. Three test readings were noted around the same region for accuracy at a particular place.

3.4.3 Microstructural study

This investigation reveals how the operating parameters of FSW have an impact on the microstructural changes. Figure 3.16 show the procedure followed to perform the microstructural analysis. Figure 3.17 shows the specimen preparation apparatus for microstructural study. In order to investigate the microstructural variations in the welded specimen this study was conducted which has a long procedure to follow. The major steps involved in this procedure were sectioning/cutting of the welded sample, mounting of the sample, rough smoothening by grinding, fine polishing and etching. The welded specimens were sectioned along the specific areas of different weld zones using the precision cutter as shown in Figure 3.17a. The specimen mounting was done by encapsulating the specimen in compression mounting compound (phenolic resin) in a hydraulically operated press shown in Figure 3.17b.

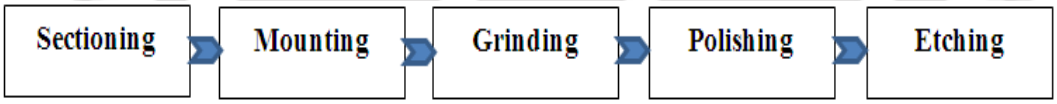

Figure 3.16 Procedure for microstructure analysis

These moulds were heated by a 350 W thermostatically controlled slip-on heater and after reaching the curing temperature the specimens were cooled by a finned slip-on cooler. Further these samples were polished by various polishing papers starting from 240 grit size to 2000 grit size. Polishing was performed by single disc with five specimen holder automated polishing machine shown in Figure 3.17c. Continuous water supply was given on the specimen for continuous rinsing action.

Figure 3.17 (a) Sectioning machine (b) Mounting press (c) Polishing machine (Make: Buehler)

Table 3.4 Chemical Etchants used for Alluminium and copper [148]

Etchant Name	Material type	Composition
Bakers reagent	All aluminium's	4-5ml of HBF_4(48%)+H_2O **Usage:** Electrolytic use
Poulant's reagent	AA1100, AA5083	12Parts of HCl+6parts of HNO_3+1part of HF(48%) and 1Part of H_2O **Usage:** Immersion or swabbing for 5secs (For Macroscopic examination)
Modified Keller's reagent	AA1100, AA5083	50ml Poulant's reagent+25ml HNO_3+40ml solution of 3g chromic acid per 10ml of water **Usage:** Immersion or swabbing for 1-4 min
Kellers reagent	AA1100, AA2000	HF-2ml+HCL- 3ml+$HNo_3$5ml+H_2O-190ml **Usage:** Immersion or swabbing for 15secs
Etchant for Copper	All Copper alloys	50ml HNo3+0.5g $AgNO_3$+50ml H_2O **Usage:** Immersing at room temperature, warm water rinsing and drying

After 2000 grit size polishing, cloth polish using metal polish (silvo for alluminium; brasso for copper samples) was done. This polishing was done with slower disc rotations of the polishing machine until it achieves a scratch free and mirror like finish. Completely polished sample was rinsed with clean water and dried with drier followed by etching. Etching was done using prepared etchant called Keller's reagent. The composition of Keller's reagent is shown in Table 3.4. This etchant gives the possibility to reveal grain boundary contrast and precipitates in several wrought and rolled alluminium alloys.

After etching the sample with appropriate reagents, the sample was thoroughly examined using the optical microscope which is shown in Figure 3.18.

Figure 3.18 Optical microscope (Make: Zeiss 4.2)

If the microstructure of the specimen was not clearly visible then the re-etching was done for 5 seconds and followed by cleaning with water. The obtained microstructure was further analysed for grain size and grain growth aspects. The average grain size of the sample was measured by the ASTM E-1382 procedure [149].

3.4.4 Compositional and fractograph analysis

Prior to the welding the, compositional studies of the base materials was examined to known the material properties for confirming as received material from vendor using FESEM. The joint properties of the weld zone were also examined by conducting elemental mapping, fractograph testing for both similar and dissimilar FSW joints performed. Figure 3.19 shows the Field emission scanning electron microscope- FESEM (make: Zeiss and model: Sigma).

Figure 3.19 Field emission scanning electron microscope (FESEM)

The compositional estimations and elemental mapping were performed to understand the material flow and mixing of Cu- Al dissimilar joint. The fractograph study was performed to understand the nature of the fractured surface of the tensile test specimens. It also provides the information of any minute tunnel hole exist in the welded sample.

3.5 Summary

In this section, the overall procedures followed on friction stir welding of both similar and dissimilar materials have been presented. This chapter has been also explained the procedures followed in numerical modelling and the mathematical formulations required for numerical simulations. Pre-welding and post-welding operations followed during experimental investigations have been reported in this chapter.

Chapter 4

Transient thermal analysis

4.1 Introduction

This chapter contains results of numerical transient thermal analysis of friction stir welding on similar and dissimilar materials. It is very essential to analyse the FSW process by numerical investigations to study the optimal conditions and their effect on the process. In order to achieve the better weld parameters and best tool geometries transient thermal analysis were conducted using the developed FE model. The most influential concern in FSW process is the heat generation between the tool and workpiece, if someone methodically recognizes this phenomena then it will be a good contribution to this process enhancement. Hence this study focusses on the issues of effect of operating parameters, tool geometries and tool plunging forces on thermal history of both similar and dissimilar metals. This section emphasis on three dimensional finite element modelling on FSW of similar and dissimilar materials. Section 4.2 contains three subsections i.e. 4.2.1 Effect of tool pin geometries of FSW, 4.2.2 Effect of tool shoulder diameter on FSW and 4.2.3 Effect of tool plunging force on FSW. Section 4.3 contains the results of Numerical studies on thermal history of FSW on dissimilar alloys. The detailed methodology of numerical modelling has been discussed previously in chapter 3. Here the analysis focussed based on the literature gaps, necessary modelling and investigations were carried out. First of all numerical thermal modelling and analysis was performed on similar materials and then the work was extended to analyse the thermal history of dissimilar materials. The obtained results of numerical analysis using developed FE model have been immensely discussed below.

4.2 Results and Discussions

The FE transient thermal analysis was solved by considering temperature dependent material properties, Newton's convection and distributed moving heat source. To reduce the computation time, coarse mesh was generated away from frictional heating region and finer mesh was generated along and near the frictional heating region as shown in Figure 4.1. The detailed procedure of transient thermal was discussed in the previous section i.e. Chapter 3.2.

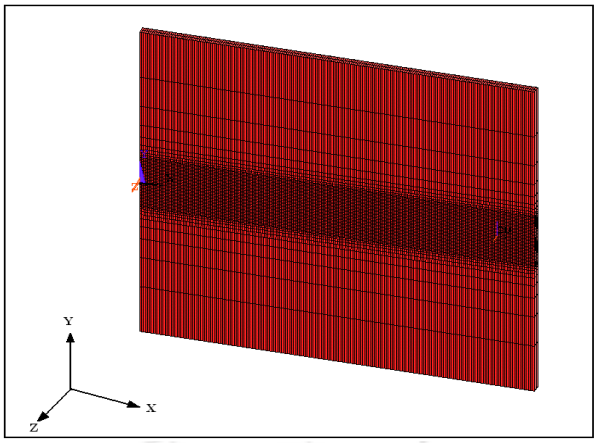

Figure 4.1 FE model and meshing view

The temperature distribution from centre of weld line to away from weld line for 6mm cylindrical probe diameter and 25mm shoulder diameter, flat circular shoulder frictional surface is shown in Figure 4.2 where the tool rotational and transverse speed were 1400 rpm and 112 mm/min respectively.

.

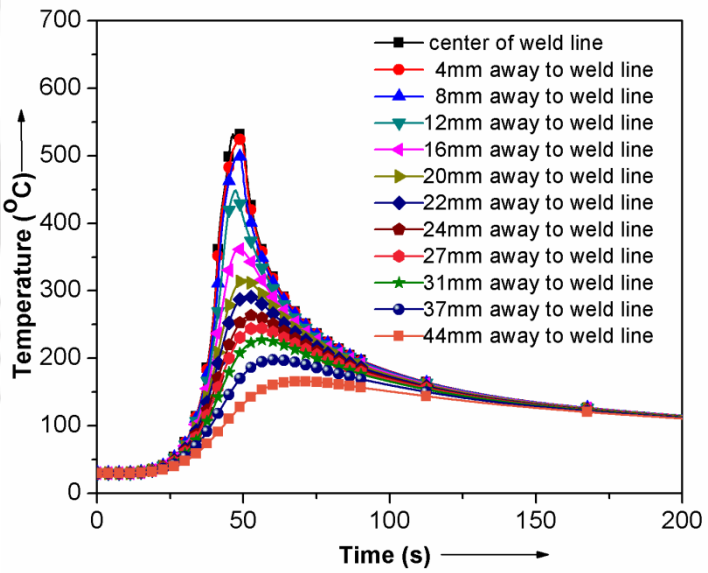

Figure 4.2 Temperature distribution from center of weld line to away from weld line

The quasi-static peak temperature distribution along the centre of weld line for 6mm cylindrical probe diameter and 25mm shoulder diameter, flat circular shoulder surface is shown in Figure 4.3 (where the tool rotational and transverse speed were 3000 rpm and 180 mm/min respectively).

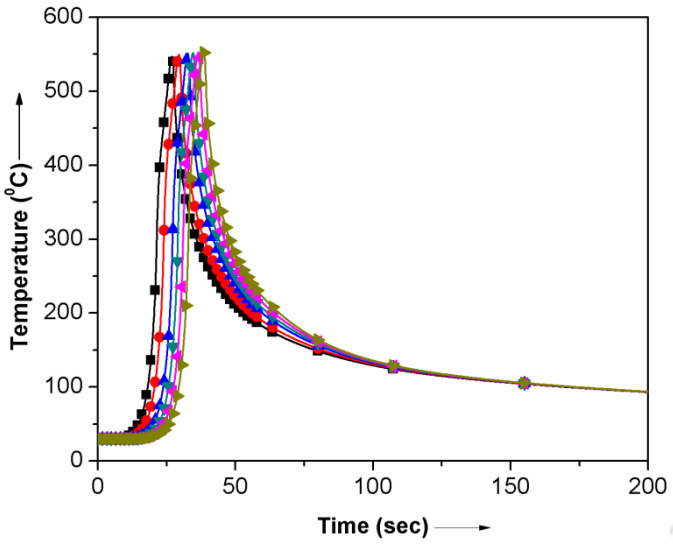

Figure 4.3 Quasi-static temperature distributions along center of weld line

The isothermal contours for a particular time step during welding are shown in Figure 4.4. The tool rotational and transverse speed was 1400 rpm and 112 mm/min respectively.

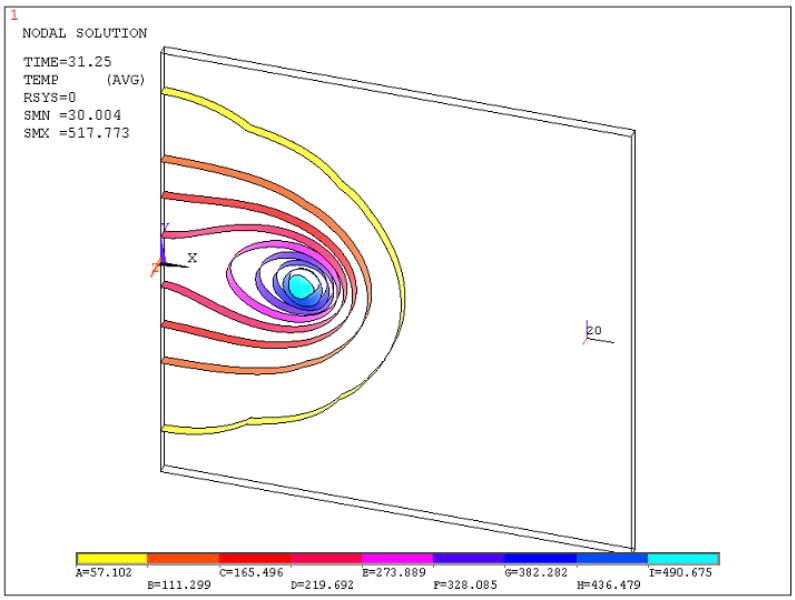

Figure 4.4 Isothermal patterns for a particular time step during welding for 6mm pin diameter

4.2.1 Effect of tool pin geometries on FSW

It is preferable to keep the tool pin diameter as small as possible to avoid occurrence of a wormhole defect. Tool plunging force reduced significantly with an increase in tool rotational speed; however, the increase in heat generation was marginal. As majority of the heat

generated in shoulder surface (i.e. about 90%) that why tool pin geometry have a marginal effect on thermal history of FSW.

Not much information on the effect of tool geometry, including that of tool pin on thermal profile, was reported in the literature. In the present study, the effect of variation of tool pin geometry on thermal profile has been presented below. In this present study two different tool geometries have been considered as shown in Figure 4.5. The process parameters used in this study are shown in Table 4.1.

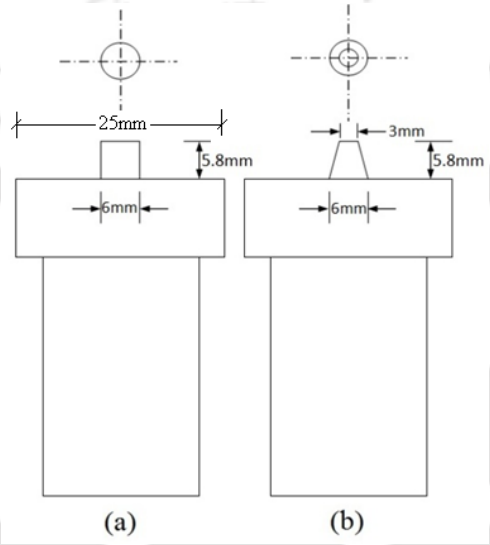

Figure 4.5 Details tool geometry for cylindrical and conical probe

Table 4.1 FSW process parameters

Rotational Speed (rpm)	Traverse speed (mm/min)	Average Plunging force (N)
1400	112	3000

The results of thermal analysis of 6mm thick aluminum alloy plate for 2 different tool geometries are discussed below.

The peak temperatures obtained from the results of thermal analysis of FSW of AA1100 considering the welding parameters given in Table 4.1 for two different tool geometries shown in Figure 4.6 are given in Table 4.2.

At the same time conical tool pins exhibited somewhat lesser peak temperature compared to that of cylindrical pin having pin diameter same as the base diameter of conical pins.

Table 4.2 Peak temperatures for different tool geometries

Sl. No.	Tool type		Peak Temperature (^{0}C)	% of melting temperature
1	Cylindrical	Flat shoulder, pin dia. 6mm	539.6	81.8
2	Conical Pin	Flat shoulder, pin base dia. 6mm, tip dia 3mm	527.82	80

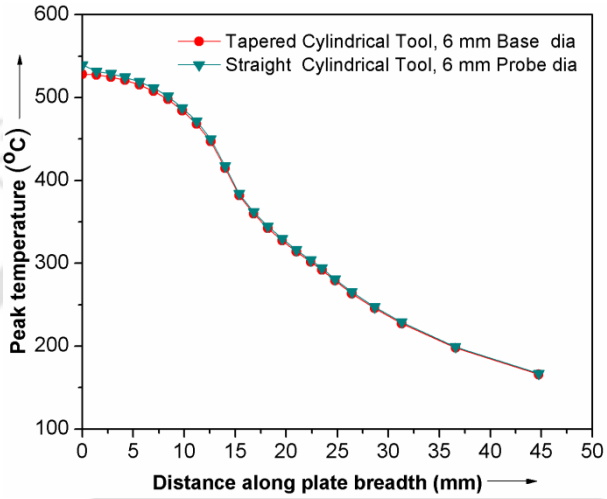

Figure 4.6 Peak temperature distributions along plate breadth perpendicular to the weld line

Keeping all other parameters constant, the variation of peak temperature distribution for 5 mm and 6 mm cylindrical tool pin diameters are shown in Figure 4.7. Figure 4.7 shows the comparison of peak temperature distribution with distance perpendicular to the weld line.

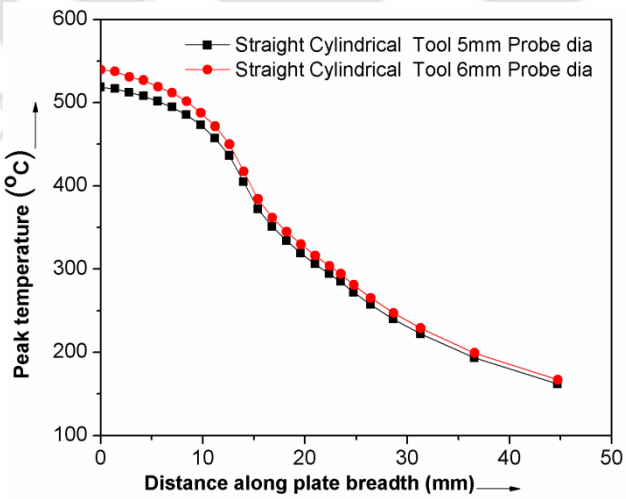

Figure 4.7 Comparison of peak temperature distribution with distance perpendicular to the weld line

From the above Figure 4.7 one can observe that for particular welding parameters the magnitude of peak temperature is slightly varied with different pin diameters. Like the maximum temperature for flat cylindrical shoulder with 5mm probe diameter is 518.83 ^{o}C and for flat cylindrical shoulder with 6mm probe diameter is 539.68 ^{o}C. And one can also observe that the peak temperature increases with the increment of pin diameter.

4.2.2 Effect of tool shoulder diameter and tool plunging force

4.2.2.1 Effect of tool shoulder diameter

The FSW of AA1000 was performed for finding out the effect of shoulder diameter and effective shoulder diameter for acquiring the required useful temperature for FSW process. Here, FSW tools having flat cylindrical shoulder and cylindrical tool pin were used as shown in Figure 4.8. Similar tool geometry was used by varying shoulder diameter. For FE analysis brick elements were considered with fine meshing in the weld zone. The details of the FE modelling have been discussed in Chapter 3, section 3.2.4.

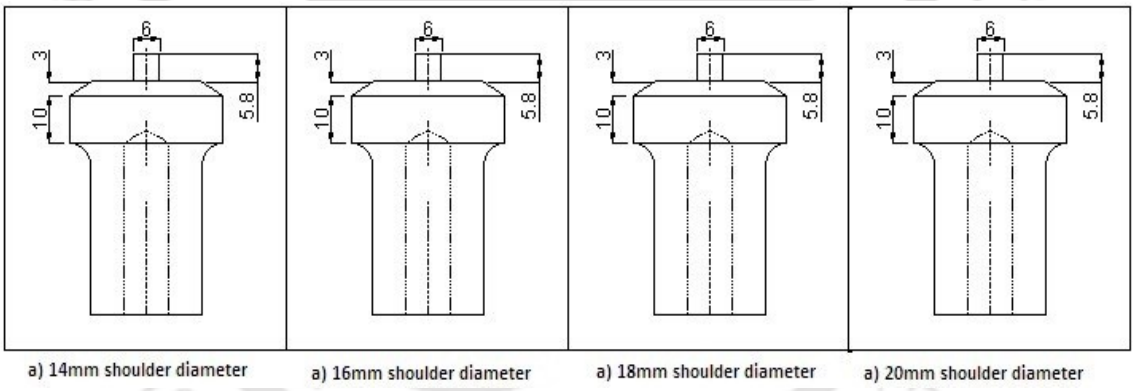

Figure 4.8 Tool geometry used

Keeping all the process parameters constant as shown in Table 4.3, the effect of shoulder diameters on FSW were studied.

Table 4.3 Process parameter and shoulder diameters

Plate Thickness (mm)	Rotational Speed (rpm)	Traverse speed (mm/min)	Varying shoulder diameter (mm)	Average Plunging force (N)
6.0	1400	112	12 to 24	3250

The results of FE thermal analysis are shown in Figures 4.9 to 4.17. Figures 4.9 and 4.10 represent the temperature contour on the top surface of the weld plate at a particular time for two different shoulder diameters i.e. for 12mm and 24mm. The minimum and maximum temperature acquired by using the FSW tool of shoulder diameter 12mm is 30.009^{0}C, 399.537^{0}C and by using 24mm shoulder diameter tool is 30.020C, 561.292^{0}C.

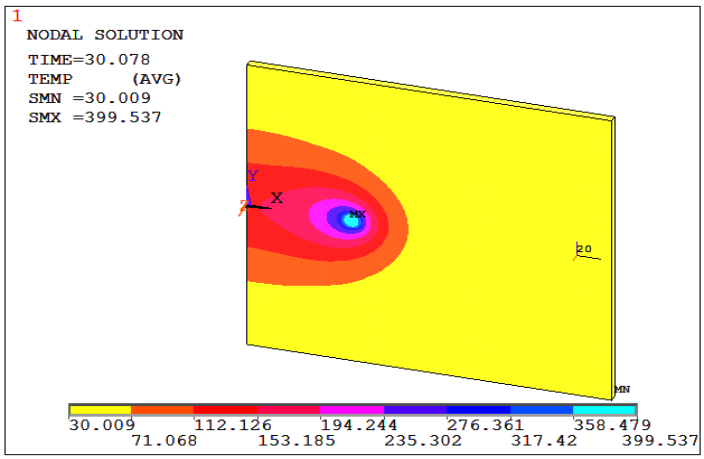

Figure 4.9 Temperature contour for 12mm shoulder diameter

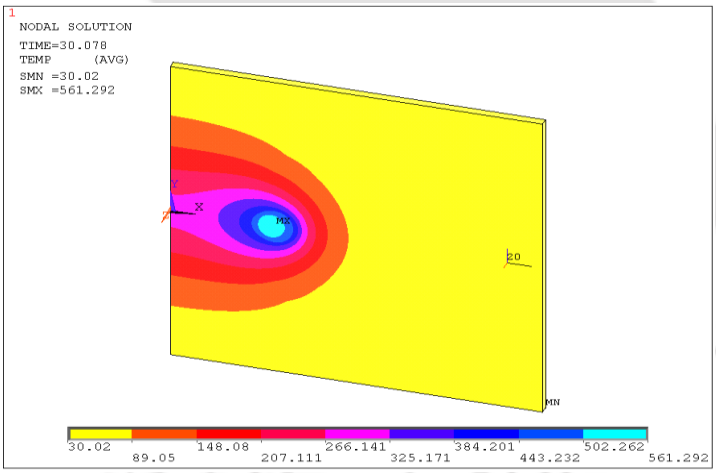

Figure 4.10 Temperature contour for 24mm shoulder diameter

Figures 4.11 and 4.12 represent the temperature contours along the cross section (i.e. along thickness) of the weld plate at a particular time for two different shoulder diameters for 20mm and 24mm respectively. In this cross sectional views, it is clearly noticeable the different zones of FSW weldments. The light blue colour regions at the centre indicates the nugget region, next to it indicates thermo-mechanically effected region, heat effected region and unaffected base metal region. In the below Figures 4.11 and 4.12 it is very clear that by

increasing the shoulder diameter the area of the nugget region also increasing. Having larger nugget region is also not preferable.

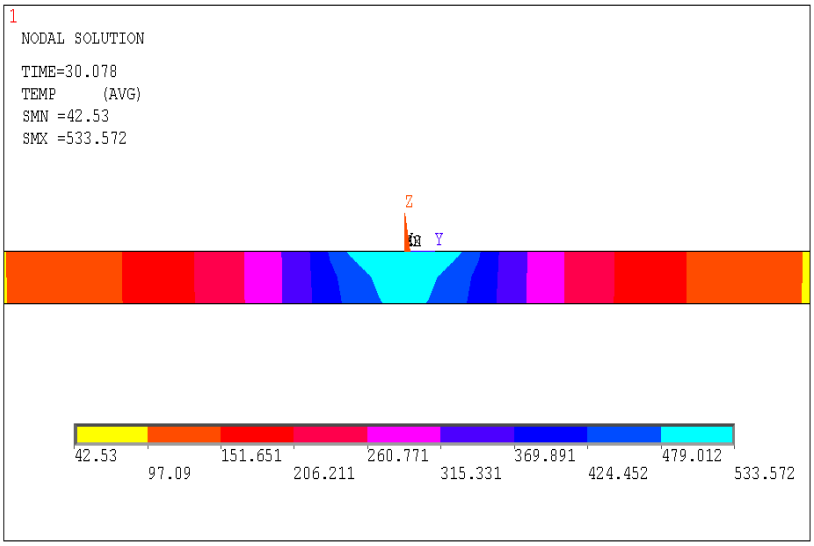

Figure 4.11 Thermal contours 20mm shoulder diameter

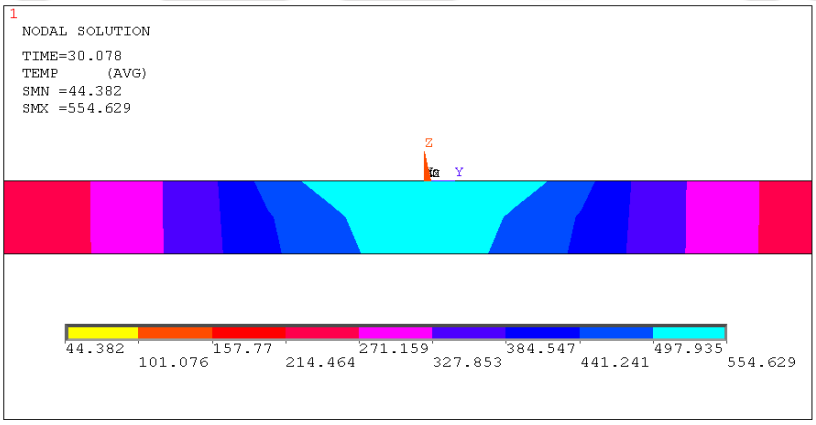

Figure 4.12 Thermal contours with 24mm shoulder diameter

Figures 4.13 and 4.14 represent the transient temperature distribution along the centre of weld line and 16mm away from centreline respectively for six tools of different shoulder diameters. The maximum temperatures at centre line vary from 390-560^{0}C for six different tools and maximum temperatures measured at 16mm away from centreline vary from 190-370^{0}C. By the plots it is noticed that by reducing the shoulder size, peak temperatures were reduced and the time required to heat loss/cooling is more for larger shoulder size tools, i.e. slow cooling rates for larger sized tools. After peak temperature to reach 150^{0}C, 12mm shoulder size tool is reaching in 60 seconds, and 24mm shoulder size tool is reaching 120 seconds, that means if we increase twice the shoulder diameter cooling rate decreased by two times. The melting point of the pure aluminium (AA1000) series is 660^{0}C. It is clear from the

published literature (Biswas and Mandal [150]) that the best suited temperature for FSW is the 80-90% of its liquidus temperature and it is equal to 528^0C. From the Figure 4.16 the peak temperature obtained with the tool of 20mm shoulder diameter is 540^0C; therefore it is very preferable to choose the tool shoulder diameter within the range of 18-20mm.

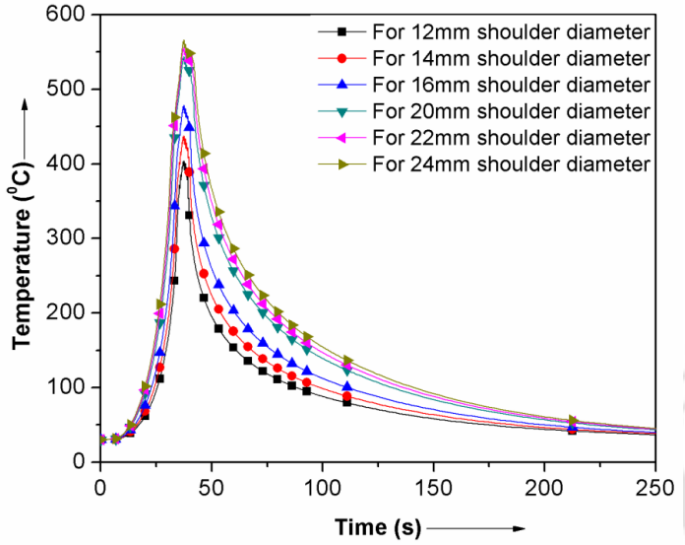

Figure 4.13 Temperature distributions at centre of weld line

From the Figures 4.13 and 4.14 it was noticed that the difference of the peak temperatures between 12mm shoulder diameter and 24mm shoulder diameter is near about 1700C. From the numerical results it is also clear that the time required obtaining the peak temperatures were within the range of 40-50seconds. That means the dwell or ideal time to keep the tool constant at a particular position after plunging should be 40 seconds or tool traversing should start 40 seconds after the tool plunging completed lead the best welds.

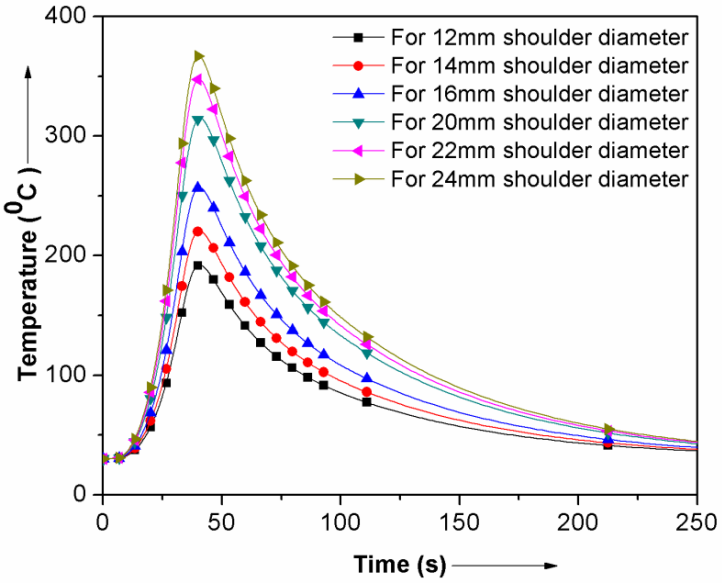

Figure 4.14 Temperature distributions at 16mm away from centre of weld line

Figure 4.15 shows the Peak temperature distribution perpendicular to the centre of weld line with different shoulder diameter and Figure 4.16 represents the maximum temperature raised due to different shoulder diameters keeping all other welding parameters constant as shown in Table 3.

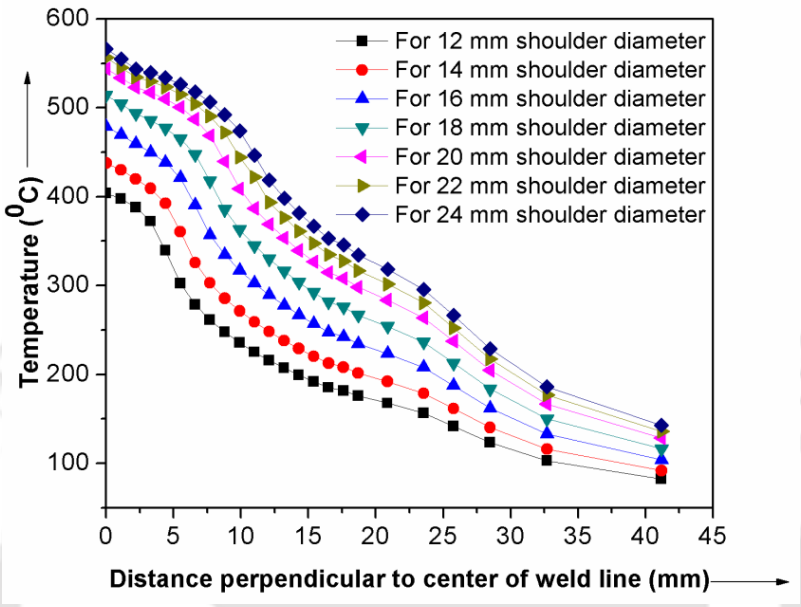

Figure 4.15 Peak temperature distribution perpendicular to the centre of weld line

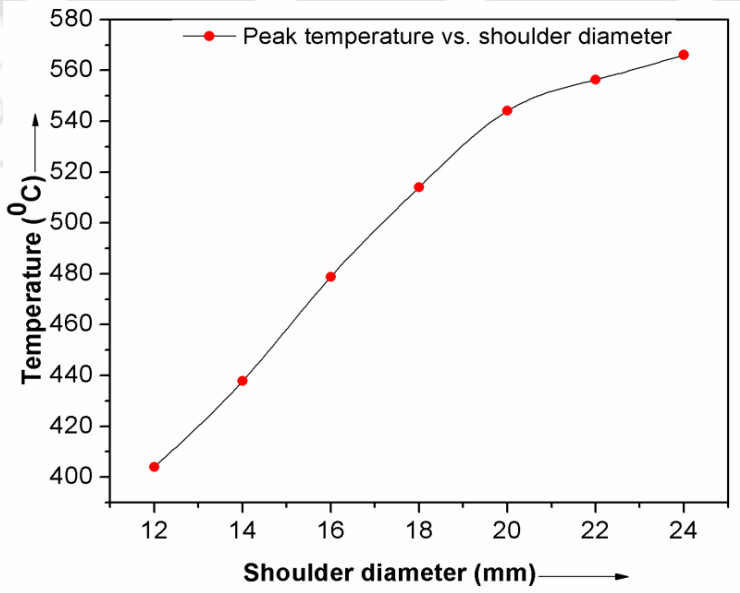

Figure 4.16 Shoulder diameters vs. maximum temperature

From Figure 4.17 it was observed that the tools of shoulder diameter and pin ratio of up to around 3.3 the increment of peak temperature is high. But for the tools beyond the 3.3, the increment of peak temperature is lower compare to the smaller ratio.

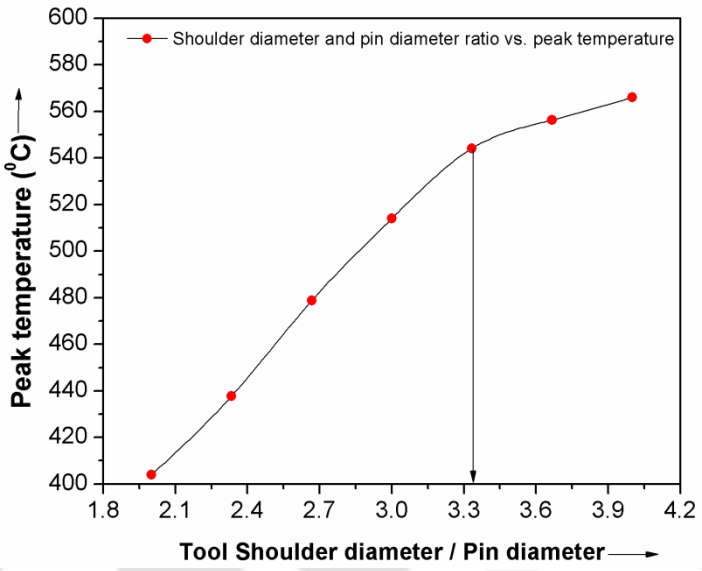

Figure 4.17 Shoulder diameter and pin diameter ratio vs. maximum temperature

Many experiments were conducted and simultaneously temperature has measured. The experimental and numerical temperature data for flat shoulder with cylindrical pin of 6mm diameter as shown in Figure 4.18. The welding was carried out with tool traverse and rotational speed of 112 mm/min and 1400 rpm respectively for different tools of varying shoulder diameters between 12-24mm. Numerical temperature distribution results at 5mm and 20mm away from centre line is well coincided with the experimental results. There is a very less time difference to obtain peak temperatures is noticed in numerical and experimental data acquired. Figure 4.18 represents numerical and experimental temperature distribution at 5mm and 20mm away from weld centre line of 18mm shoulder diameter.

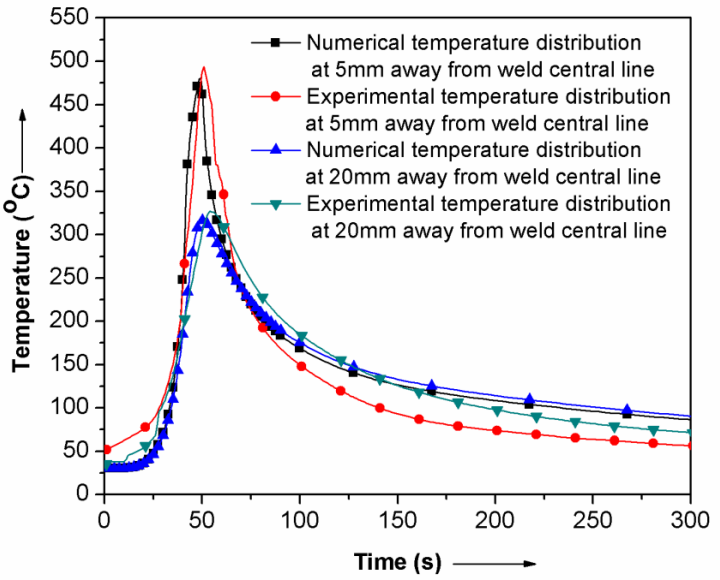

Figure 4.18 Numerical and experimental temperature distribution at 5mm and 20mm away from weld centre line of 18mm shoulder tool

Figure 4.19 shows a sample result of numerical and experimental temperature distribution welded with 20mm flat cylindrical shoulder tool. The temperature was recorded 20mm away from centre of weld line.

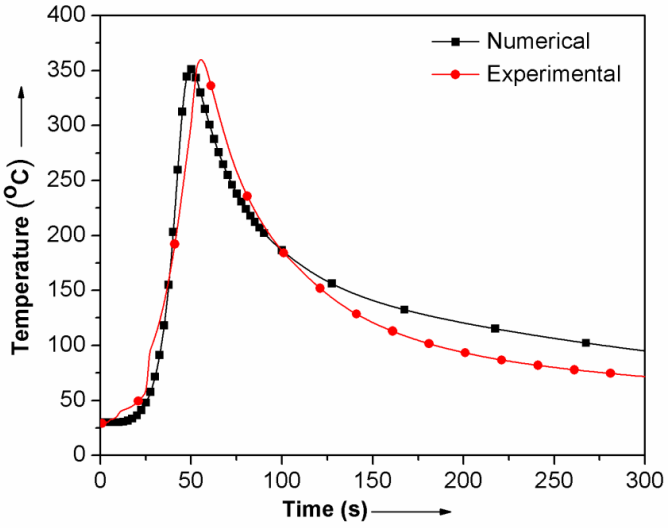

Figure 4.19 Numerical and experimental temperature distribution for welding with 20mm shoulder tool.

The welding was carried out with tool rotational and transverse speed 1400 rpm and 112mm/min respectively. The measured thermal data compared well with the calculated ones as can be seen in the Figures 4.18 and 4.19. Some mismatch can be observed in the cooling rate below about 150 ^{0}C. However more importantly, the peak temperatures measured, which have major influence on the overall welding process, were found to be in very good agreement with the calculated ones.

4.2.2.2 Effect of tool plunging force

After optimizing the tool shoulder diameter the same was used i.e. 20mm, to predict the effect of plunging force on thermal history of FSW by varying the plunging force from 2200N to 3250N. Figure 4.20 represents the transient temperature distribution along the center of weld line for three different plunging forces. Figure 4.21 shows the peak temperature perpendicular to the weld center line for different plunging forces.

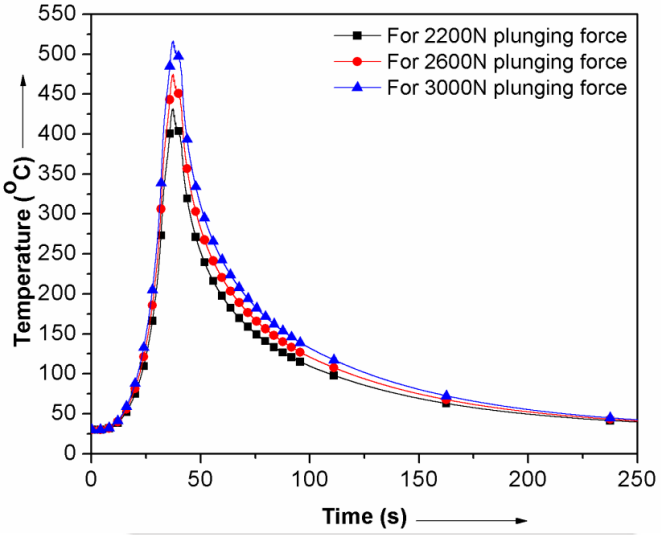

Figure 4.20 Time vs. Temperature distribution at center of weld line

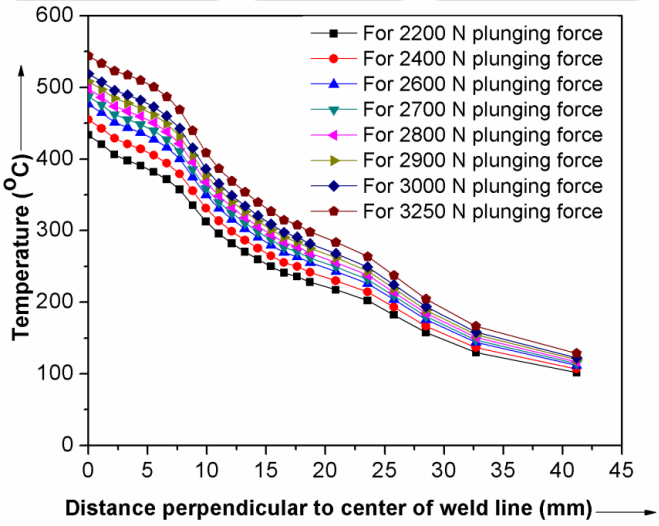

Figure 4.21 Peak temperature distribution perpendicular to the centre of weld line for various plunging forces

Except shoulder diameter all other parameters kept constant as stated in Table 4.3. The maximum temperatures at center line vary from 440-540^{0}C for different plunging forces as shown in Figure 4.21. It has seen that for every 100N increase in the tool plunging force the average peak temperature hiked to around 10^{0}C.

Twenty seven experiments were conducted and simultaneously temperature was measured by using Agilent data logger and K-type thermocouples. The transient temperature distributions were verified with experimental results. Experimental and numerical transient thermal profile is shown in Figure 4.18 and Figure 4.19. The process parameters used for experiment is shown in Table 4.4. After verifying the transient thermal history, the experimental peak temperatures were recorded for varying shoulder diameter and for varying tool plunging force. The comparison between numerical and experimental peak temperature at 5mm and 21mm away from center line are shown in Figures 4.22 and 4.23.

Table 4.4 Process parameter and shoulder diameters

Thickness of Plates (mm)	Rotational Speed (rpm)	Traverse speed (mm/min)	Shoulder diameter (mm)	Average Plunging force (N)
6.0	1400	112	20	3250

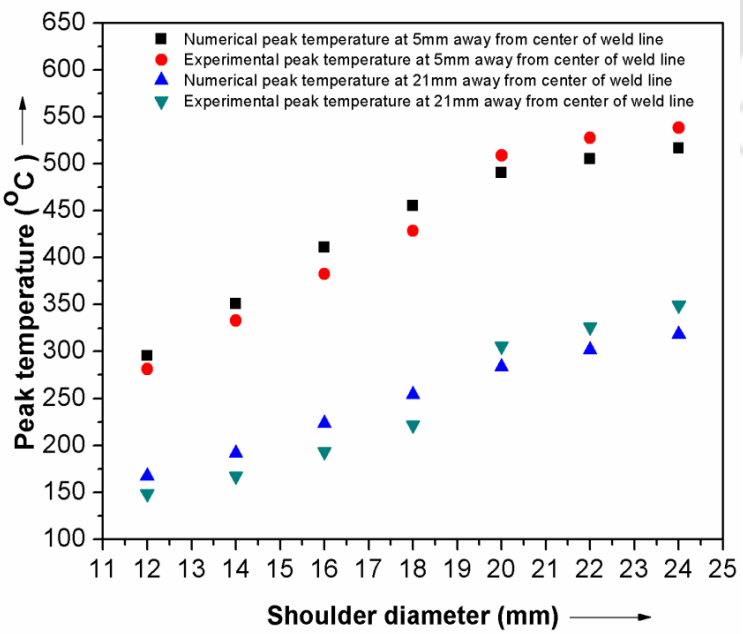

Figure 4.22 Numerical and experimental peak temperature at distance 5 mm and 21mm away from weld line

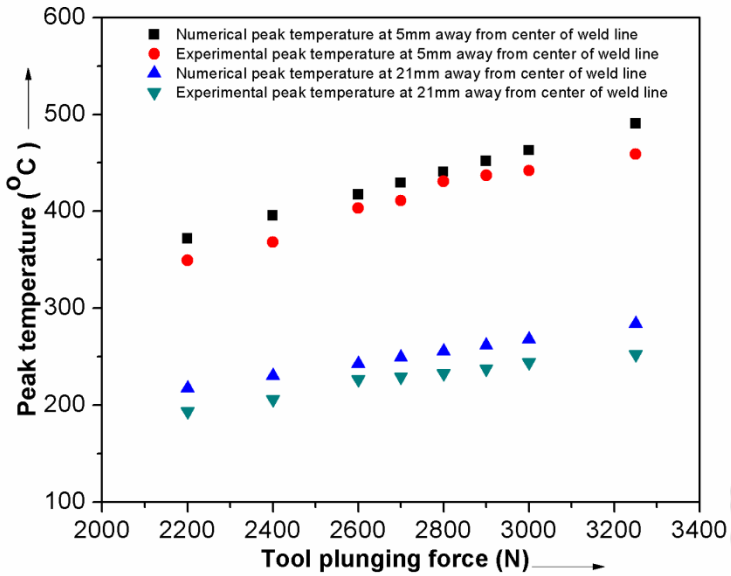

Figure 4.23 Numerical and experimental temperature vs. plunging force

4.2.1 Summary

The three-dimensional finite element model was developed for carrying out the transient thermal analysis of FSW of AA1000. The numerical results obtained were fairly evaluated and matched with the experimental results within the variation of 8%. There was an increment in the size of weld zone and peak temperature by increasing the tool shoulder diameter while keeping other process parameters constant. By increasing the shoulder diameter, cooling rate of workpiece was decreased and for the lesser shoulder diameter tools cooling rate was more. The time required to change temperature from 300^0C to 100^0C for 24mm shoulder diameter tool is 80 seconds where as for workpiece welded by 12mm tool is 50 seconds.

In the case of lower shoulder diameter tools, i.e.12mm to 20mm, for every 2mm increment in the shoulder diameter 6.5% of peak temperature raised and for bigger shoulder diameter tools (above 20mm diameter) for every 2mm raise in shoulder diameter only 1.8% of peak temperature was raised. The optimum temperature was obtained at around 3.3 ratio of tool shoulder diameter and pin diameter. By increasing the plunging force the temperature between the tool and the workpiece interface increases. It has been seen that for every 100N increase in the tool plunging force the average peak temperature hiked about 10^0C. And also it has been seen that with 10% increment of plunging force the peak temperature increment is

about 4.5%. The numerical and experimental peak temperature for varying shoulder diameters and varying plunging forces matched fairly well within the variation of 11%.

4.3 Numerical studies on thermal history of FSW on dissimilar alloys

In the present study FE transient thermal analysis of FSW for dissimilar material i.e. Al and Cu was done. Here, FSW tools having flat cylindrical shoulder and cylindrical tool pin is used which have 20mm shoulder diameter and 6mm pin diameter. For FE analysis brick elements were considered with fine meshing in the weld zone. The problem was solved by considering temperature dependent material properties. To reduce the computation time, coarse mesh was generated away from frictional heating region and finer mesh was generated along and near the frictional heating region. Numerical thermal history was estimated for FSW of 6mm thick Aluminum and 6mm Copper plates for different process parameters.

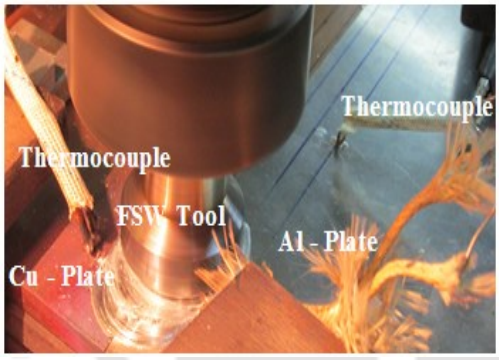

Figure 4.24 Cu-Al FSW process

Figure 4.25 Cu-Al FSW plate

Several test samples of 200 mm long and 100 mm wide taken from 6 mm thick AA1100 and B370 copper (Cu) plates were welded with the below referred FSW tools. A semi-automatic milling machine was modified and used as a FSW machine and the specifications are motor capacity: 7.5 HP, Rotational Speeds: 50–1500 rpm, Traversing Speeds: 22–555 mm/min. The tool was rigidly fixed on an arbour. The clamping of workpieces was done such that the movement of workpieces restricted in all degrees of freedom to with stand mainly plunging and translational forces of the tool. A typical FSW setup and a dissimilar metal weldment (i.e. Al and Cu) are shown in Figs.4.24 and 4.25.

Aluminum plate was kept in the advancing side and copper was kept in retreating side and the tool was kept at the center of the butted line. K type thermocouples were placed 12mm away from the weld center line. The FSW tool used in this experimentation was fabricated using the SS310 steel material. Agilent data acquisition system 34972A was used to record the

temperature data form both the alluminium copper plates. The results of FE thermal analysis results for dissimilar metals are shown in Figure 4.26 to 4.33.

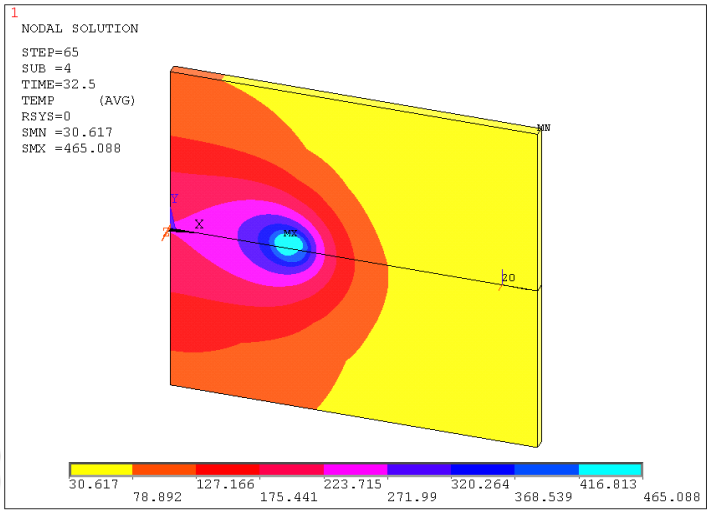

Figure 4.26 Temperature contour for traverse speed (t_s) = 120 mm/min, Rotational speed (r_s) = 1000 rpm and plunging force (p) = 4000 N

Figure 4.26 shows the temperature contour for particular process parameters i.e. for traverse speed (t_s) of 120 mm/min, rotational speed (r_s) of 1000 rpm and plunging force of 4000 N. The upper part is aluminum whereas lower part is copper. The maximum temperatures attained in Al and Cu for the above parameters is shown in Table 4.3 below.

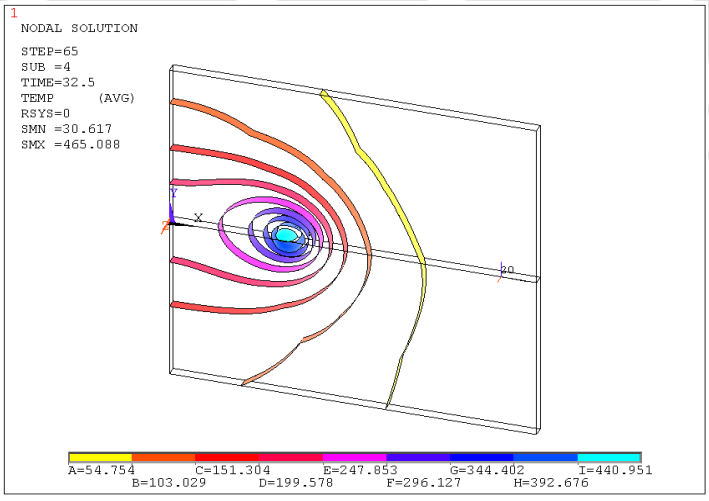

Figure 4.27 Temperature iso-contour for traverse speed (t_s) = 120 mm/min, rotational speed (r_s) = 1000 rpm and plunging force (p) = 4000 N

The isothermal contours for a particular time step during welding are shown in Figure 4.27. The variation in contour pattern on both sides i.e. upper Aluminum and lower Copper side

can be easily seen. It was observed that the temperature contours are not uniform. The temperature raises more in Al plate compare to Cu plate.

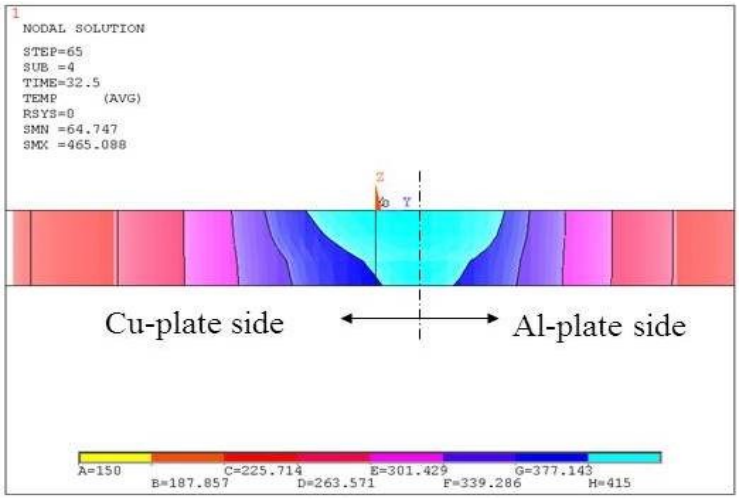

Figure 4.28 Cross-sectional temperature contour for traverse speed (t_s) = 120 mm/min, rotational speed (r_s) = 1000 rpm and plunging force (p) = 4000 N

The cross sectional temperature contour for traverse speed (t_s) of 120 mm/min, rotational speed (r_s) of 1000 rpm and plunging force of 4000 N is shown in Figure 4.28. Figure 4.29 and 4.30 represent the peak temperature perpendicular to the weld center line for different welding parameters.

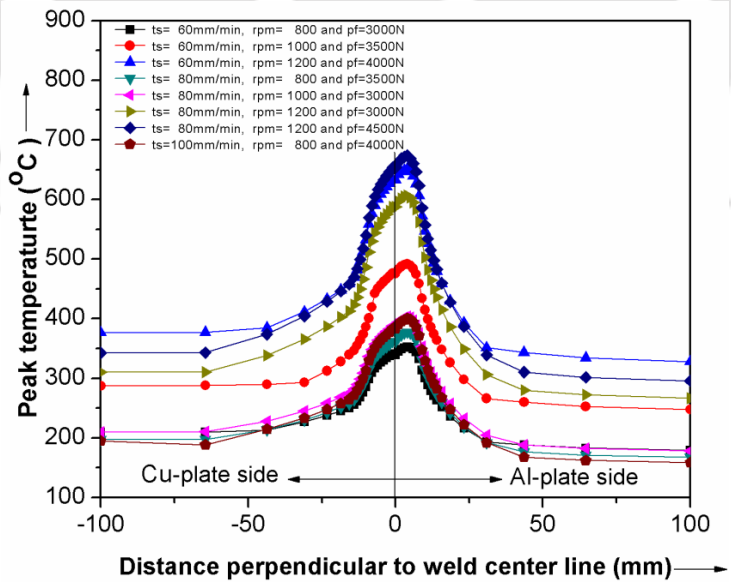

Figure 4.29 Peak temperature distributions at distance perpendicular to the centre of the weld line

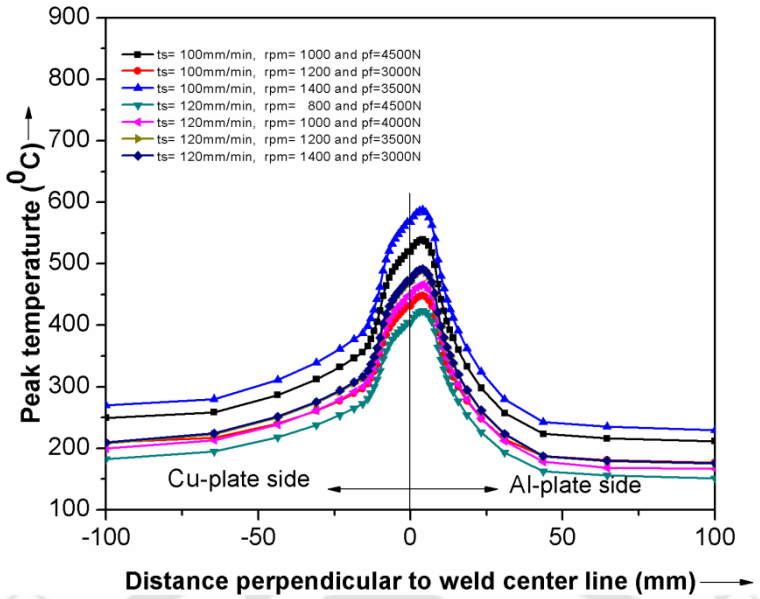

Figure 4.30 Peak temperature distributions at distance perpendicular to the centre of the weld line

The maximum temperatures at varying process parameters are listed and shown in Table 4.5. It has seen that the peak temperature varies non-uniformly about the center of weld line. All the finite element simulation results were tabulated and shown in Table 4.5.

Table 4.5 Process parameters versus maximum temperature

Tool transverse speed (mm/min)	Tool rotational speed (rpm)	Tool plunging force (N)	Maximum temperature at Cu Plate (^{0}C)	Maximum temperature at Al Plate (^{0}C)
60	800	3000	341.3494	353.0626
60	1000	3500	476.1225	491.9982
60	1200	4000	633.4853	651.2786
80	800	3500	361.869	377.7204
80	1000	3000	387.7978	403.5882
80	1200	4500	587.7266	606.9151
100	800	4000	382.9915	400.5528
100	1000	4500	519.9004	537.8155
100	1200	3000	431.2295	448.8898
100	1400	3500	567.6962	587.7519
120	800	4500	404.6735	423.562
120	1000	4000	447.0008	466.4833

120	1200	3500	469.4234	489.0886
120	1400	3000	472.7387	492.1551

A suitable co-relationship was established between the welding process parameters and peak temperatures attain both for Al and Cu plates. The co-relationships are shown in Figure 4.31 and Figure 4.32 respectively.

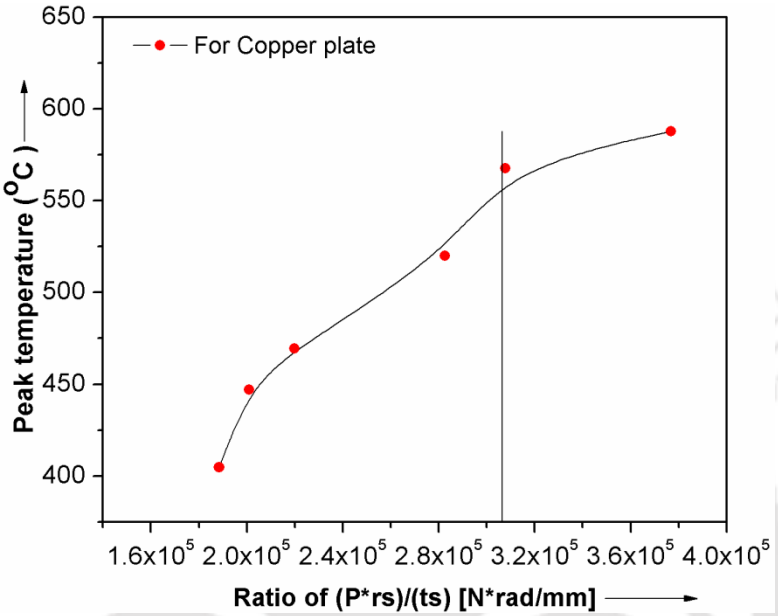

Figure 4.31 Plot of peak temperature versus Pr_s / t_s ratio [N rad/mm] for copper

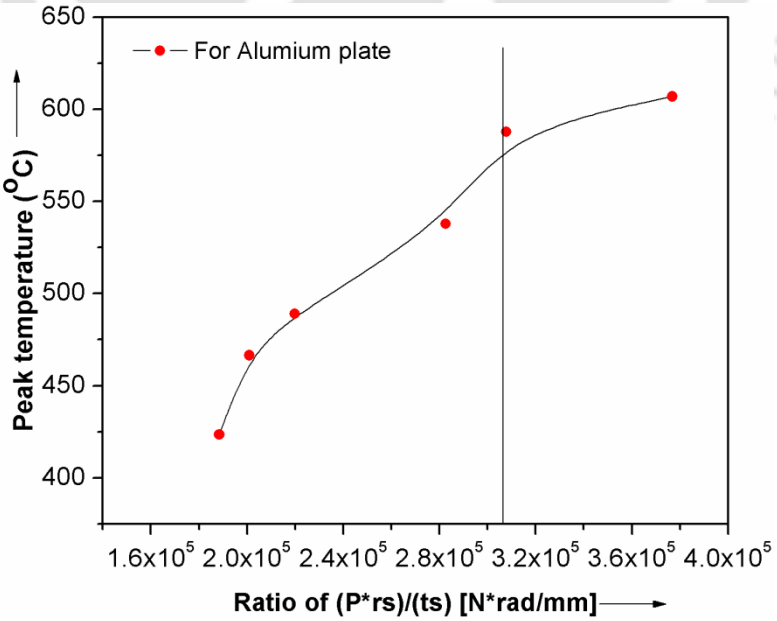

Figure 4.32 Plot of peak temperature versus Pr_s / t_s ratio [N rad/mm] for aluminium

From Figure 4.30 and 4.31 from the plots it can be seen that the peak temperature increases rapidly for the Pr_s / t_s ratio up to $3x10^5$ and beyond that the rise in the peak temperature is slow. It can be seen that rise in temperature is more in aluminium than copper.

The above FE numerical results are compared with the obtained experimental ones and found that the results of FE model of dissimilar Cu-Al alloy combination are fairly matched with the experimental results. Figure 4.33 shows the comparisons for both FE model and experimental FSW weldment shape.

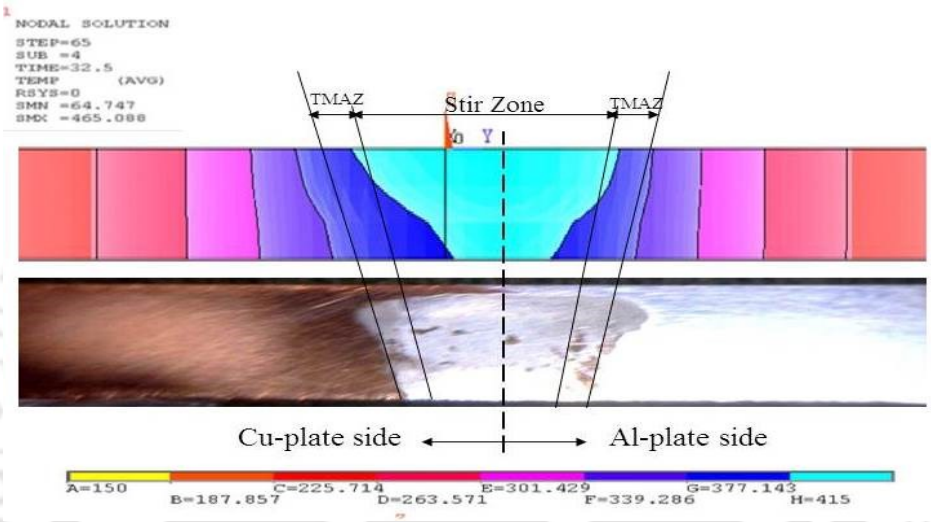

Figure 4.33 Comparisons of FE model and experimental weldment

The developed FE model is very useful to understand the temperature distribution throughout the two dissimilar metal plates. The temperature distribution at different weld zones can also be observed in the Figure 4.26. The maximum temperature achieved at center of the weld is about 460^0 C.

4.3.1 Summary

A 3dimensional finite element modelling approach was successfully used for the simulation and analysis of the dissimilar metal FSW, by using the simulation software ANSYS. The predicted overall thermal contours are fairly evaluated with the experimental results. It has seen that the peak temperature varies non-uniformly about the center of weld line at two dissimilar metal plates. The computed results were compared with experimental results to understand the influence of process parameters on the heat generation and weld quality. It was seen that the plunge force and tool rotational speed has major influence in the heat generation and weld quality. The average peak temperature difference between two dissimilar

materials is about 15^0C. i.e. alluminium side it is 15^0C more. Sound welds with defect-free joint can be produced by arranging Aluminium on advancing side with sufficient probe offset to Al side and with tool plunging force more than 3500N. Insufficient tool plunging force leads to the less heat generation and there by tunnel defects are produced due to the improper ramming effect on weld joint for this kind of incompatible material combination.

Chapter 5

FSW of similar materials

5.1 Introduction

This chapter focusses on the experimental investigations and analysis of the the quality of FSW weldments for similar materials. This chapter contains the following two sub-sections i.e.

5.2 Effect of tool pin geometries and process parameters on FSW of aluminum alloy and

5.3 FSW of thick sections of aluminum alloy

The section 5.2 deals with detailed experimental of various operating parameters on FSW of 6mm thick alluminium (AA1100) plates. Considering the improvements seen in the results of section 5.2 further investigations has done. The section 5.3 has focused on the welding of thick alluminium plates using the suitable optimal operating parameters and tool geometries obtained in the section 5.2. As per the defined objectives based on the gaps found in literatures the present chapter has been investigated.

5.2 Effect of tool pin geometries and operating parameters on weld quality of aluminum alloy

From the published literature study it was noticed that many authors are using some very exotic and complicated tool geometries, which are extremely difficult to manufacture. It was also observed that the tool pin profiles tend to wear out very fast eventually leading to a cylindrical/conical form, particularly while working with higher tensile strength materials. Though these complicated pin geometries were optimized for achieving the desired weld quality, consistently in the long run welds it becomes difficult to maintain because of wear and tear of the tool pins. Eventually they assume the shape of surface of revolution. Hence in the present work it was decided to study the performance of FSW tools having simple regular geometrical forms, like straight cylindrical, tapered cylindrical, trapezoidal, straight hexagonal and simple threaded. On prolonged usage, even if these tools wear down, they will attain tapered cylindrical or cylindrical shape. Therefore a systematic study of these regular simple geometric shapes was taken up to compare the effects of trapezoidal, hexagonal and threaded tool pins with tapered cylindrical and cylindrical pins.

The Previous investigation Chapter 4.2 was focussed on the effective shoulder diameter for FSW of 6mm thick aluminum plates and noticed that around 18-22mm shoulder diameter tools produces required temperature. In that study (i.e. section 4.2) the effect of tool pin geometry was ignored. Hence, in the present section an attempt was made to investigate the effect of various tool pin geometries having regular geometric shapes and process parameters on mechanical properties and microstructural characteristics of the welded joint made from commercial aluminum alloy. The investigation was based on extensive experimentations. Material SS310 was used to fabricate the FSW tools. The material composition and the relevant physical properties of SS310 are shown in Tables 5.1 and 5.2, respectively. The chosen tool geometries and the fabricated tools are shown in Figures 5.1 and 5.2 respectively. The welding parameters used in this present study are shown in Table 5.4.

Table 5.1 Composition of SS310 by percentage

Fe	C	Cr	Mn	Ni	P	S	Si
48–53	0.25	24–26	2	19–22	0.045	0.03	1.5

Table 5.2 Physical properties of SS310

Hardness, Brinell's	160
Tensile strength, ultimate (MPa)	655
Tensile strength, yield (MPa)	275
Thermal conductivity at 100 ^{0}C (W/m^2 K)	14.2

The tool material used in this present investigation was selected based on high strength and low thermal conductivity. Due to the low thermal conductivity the heat loss in the tool is less.

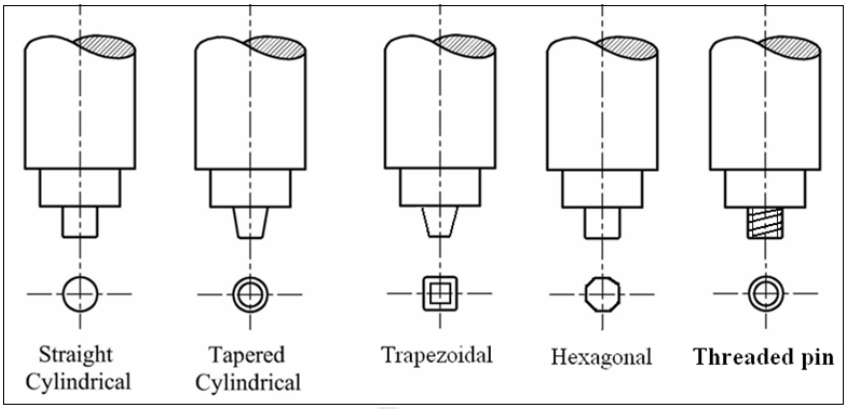

Figure 5.1 Different FSW tool geometries

Figure 5.2 Fabricated FSW tools

Table 5.3 Names of the tools used

Tool No.	Type of tool
1	Cylindrical probe of 6mm diameter
2	Cylindrical probe of 5mm diameter
3	Trapezoidal probe
4	Tapered cylindrical probe
5	Hexagonal probe
6	Threaded probe

Table 5.4 Process parameters for 6mm thick aluminum plates

Expt. No.	Tool rotational speed (rpm)	Tool transverse speed (mm/min)
1	1000	80
2		112
3		160
4	1400	80
5		112
6		160
7	2000	80
8		112
9		160

5.2.1 Metallographic examination

Metallographic tests on the transverse cross sections of different welded samples were carried out to study the microstructures of different zones of the welded samples. The variation of average grain size with different tool geometries at a particular tool traverse speed (i.e. 80mm/min) and tool rotational speed (i.e. 1400rpm) was observed as given in Table 5.5.

Table 5.5 Variation of average grain size with tool geometry

	Hexagonal pin	Cylindrical pin with 6mm dia.	Cylindrical pin with 5mm dia.	Tapered cylindrical pin	Trapezoidal pin	Threaded pin
Grain size in HAZ(μm)	23.81	26.73	22.93	22.62	21.80	28.71
Grain size in WN (μm)	10.73	12.92	11.13	9.62	9.12	13.52

In all the cases substantial grain refinement was observed in weld nugget zone (WN). The maximum reduction of grain size was observed in case of FSW tools having tapered cylindrical pin and trapezoidal pin. The effect of variation of tool rotational speed and tool traverse speed on grain size of heat affected zone (HAZ) and weld nugget (WN) were further studied. Since tools having trapezoidal pin geometry resulted in maximum grain refinement,

this particular pin geometry was considered for studying the effect of process parameters on the resulting grain structure at HAZ and WN. The measured grain sizes obtained for varying process parameters are listed in Table 5.6. Increase in tool rotational speed at a given welding speed increases the strain rate of the plasticized material, thus affecting the resulting microstructure of the stirred zone, i.e. the weld nugget. Increased strain rate with reduced weld speed, i.e. increasing the dwell time of the tool pin causes higher levels of grain refinement. Figures 5.3, 5.4 represent the microstructures of the samples welded by using trapezoidal pin tools and parameters of Expt. No 1 and 2 as shown in Table 5.4.

Table 5.6 Variation of average grain size with FSW process parameters

Process parameters		Average grain size (µm)	
Welding speed (mm/min)	Tool rotational speed (rpm)	HAZ	WN
80	1000	22.52	10.74
	1400	21.80	9.12
112	1000	23.70	12.84
	1400	22.90	10.55
	2000	21.92	10.27

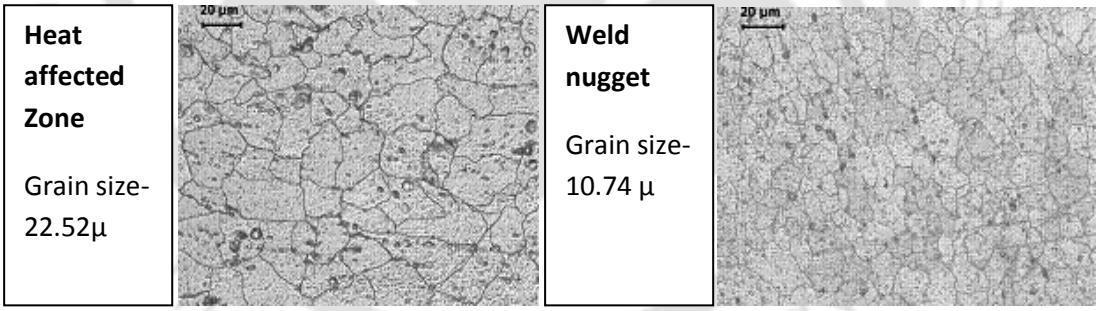

Figure 5.3 Trapezoidal pin tool 1000rpm 80 mm/min feed

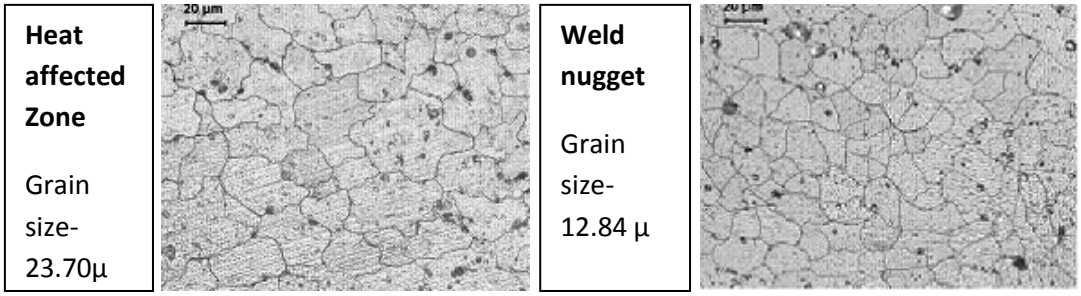

Figure 5.4 Trapezoidal pin tool 1000rpm112 mm/min feed

5.2.2 Vickers micro hardness

Hardness measurements were taken on the cross sections perpendicular to the welding direction. Welding was carried out using trapezoidal tool with varying process parameters. Test samples for hardness measurement were taken from two groups of welded samples. The 1st group (Expt No: 1, 2, 3) comprised of test pieces welded at constant welding speed with increasing tool rotational speed from 1000 to 2000rpm which is shown in Table 5.4. Whereas in case of the 2nd group (Expt No: 2, 5, 8), the tool rpm was kept constant and the weld speed was increased from 80 mm/min to 160 mm/min.

The hardness at the different zones of the test samples was measured. The variation of hardness at different zones for the test pieces in group-1 is shown in Figure 5.5. As such no specific trend could be observed accepting that the hardness in the weld nugget and thermo mechanically affected zone was found to have lower hardness than that of the parent metal.

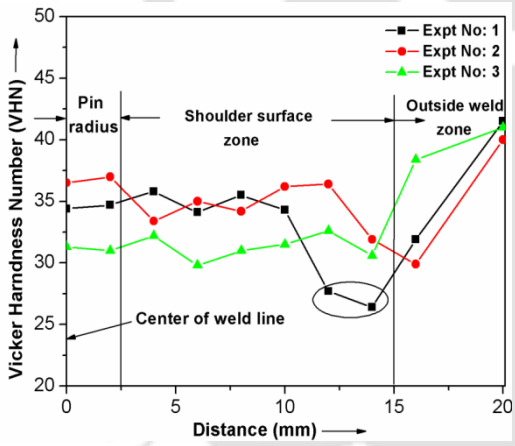

Figure 5.5 Hardness at different zones for varying weld speed, at 1000 rpm

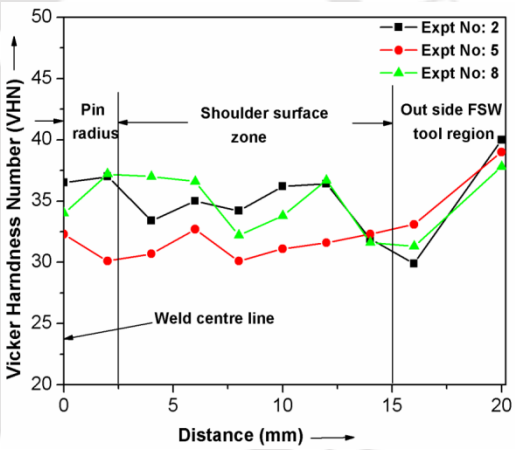

Figure 5.6 Hardness at different zones for varying tool rpm, at 112mm/min

The variation of hardness values for the group-2 test pieces is shown in Figure 5.6. Here one can distinctly observe the effect of increasing welding speed. With increase in weld speed from 80 mm/min to 160 mm/min a clear decrease in hardness was observed as shown in Figure 5.5. The encircled points in the plots deviated excessively out of the normal scatter of the data. This was due to some faulty measurement or some unknown reasons and accordingly these data were ignored. Figure 5.6 represents the variations in hardness for the specimens welded at 112mm/min constant speed.

The effect of different tool pin geometries on hardness was studied on test pieces welded at 1400 rpm with 112 mm/min speed. The six different tool used in this study have been given in Table 5.3. The hardness measured at different zones of the welded samples was plotted as shown in Figure 5.7. An overall reduction in hardness was observed in the weld nugget and thermo mechanically affected zone for varying pin geometry. However maximum reduction in hardness took place in case of threaded, conical, and trapezoidal pin configurations.

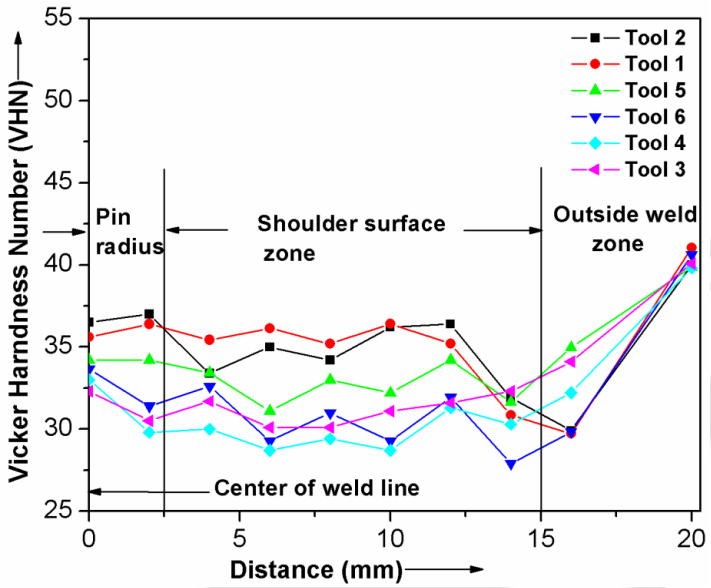

Figure 5.7 Vickers Hardness at different zones for varying FSW tool pin geometries

5.2.3 Tensile strength

The tensile test specimens were taken perpendicular to the welding direction from the welded test samples. All tensile tests were performed at a constant crosshead displacement rate of 1 mm/min using a Tinius Olsen tensile testing machine. Some of the test samples are shown in Figure 5.8.

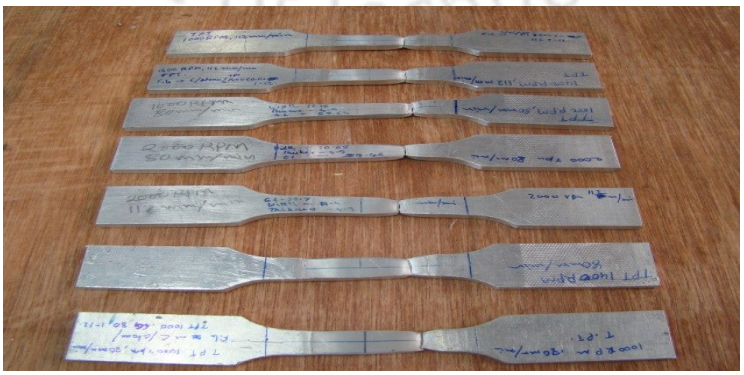

Figure 5.8 Tensile test samples

The tests were carried out to study the load-deflection/stress-strain characteristics for the following 2 conditions:

i) Different tool rpm and traverse speed, keeping the tool geometry fixed.
ii) Different pin geometries, keeping tool rpm and traverse speed constant.

The effect of variation of tool pin geometry on the load-deflection/stress-strain characteristics of the tensile test specimens welded at 80 mm/min speed with 1400 rpm is shown in Figure 5.9. Here one can observe that the samples welded with FSW tools having trapezoidal pin (Tool 3) and tapered cylindrical pin geometry (Tool 4) exhibited about 50% increase in the ductility compared to that of the original base metal (BM).

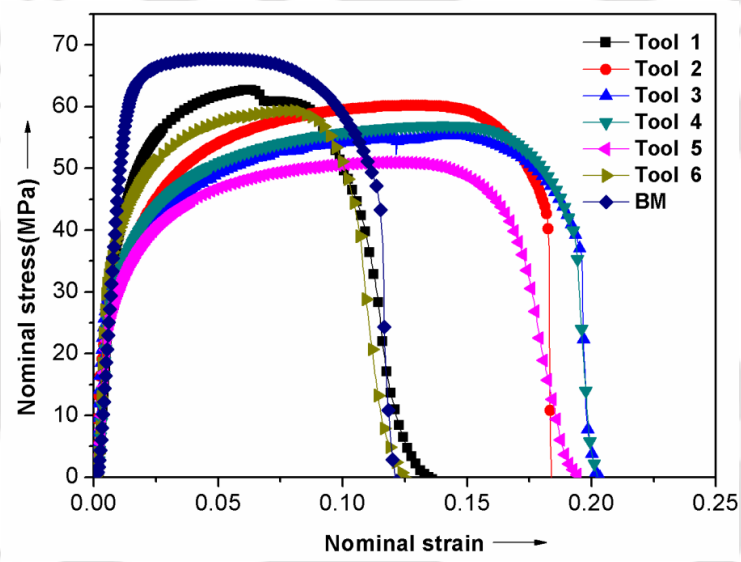

Figure 5.9 Effect of variation of tool pin geometries on engineering stress-strain characteristics of the test specimens

The effect of variation of tool rotational speed and welding speed is shown in Figure 5.10. Here all the welding was carried out using a tool having 5mm diameter straight cylindrical pin. With the variation in tool rpm and traverse speed, a definite amount of variation occurred in tensile strength and elongation of the test samples.

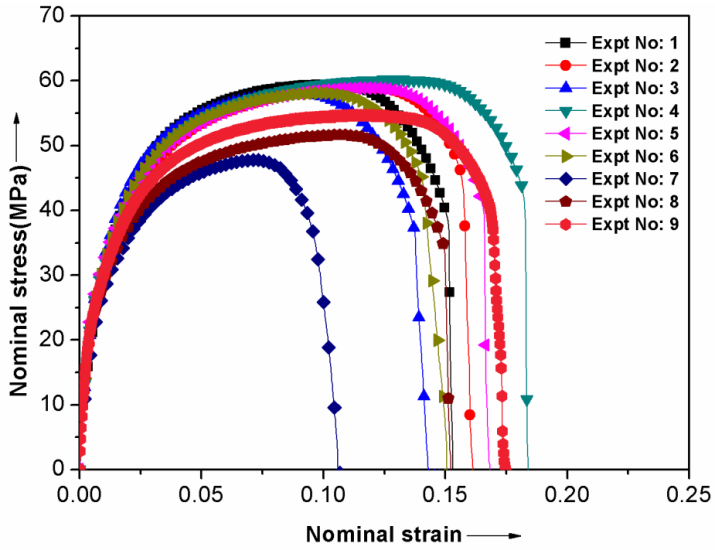

Figure 5.10 Effect of tool rpm and welding speed on engineering stress-strain characteristics of the test specimens

To achieve a good weld joint using FSW, the first and foremost requirement is full consolidation of material at the mating edges of the plates through adequate stirring action by the FSW tool pin. Plasticization of the material takes place under the action of heat generated through friction and mechanical deformation at the tool-work piece interfaces. Hence the contribution towards heat generation by the pin is quite insignificant. However the pin plays an important role towards shearing of the material and thereby consolidating the material at the mating edges.

The extreme mechanical deformations caused by the shearing action resulted in finer grain structure at the weld nugget. The trapezoidal pin (Tool 3) showed maximum grain refinement. Maximum shearing of metal in the nugget zone was expected under the action of tapered pin configurations because of the downward component of the frictional force at the pin surface. Thus consistently lowest level of hardness was observed in the weld nugget produced by tools having tapered pins. Thereby the welding produced by these tools naturally exhibited higher ductility in the test samples. Thus one can observe that taper configuration of pin geometries leads to desirable mechanical properties.

On the other hand the microstructure and thereby the mechanical properties depend on the pin geometry, at the same time it also depends on the combined action of tool rotational speed as well as tool traverse speed. With increase in tool rpm the stirring action increases causing higher ductility. Therefore at lower traverse speed higher tool rpm causes higher degree of

straining leading to formation of finer grains at the weld nugget. If the rpm is further increased keeping welding speed low, it causes an effect of saturation in the stirring action thereby saturation in the straining of the material leading to reduction in sticking condition. These results in formation of worm-hole defects which is reflected in loss of strength of the test samples. Similarly, if the weld speed is too high, the stirring action will suffer causing inadequate consolidation of material at the weld butt. This leads to worm-hole defects as well as there will be loss in ductility and increase in hardness due to inadequate grain refinement. Hence it was felt that a more adequate parameter would be the ratio of tool rpm to tool traverse speed.

The maximum load (tensile strength) sustained by the test specimens and the elongation (ductility) were plotted against the ratio of tool rpm to tool traverse speed as shown in the Figures.5.11 and 5.12 respectively. As expected the plots clearly indicate a distinct dependence of the mechanical properties on the rpm- traverse speed ratio.

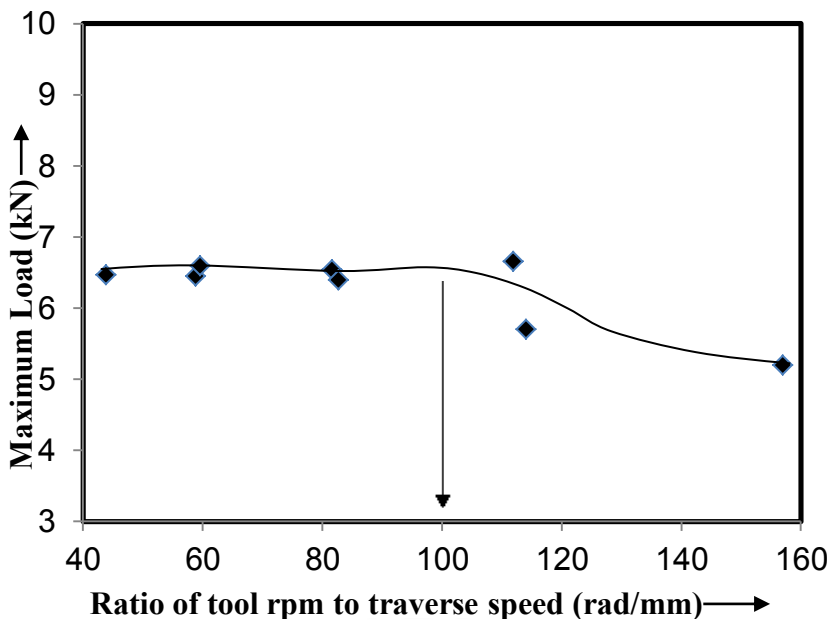

Figure 5.11 Effect of the ratio of tool rpm to tool traverse speed on maximum load

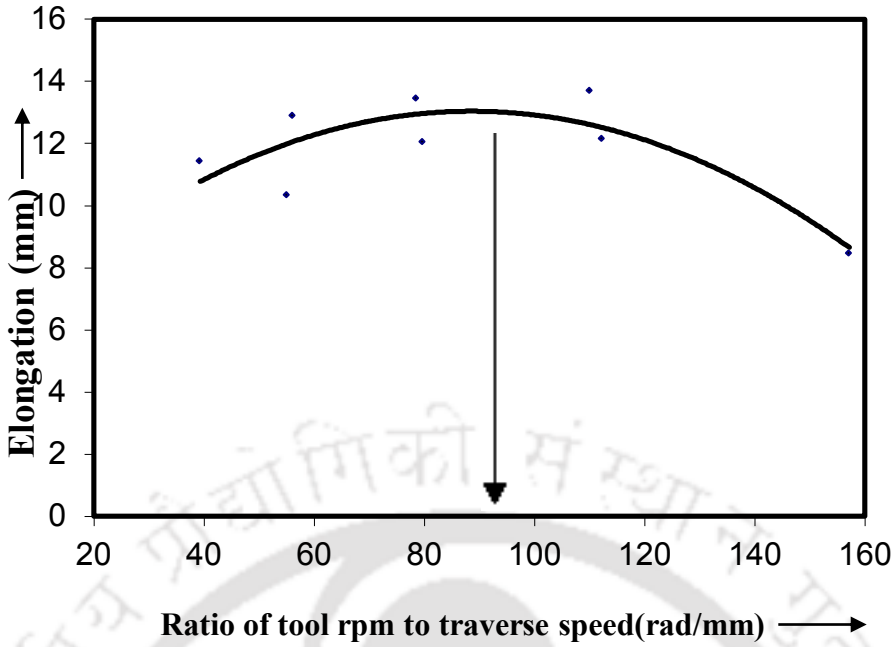

Figure 5.12 Variation of elongation of test specimens with the ratio of tool rpm to tool traverse speed

A sharp drop in the maximum load (tensile strength) beyond about 100 rad/mm can be seen in Figure 5.11, whereas at about 93 rad/mm it relates to maximum elongation as shown in Figure 5.12. Hence one can take a suitable ratio of tool rpm to tool traverse speed between around 95 to 100 rad/mm to decide on the weld parameters to achieve friction stir welded joints free of defects having maximum ductility as well as load bearing capacity.

5.2.4 Summary

This investigation showed that friction stir welding of commercial grade aluminum alloys (AA1100) can be successfully done achieving the desired properties using tools having tapered cylindrical or trapezoidal pin geometry. The overall mechanical response highly depends on the ratio of tool rpm to tool traverse speed. It was found that to achieve friction stir welded joints having maximum ductility as well as load bearing capacity a suitable ratio of tool rpm to tool traverse speed between around 95 to 100 rad/mm should be considered to decide on the weld parameters.

5.3 Friction stir Welding of thick aluminum alloy plates

The present section provides a methodology on Friction Stir Welding of thick aluminum alloy plates (i.e. 12mm thick). Most of the investigations on friction stir welding (FSW) of aluminum alloy plate thickness limited to about 5 to 6 mm. In this present study an attempt was made to weld comparatively higher thick plates. Here, the various aspects concerning the process parameters and FSW tool geometry were studied on friction stir welding of 12 mm thick commercial grade aluminum alloy.

In the present study two different tool geometries were considered. They were, a) Tapered cylindrical probe and b) Trapezoidal probe. These tool geometries were selected based on the previous studies (i.e. in section 5.2) used successfully to weld thick alluminium alloy plates. The FSW tool material used in present study was stainless steel grade 310 i.e. SS310. The material composition and the relevant physical properties of the material used for manufacturing the tools are shown in Tables 1 and 2, respectively. The two fabricated tools for FSW of 12mm thick plates are shown in Figure 5.13 and Figure 5.14 respectively.

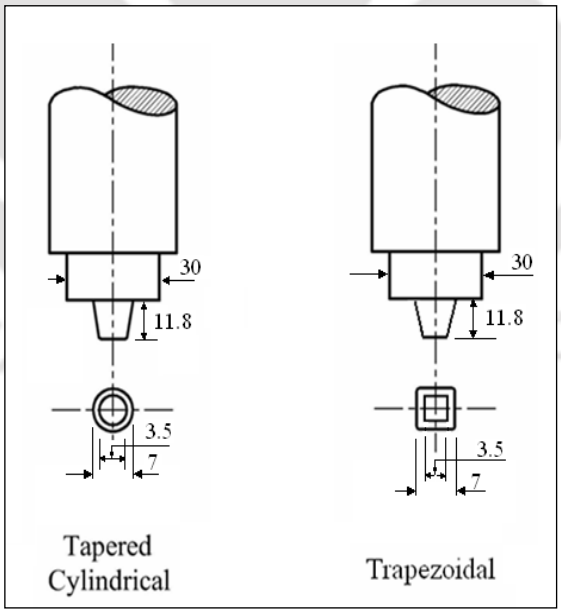

Figure 5.13 Different FSW tool geometries (all dimensions are in 'mm')

Figure 5.14 Designed and developed FSW tools

Several test samples were welded with various combinations of tool rpm and welding speed for both the tool geometries. However it was observed that low tool rpm resulted in consistently poor quality of welding. Whereas best results were obtained with tool rpm of 2000 in conjunction with low weld speed. This happened because of high tool rpm with low weld speed caused severe mechanical stirring of the metal causing reduction in grain size leading to higher strength of the welded joints. That is why in this paper; the results with 2000 rpm tool rotational speed were reported.

5.3.1 Tensile Properties

The FSW tools and process parameters were evaluated by testing the weld samples. In FSW process stirring/churning of metal takes place in the weld nugget zone and thus the grain refinement expected in this weld zone. The FSW welds were cut according to the ASTM specifications for tensile testing as shown in Figure 5.15.

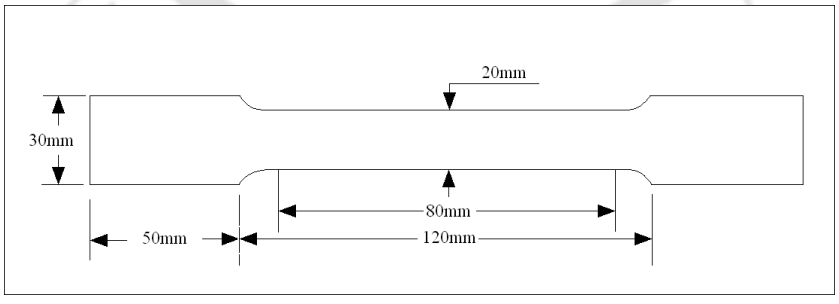

Figure 5.15 Detail dimension of tensile test specimen

Welding was carried out with different sets of welding parameters with trapezoidal probe and tapered cylindrical probe FSW tools as shown in Tables 5.7 and 5.8 respectively.

Table 5.7 Welding process parameters for trapezoidal probe geometry

Sl. No.	Plate thickness (mm)	Tool rotational speed (rpm)	Tool transverse speed (mm/min)	Observation from Tensile test (Breaking zone)	Quality of weld
1	12	2000	28	Outside the welding zone	Good
2	12	2000	40	Outside the welding zone	Good
3	12	2000	56	Outside the welding zone	Good
4	12	2000	80	Middle of the welding zone	Poor
5	12	2000	112	Middle of the welding zone	Poor

Table 5.8 Welding process parameters for tapered cylindrical probe geometry

Sl. No.	Plate thickness (mm)	Tool rotational speed (rpm)	Tool transverse speed (mm/min)	Observation from Tensile test (Breaking position)	Quality of weld
1	12	2000	28	Outside the welding zone	Good
2	12	2000	40	Outside the welding zone	Good
3	12	2000	56	Middle of the welding zone	Poor
4	12	2000	80	Middle of the welding zone	Poor
5	12	2000	112	Middle of the welding zone	Poor

The tested tensile samples for tapered cylindrical probe geometry are shown in Figures 5.16 and 5.17 respectively. Figures 5.16(a) and 5.16(b) represent the tensile test samples for the welding parameters as shown in Sl. No. 2 of Table 5.7. Figure 5.16 (c) represents the tensile test sample for the welding parameters as shown in Sl. No. 1 of Table 5.7. Figure 5.17(a) represents the tensile test samples for the welding parameters as shown in Sl. No. 3 of Table 5.8. Figure 5.17(b) represents the tensile test sample for the welding parameters as shown in Sl. No. 4 of Table 5.8.

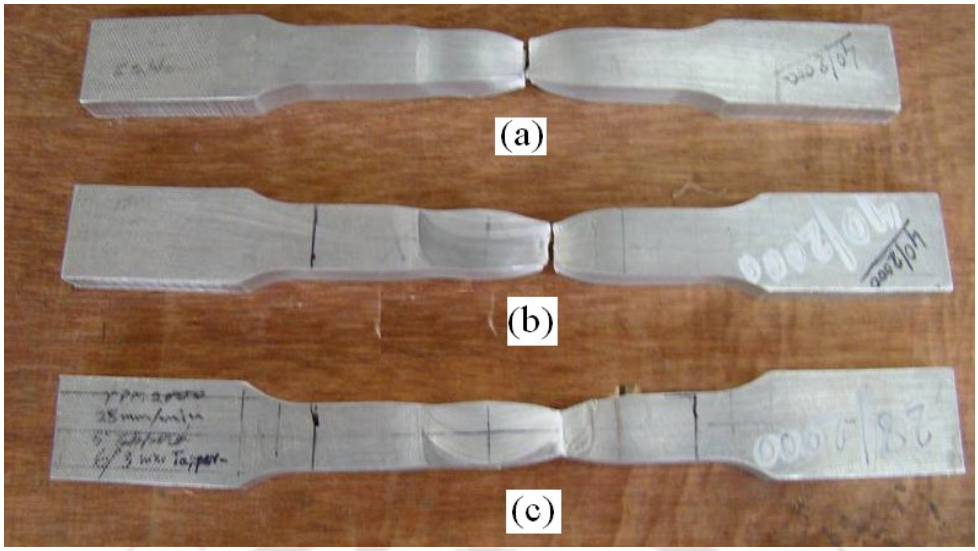

Figure 5.16 Some of the tested tensile specimens of FSW Joints of good quality

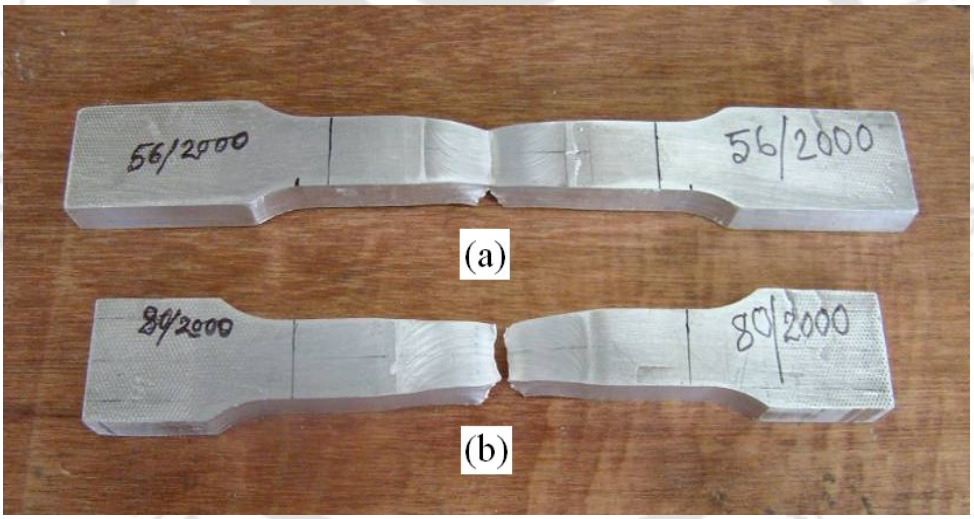

Figure 5.17 some of the tested tensile specimens of FSW Joints of bad quality

The tensile test results with varying tool traverse speed and constant rotational speed for trapezoidal tool pin geometry are shown in Figures 5.18 to 5.21. Here one can observe a very distinct and conspicuous effect on the maximum elongation with variation of traverse speed. With increasing welding speed for a particular tool rpm, a sharp drop in maximum elongation was observed. Here it was also observed that with increasing welding speed for a particular tool rpm, a sharp drop in nominal stress and strain as shown in Figure 5.21.

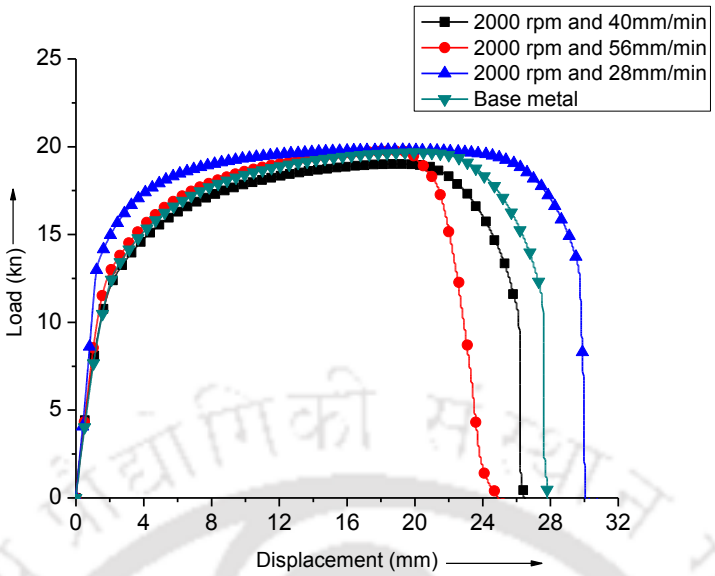

Figure 5.18 Load vs. displacement for Trapezoidal probe geometry

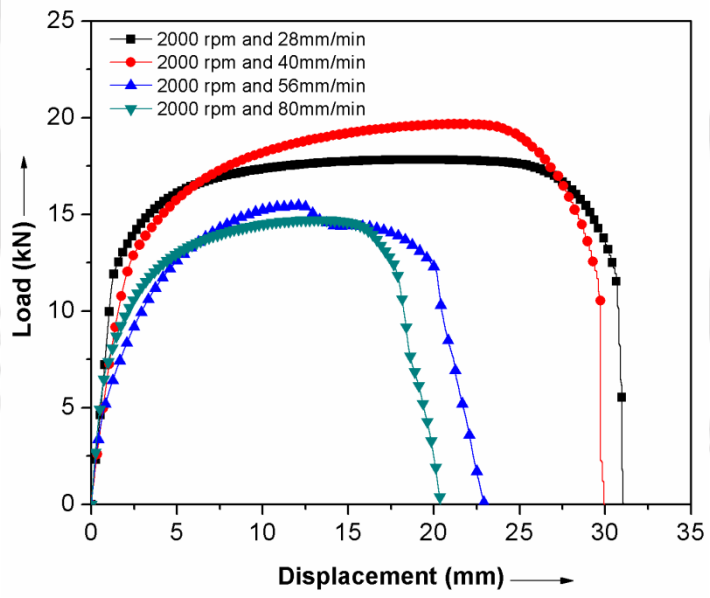

Figure 5.19 Load vs. displacement for tapered cylindrical probe geometry

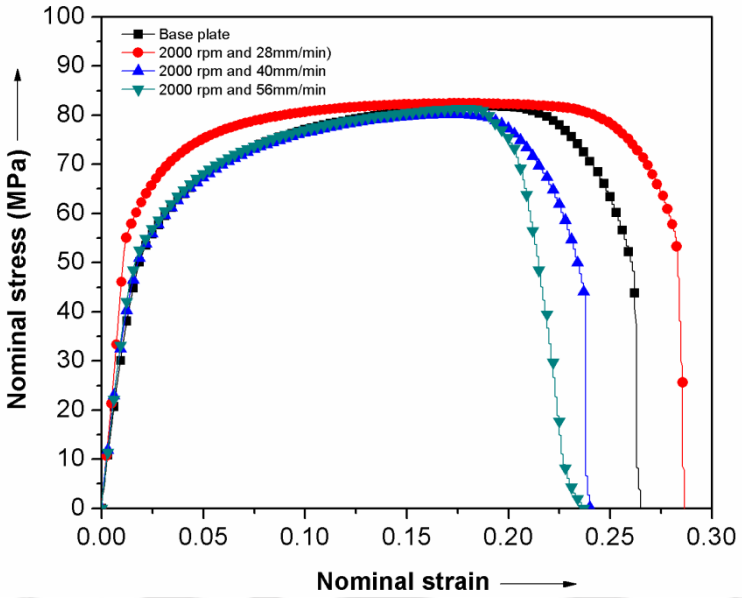

Figure 5.20 Nominal stress vs. Nominal strain for Trapezoidal probe geometry

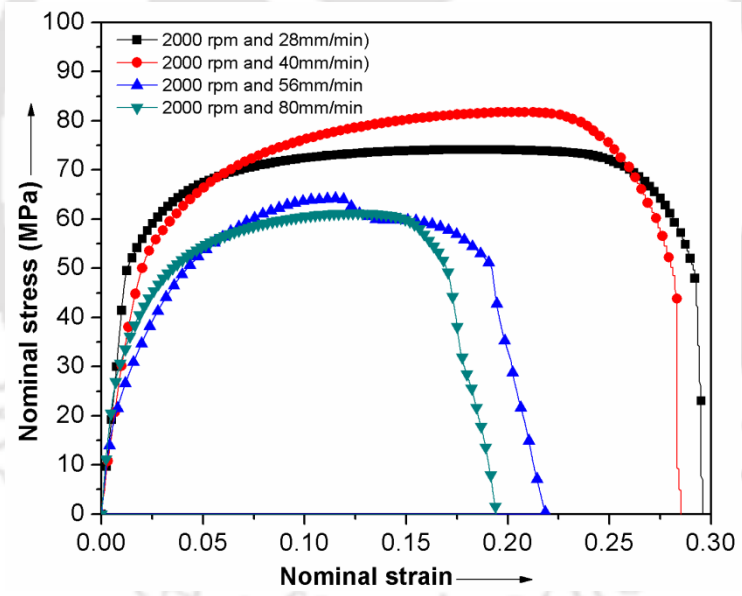

Figure 5.21 Nominal stress vs. Nominal strain for tapered cylindrical probe geometry

5.3.2 Effect of dwell time on mechanical properties

Initially the material was preheated by the stationary, rotating tool in order to achieve a sufficient temperature ahead of the tool. This period may also include the plunge of the tool into the workpiece. Here the dwell time was taken as the summation of plunging time of the tool into the workpiece and preheating time of stationary rotating tool. Keeping the plunging

time constant and varying the preheating time, i.e. the dwell time was varied. To study the effect of dwell time, the tensile test specimens were taken 50mm away from the starting position of welding as shown in Figure 5.22. The effect of dwell time on tensile properties of FSW samples welded by conical probe FSW tool is shown in Figure 5.23.

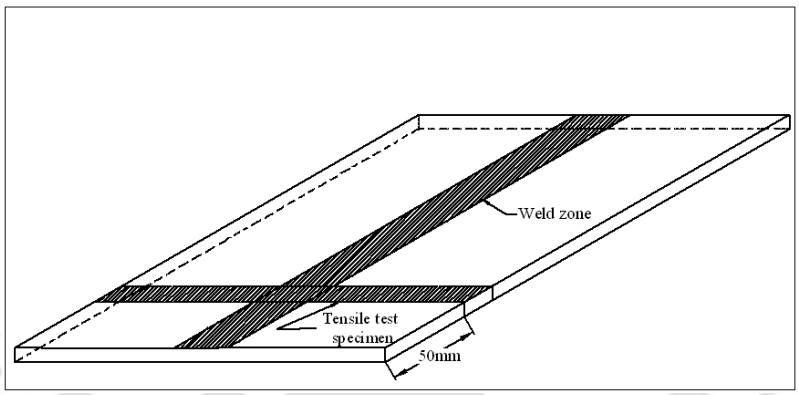

Figure 5.22 Position of tensile test specimen

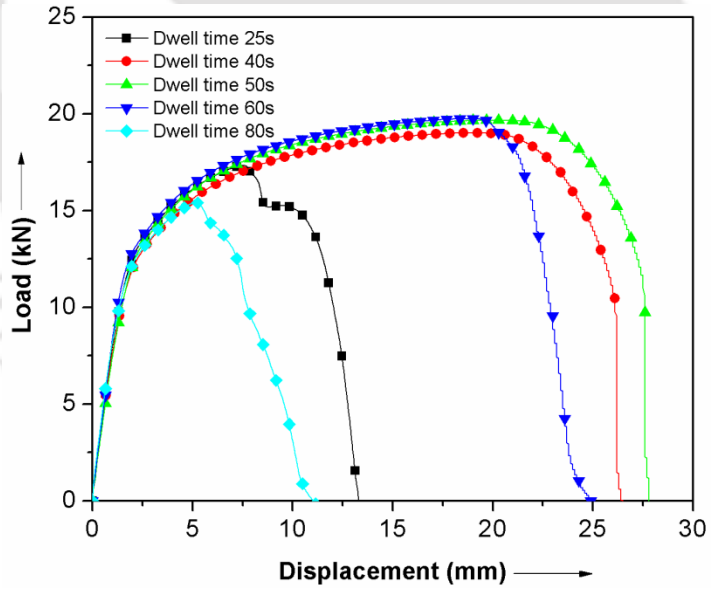

Figure 5.23 Effect of dwell time on tensile properties of FSW weld samples

From Figure 5.23 it can be observed that dwell time have significant effect on tensile property. It was observed that it has a very significant effect closer to the starting position of welding. A sharp drop in elongation was observed both at very low and high dwell time. From macroscopic view of weld cross section, it was observed that at very low dwell time (i.e. lack of heating) proper mixing of material did not take place at the weld nugget as shown

in Figure 5.24. Whereas with high dwell time causing higher temperature rise wormhole defects were observed in the weld zone as shown in Figure 5.23.

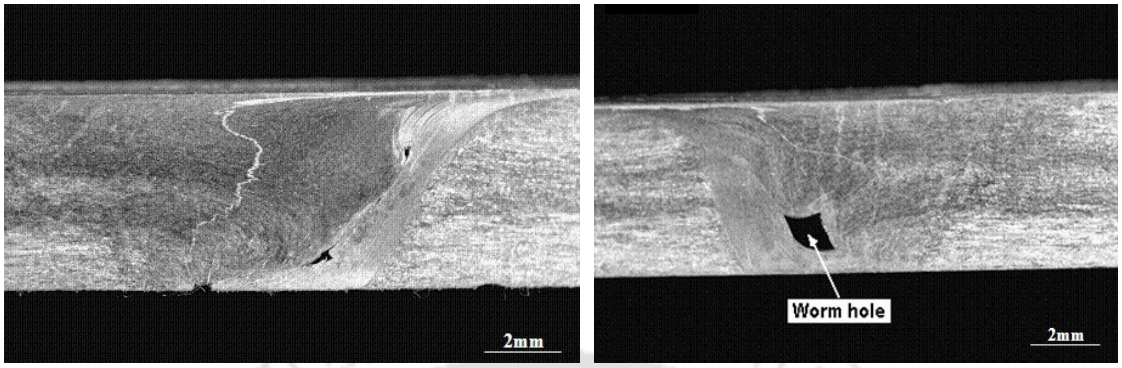

(a) (b)

Figure 5.24 Macrographs (a) Improper mixing of material (b) Wormhole due to high dwell time

5.3.3 Microstructure

The microstructures were observed by metallurgical microscope which is shown in Figure 3.18 in chapter 3. The microstructures of two different tool geometries are shown in Figures 5.25 and 5.26.

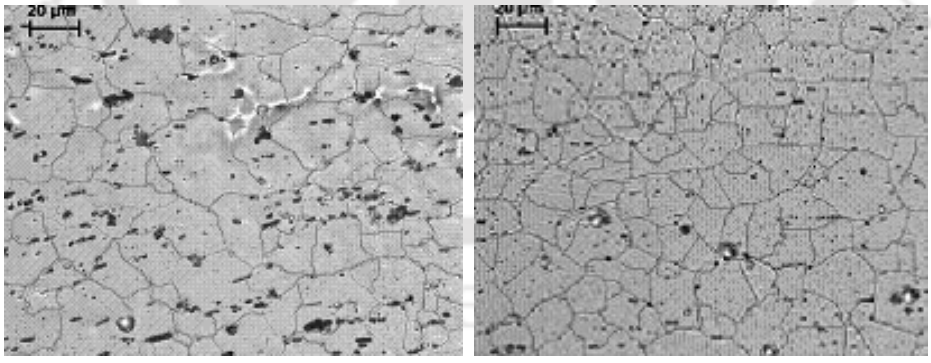

a) TMA Zone
Average Grain size-23.27µ

b) Weld nugget Zone
Average Grain size-10.51µ

Figures 5.25 Trapezoidal pin with tool rotational speed 2000rpm and welding speed 40 mm/min

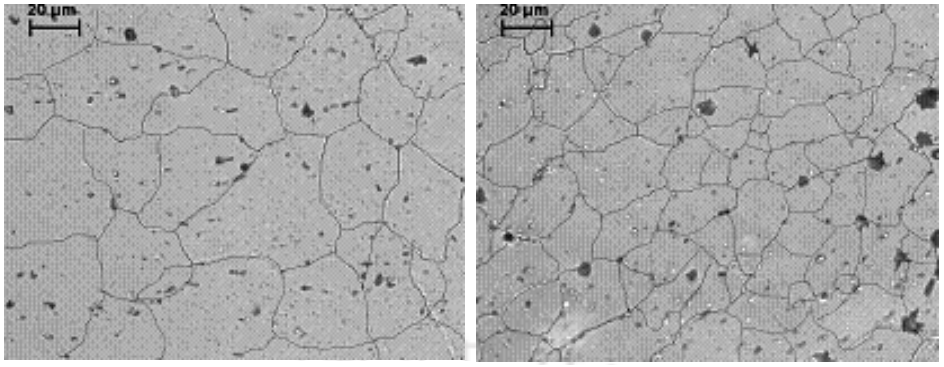

a) Thermo-mechanically affected Zone
Average Grain size-25.93µ

b) Weld nugget Zone
Average Grain size-11.96µ

Figure 5.26 Tapered cylindrical pin with tool rotational speed 2000rpm and welding speed 40 mm/min

From Figures 5.25 and 5.26, it was observed that the grain size reduced in weld nugget zone and it was elongated in thermo-mechanically affected zone.

5.3.4 Micro-hardness

The microhardness of the FSW samples was measured using a computerized microhardness tester shown in Figure 3.15 in chapter 3. Hardness measurements were taken on the cross sections perpendicular to the welding direction. With increase in weld speed from 28 mm/min to 56mm/min a distinct decrease in hardness was observed as shown in Figure 5.27. The weld nugget exhibited microhardness a little higher compared to that of the thermo-mechanically affected zone (TMAZ) and heat affected zone (HAZ). It is to be considered here that the microhardness of the weld nugget and TMAZ are material specific to some extent and the material used for the investigation was commercial grade aluminum alloy. The microhardness characteristics of the weld and TMAZ might be different for other non- heat treatable aluminum alloy. The hardness values were found minimum in the heat affected zone i.e. near the parent metal and tool shoulder edge junction region. In general the hardness values are less in the weld and TMAZ compared to that of the parent metal.

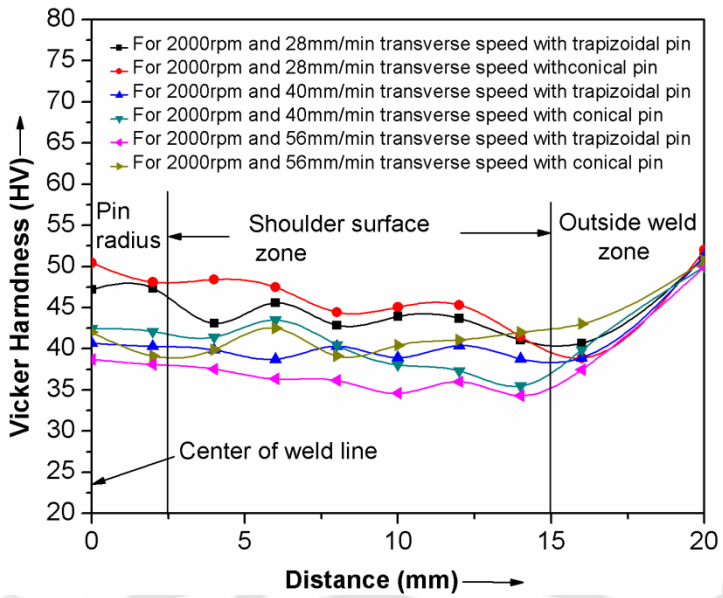

Figure 5.27 Vickers Hardness at different zones of weld samples

5.3.5. Summary

Successful friction stir welded joints were achieved for 12mm thick commercial grade aluminum alloy plates. Higher tool rpm with low welding speed resulted in finer grain structure leading to higher strength as well as higher ductility of welded joints. The tensile strength of the FS welds was found to be similar to that of base metal. Lower welding speed resulted in higher ductility exhibited through higher elongation. This indicates that lower range of weld speed is suitable for achieving superior mechanical properties. Dwell time have significant effect on tensile property and quality of welded joint. It has a very significant effect closer to the starting position of welding. At very low and high dwell time the ductility of welded joints reduces significantly.

With increase in weld speed the hardness increase in weld nugget zone (NZ) and thermo-mechanically affected zone (TMAZ) showed a decreasing trend. It was also observed that the weld nugget exhibited marginally higher microhardness as compared to the thermo-mechanically affected zone (TMAZ) and heat affected zone (HAZ). The hardness values were found to be a minimum near the parent metal and tool shoulder edge junction region. In general the hardness values were less in the weld and TMAZ compared to that of the parent metal. The average micro-hardness of the NZ and TMAZ was found to be more for conical probe compared to the trapezoidal probe for same welding parameters. This might be due to the better stirring of the material due to the trapezoidal probe.

Chapter 6

FSW of dissimilar materials

6.1 Introduction

The importance of this chapter is to analyse the quality of FSW weldments for dissimilar materials. This chapter covers two sub-topics i.e.

6.2 FSW of aluminum and copper alloy plates and

6.3 Parametric investigation of FSW on dissimilar aluminum alloys

Section 6.2 focusses on the mechanical and microstructural properties of dissimilar FSW welds, i.e. aluminum to copper. Section 6.3 consists of friction stir welding of dissimilar alluminium alloys, i.e. AA1100 to AA5083. In this study, the optimisation of process parameters has been done for obtaining the acceptable dissimilar welds using grey-taguchi technique.

6.2 FSW of alluminium and copper alloy plates

The present section manifests that FSW is a feasible avenue for joining of 1100 aluminium (Al) to B370 copper (Cu) plates. In this study the effect of different process parameters (i.e. tool geometries, tool rotational speed, tool traverse speed and tool plunging depth) on weld quality have been investigated. Figure 6.1 illustrates the experimental setup and Figure 6.2 shows the tool used in the present work. Tools were fabricated using D3 Tool steel. This work contains both microstructural study and mechanical properties study.

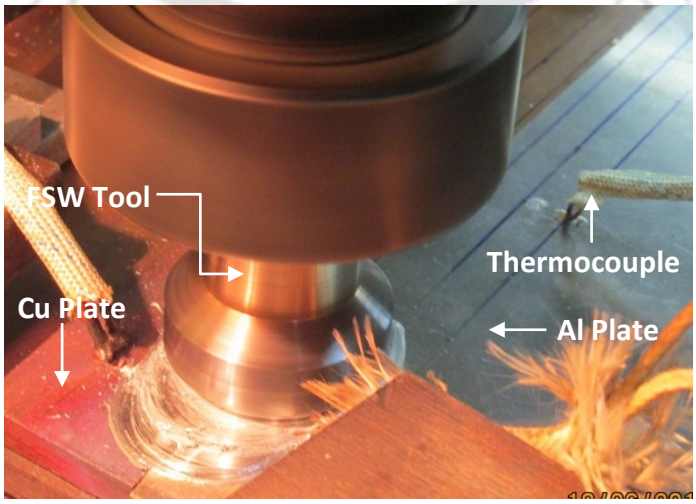

Figure 6.1 FSW set up

Commercial alluminium alloy i.e. AA1100 and pure rolled copper plates B370 of 200 mm X 100 mm X 6 mm sizes were butt joined by friction stir welding. The hard copper plate was kept in retreating side and the aluminum plate was kept in advancing plate. Two types of tools were used in this work .i.e. Right helix threaded tool (RHT) and left helix threaded tool (LHT) with flat cylindrical shoulder and cylindrical pin. The dimensions of the tool are 28 mm shoulder diameter, 6 mm pin diameter, 5.7 mm-pin height and 1.1mm pitch of thread. The larger shoulder diameter was chosen in order to maximize the heat input. Vertical milling machine of 7.5 HP motor capacities was modified and used for FSW purpose. Prior to the welding, the edges of the welded samples are grinded and cleaned with the methanol and wiped with the clean cloth to remove oxide films, oil and grease. The copper plates are kept on retreating side and aluminum in advancing side. Tool pin was kept in offset positions i.e. 2mm in copper plate and 4mm in aluminum plate. The workpieces were clamped rigidly on a backing bar to prevent the abutting of joint faces.

Figure 6.2 Fabricated Tools

Several double blind experiments were carried out using the same tools of different profiles (Tapered pin, Trapezoidal pin, Cylindrical pin etc.) which were used in the previous work discussed in Section 5.2. It was noticed that unthreaded tools generates continuous voids and sometimes the thermal cracks in the weldments of this dissimilar material combinations (i.e. Al-alloy and Cu-alloy). Therefore the threaded tools shown in the Figure 6.2 were used in this work for carrying out the FSW experiments. Design of experiments were performed based on the following three important steps, (i) Identification of important process parameters and variables (ii) Fixing the upper and lower limits of parameters and variables (iii) and Developing the Taguchi DOE design matrix. The selected design matrix is L-16

obtained by 2^4 (Two levels and four parameters). Table 6.1 shows the design of experiments followed in the present work.

Table 6.1 Design of experiments

Expt no	RPM	WS	Tool	PD
E1	1100	98	RHT	0.8
E2	1100	98	RHT	1.6
E3	1100	98	LHT	0.8
E4	1100	98	LHT	1.6
E5	1100	132	RHT	0.8
E6	1100	132	RHT	1.6
E7	1100	132	LHT	0.8
E8	1100	132	LHT	1.6
E9	1500	98	RHT	0.8
E10	1500	98	RHT	1.6
E11	1500	98	LHT	0.8
E12	1500	98	LHT	1.6
E13	1500	132	RHT	0.8
E14	1500	132	RHT	1.6
E15	1500	132	LHT	0.8
E16	1500	132	LHT	1.6

This section gives the mechanical results of dissimilar Cu-Al joints i.e. hardness and tensile strengths of the welded joints for all the E16 experiments. These mechanical results are further validated by comparing with the microstructural and factographical studies.

6.2.1 Microhardness

A constant load of 500gf applied for 10 seconds by using a digital micro hardness tester (buehler), and measurements are taken on every 1mm distance away to the weld centre line on both sides of the weld. Hardness measurements were taken on cross-sections perpendicular to the welding direction. Test samples for the hardness measurement were taken from two groups of welded samples. The first group consists of test pieces welded using RHT tool and the second group of samples welded with LHT tool. Hardness variations on horizontal distance from the weld centre line are shown in Figure 6.3 and Figure 6.4. It was observed that the homogeneous trend appeared in the hardness plots for almost all the samples, but for the welds of samples E13, E14 manifests the dropdown in nature. This

lowered hardness reveals the truth of void existence. Figure 6.3 shows the hardness plots for the welds using RHT tool.

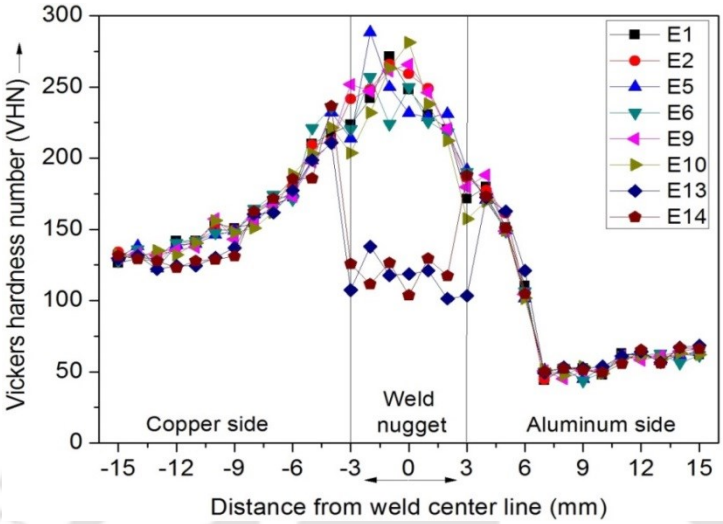

Figure 6.3 Hardness values for the samples welded by right helix threaded tool (RHT)

Figure 6.4 shows the hardness plots of the weldments produced using the LHT tool. During tool stirring and traversing, the softened Al alloy reacted strongly with copper pieces spread throughout the nugget zone, which resulted in the formation of the Al–Cu intermetallic compounds $CuAl_2$, These intermetallic compounds have significant effect on hardness distribution pattern of the Cu-Al welds.

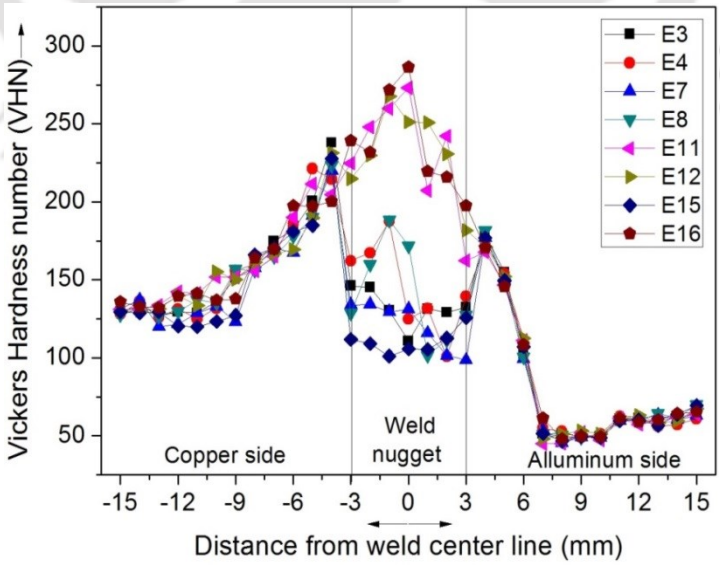

Figure 6.4 Hardness values for the samples welded by left helix threaded tool (LHT)

It was noticed that the greater improvement in the hardness at nugget zone was achieved for dissimilar Cu-Al FSW joints. From the Figure 6.4, it was observed that the samples E3, E4, E7, E8, and E15 clearly manifest the lesser hardness at nugget zone. This may be occurred due to improper mixing of the both the materials, minute voids were also formed at weld nugget zone. It was further seen that the material mixing was not appropriate using LHT tool (Table.6.2; macrograph for sample E3, E4, E7, E8, E15), because the threads on the tool pin was left hand threads and the direction of the tool rotation was clockwise which leads to improper mixing of material in weld zone. The reason for the increment of hardness in weld nugget zone is the formation of hard and brittle intermetallic components phases of Al–Cu.

6.2.2 Tensile strength

Tensile testing was performed for all the welded samples and base metals. Stress vs. Elongation plot for the base materials is shown in Figure 6.5. The effects of process parameters for the two tool pin profiles on FSW of Cu-Al joints are shown in Figure 6.6 and 6.7. The trend was common in all the joints, irrespective of the tool pin profile. The joint produced by the Right Helix Threaded (RHT) pin profiled tool exhibits a high tensile strength when compared to the other joints. The similar result was also observed in the hardness results.

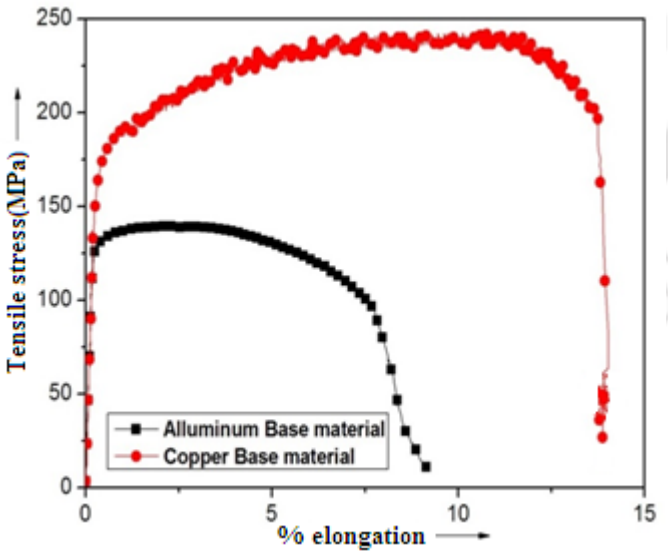

Figure 6.5 Stress vs. elongation plots for the base materials

Significant difference in the tensile strength of base materials was observed from the study which is shown in Figure 6.5. Tensile strengths of welded test samples vary from 60 to 100 MPa depending upon the welding conditions. Most of the specimens broke away to the weld

nugget region and parentage of elongation measured across the weldment using an extensometer showed elongation/ductility ranging from 0.7% to 3.0%. The variation of tensile stress and percentage of elongation for all the welded samples are shown in Figure 6.6 and 6.7 As seen in the hardness results the joints E3, E4, E7, E8 doesn't give impressive results due to improper mixing of the two materials but the joints E1, E2, E5, E6, E9, E10, E11, E12, E13, E14 exhibited good tensile properties.

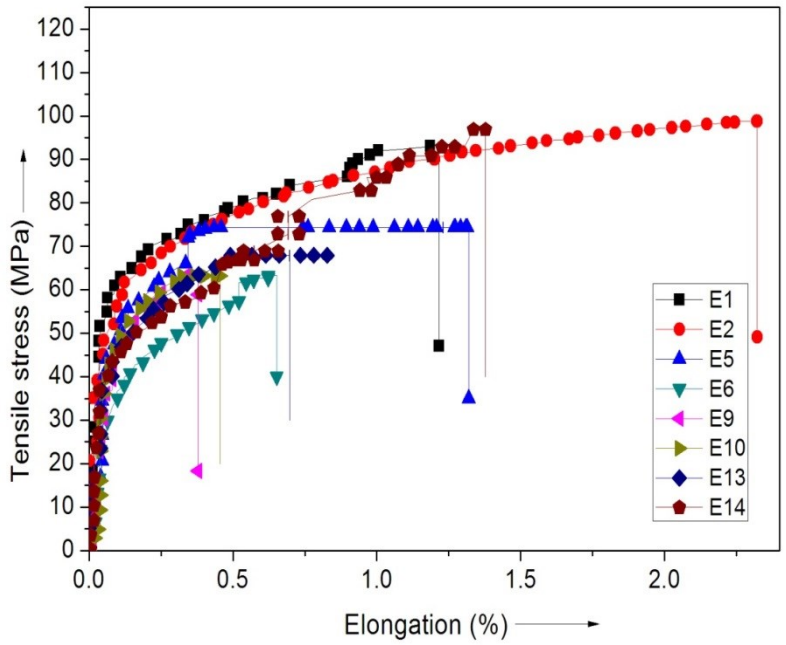

Figure 6.6 Stress vs. elongation plots for the specimens welded by RHT tool

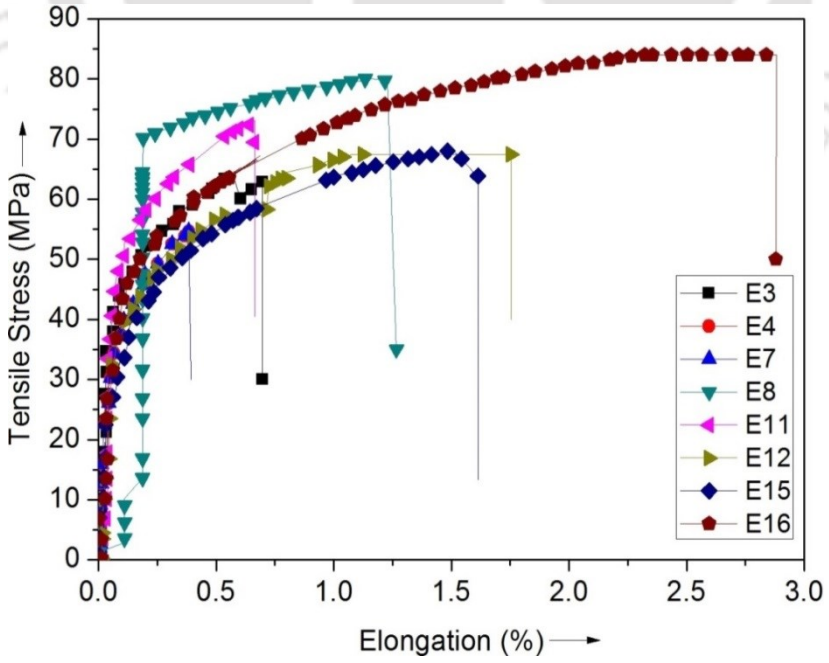

Figure 6.7 Stress vs. elongation plots for the specimens welded by LHT tool

The tensile failure was seen away to the welding nugget zone i.e. at the interface of heat affected zone (HAZ) and base metal zone of Al alloy, indicating that the weld nugget has a higher joint strength. This was proved by the hardness results; the average hardness at the nugget was improved and was recorded almost three times of the parent base material (i.e. Al-alloy). The comprehensive results of all the microhardness, tensile properties and joint efficiency of the sixteen weldments E1-E16 are shown in Table 6.2. Joint efficiency was calculated based on UTS (ultimate tensile stress) of the joint to the UTS of the weak base material and remark on the weld quality was also stated in the Table 6.2. The joint efficiencies for the welds produced by the RHT are superior to that of the welds of LHT tool.

Table 6.2 Results of mechanical and weld zone in thickness direction

Exp no	VHN*	UTS	% Elongation	Joint Efficiency	Weld zone	Remarks
E1	274	92.5	1.6	71.15	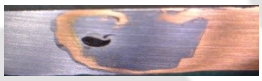	Worm hole due to slower tool traverse speed.
E2	273	98	2.3	75.3		Sound weld, failed away to weld zone.
E3	140	63.5	0.7	48.84		Improper mixing.
E4	185	55	0.4	42.3		Narrow keyway just below the tool shoulder.
E5	285	74.5	1.25	57.69		Sound weld, failed away to weld zone,
E6	260	62.5	0.62	48.07		Sound weld, failed away to weld zone.
E7	130	56	0.42	42.3		Faster TRS leads Intermetallic components .
E8	185	80	1.25	61.53		No defects observed.
E9	272	61	0.35	44.61		Sound weld, failed away to weld zone.
E10	280	63	0.36	48.46		Sound weld, failed away to weld zone.

E11	274	73	0.65	56.15		Sound weld, failed away to weld zone.
E12	270	68	1.75	51.92		Sound weld, failed away to weld zone.
E13	140	68	0.7	52.3		Worm hole, failed at weld zone.
E14	130	95	1.38	74.61		Worm hole, failed at weld zone.
E15	127	68.5	1.6	52.69		Defective weld, Improper mixing & lesser plunging force.
E16	280	84.2	2.8	64.7		Sound weld, failed away to weld zone.

* VHN average of three hardness values at the nugget zone.

6.2.3 Metallographic study

Microstructural study provides the distinct analysis of welded joints to understand the quality of the FSW joint. For achieving metallographic microstructure a rigid step-by-step process was followed. In sequence, the steps were the sectioning of the sample, mounting, course grinding, fine grinding, and polishing, etching and microscopic examination. The detailed experimental description has been given in the methodology chapter 3, section 3.5.3. Figure 6.8 reveals the different zones of the Cu- Al dissimilar joint.

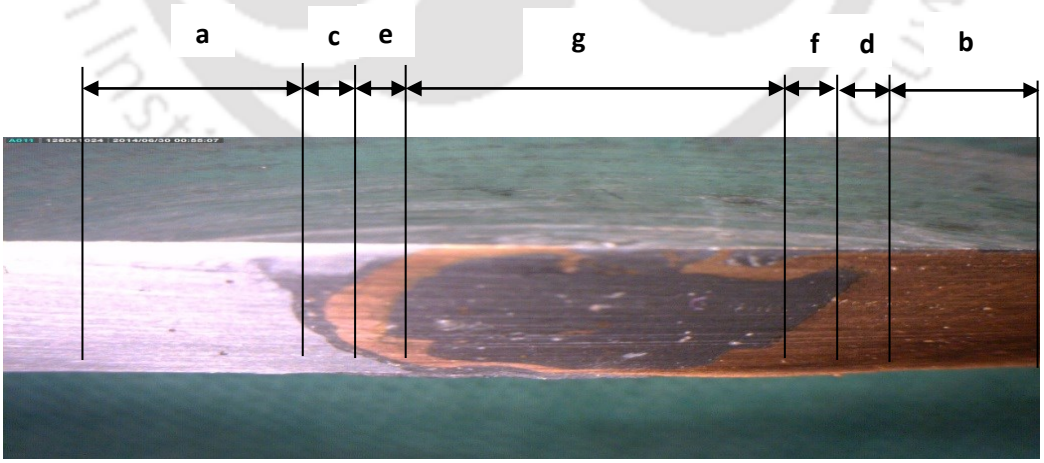

Figure 6.8 Macrograph of Cu-Al FSW Joint shows various zones. {a) Base material zone at Al side, b) base material zone at copper side, c) HAZ at Al side d) HAZ at Copper side, e) TMAZ at Al side, f) TMAZ at copper side, g) Nugget zone.}

The base material zone is an area beside the weld zone which doesn't under go any physical or metallurgical deformation, this can also called as unaffected zone. Figure 6.8a shows the

unaffected base Aluminum material and Figure 6.8b shows the unaffected copper base material. The Heat Affected Zone (HAZ) is the region which undergoes thermal effect but it does not undergo any plastic deformation. The Thermo Mechanically Affected Zone (TMAZ) is the region in which the grain elongation occurs due to the effect of thermal and mechanical force on the weld zone. Figures 6.9 to 6.12 represent some of the important microstructures obtained from the metallographic studies. Figure 6.9c and Figure 6.9d reveals the TMAZ at Al and Cu sides. Figure 6.10 is the nugget zone of the Cu- Al weld. Hard intermetallic phase components formed at the nugget zone.

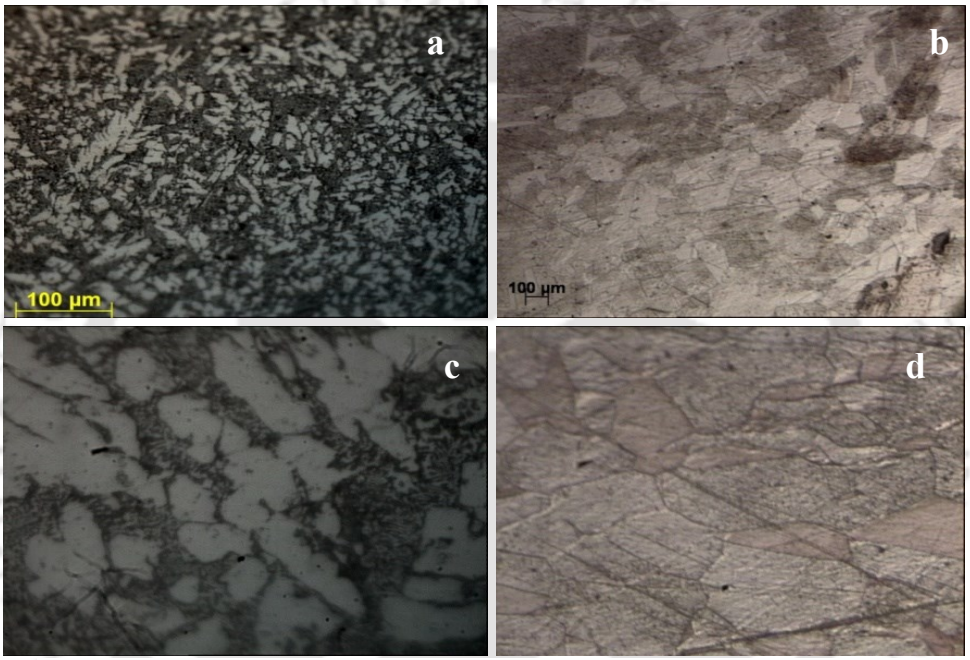

Figure 6.9 a) Base material of Alluminium b) Base material of copper
c) TMAZ at Al side and c) TMAZ at copper side.

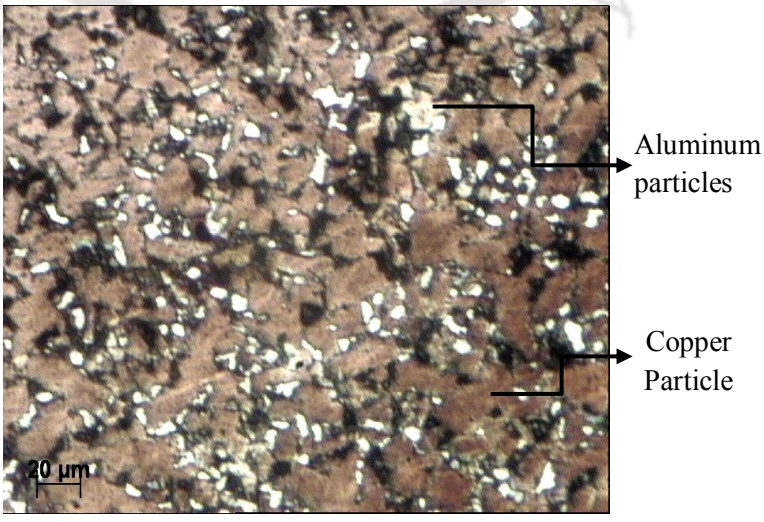

Figure 6.10 Copper and aluminum grain refinement at Nugget zone

Figure 6.11a reveals the joint produced by the process conditions E12 in which both the materials were perfectly mixed. Figure 6.11b shows the worm hole defect which was caused due to the slower tool traversing speed and the lesser tool plunging force. Figure 6.11.c reveals the void which was occurred due to the improper mixing and lesser tool plunging force. Figure 6.12 represents the micro structures at different areas of the nugget zone.

Figure 6.11 (a) Good weld (b) Tunnel defect (c) Void

Intermixing behaviour of alluminum and copper metal can observed in the Figure 6.11a. Figure 6.11b though there is a worm hole noticed in this macrograph, but it is not not continued thorough out the joint. This was supported by the tensile result of the E1 experiment. The tensile strength of the E1 sample is about 92.15 MPa. Figure 6.11c reveals the void which was occurred due to the improper mixing and lesser tool plunging force. The reason for the poor hardness in some samples at nugget zone can be percieved. These voids are occurred due to the slower tool traversing speeds or with the less tool plunge depths.

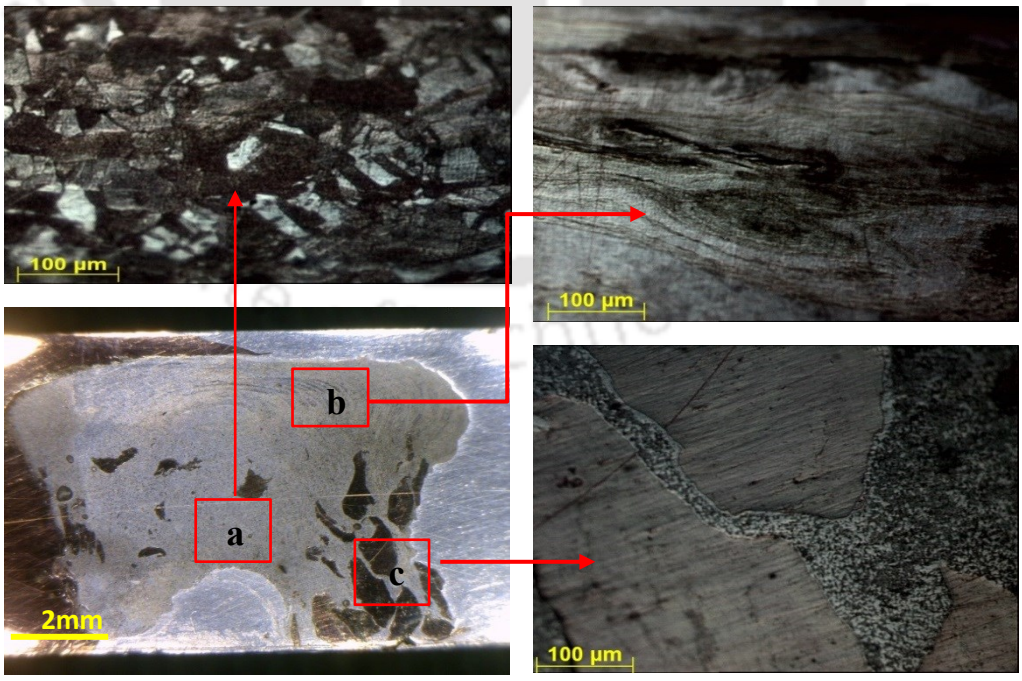

Figure 6.12 Microstructure at different areas in the nugget zone of Cu-Al FSW joint

Figure 6.12 represents the various microstructure patterns observed in the weld nugget. The microstructural studies interpret the joint quality and also to comprehend the influence of grain refinement in the improvement of mechanical properties. The present micro graphs showns a homogeneous trend appears in the nugget zone microstructures but at some portions tough copper pieces has been shifted towards alluminium side Figure 6.12c.

6.2.4 Elemental scanning

To understand the phenomena of material mixing and the homogeneity of dissimilar material stirring, elemental analysis was performed by using EDX-FESEM (Ziess-sigma). Figure 6.13 represents the elemental scan of nugget zone which reveals the various alloying elements present in the nugget zone of Cu-Al dissimilar weldment.

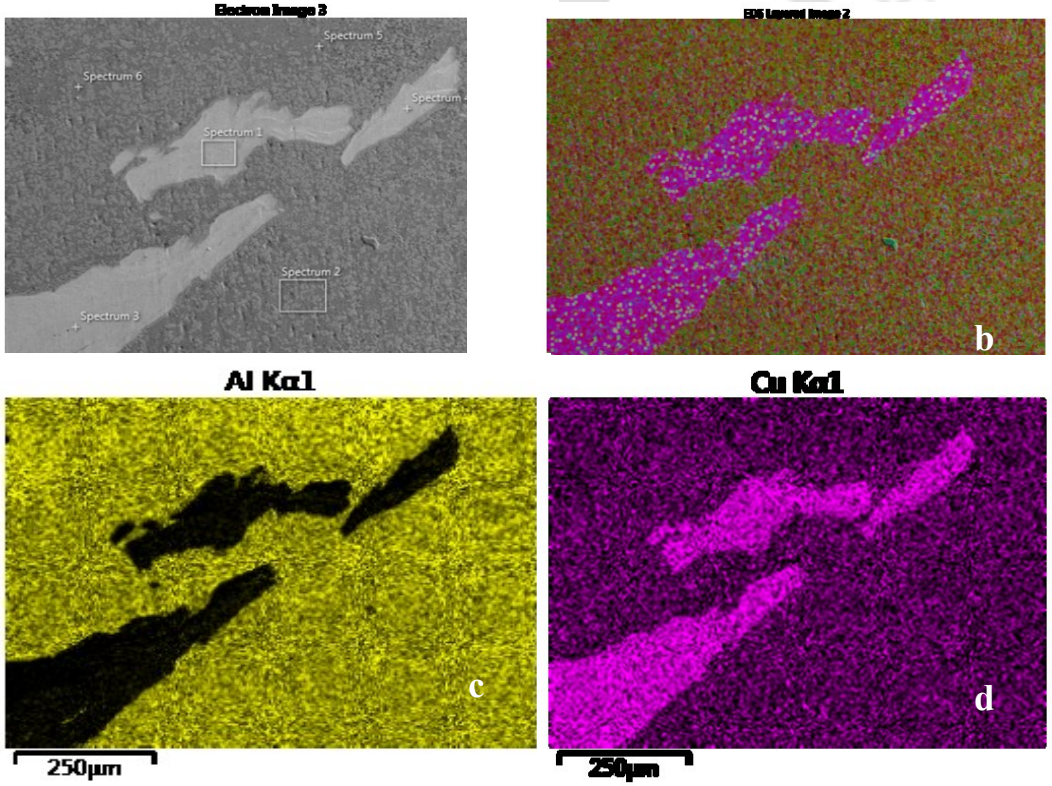

Figure 6.13 Elemental plotting by FESEM-EDX

Figure 6.13a is the sample taken from the nugget zone of Cu-Al, Figure 6.13b pretends the entire elemental map of the sample which consists elements present in the material. Figure 6.13c shows the distribution of aluminum elements (yellow in colour) in the sample. The black portion appears in Figure 6.13c represents it does not have alluminium material in it. The pink coloured portion in Figure 6.13d represents the presence of copper at the sample.

Spectrums 1, 2 are the scanned areas shown in Figure 6.13a. Figure 6.14 reveals the percentage of alloying elements in the sample shown in Figure 6.13a.

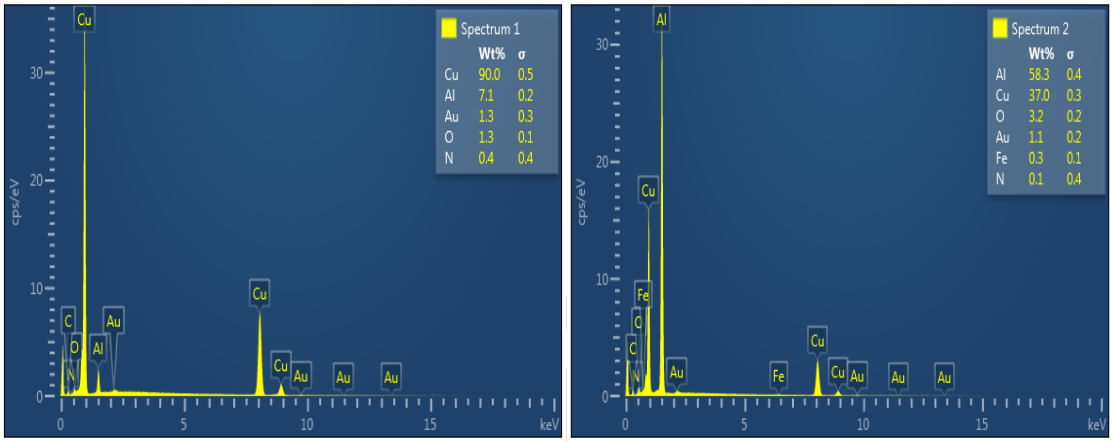

Figure 6.14 FESEM-EDX compositional analyses on FSW of Cu-Al (at Nugget portion)

From the Figure 6.14 it is evident that the zone corresponds to Spectrum 1 contains 90% of copper which is tough copper phase and for the zone corresponds to spectrum 2 in Figure 6.14 contains the 58.3% of Al and 37% Cu which indicates the homogeneous mixing of two materials.

6.2.5 Summary

Successful friction stir welding copper to alluminium was performed using two different threaded pin geometries. From this study it was seen that the plunge depth is the most influencing parameter in the weld quality of this type of combination of metals. With the increase of plunge depth both joint strength and hardness increases. Sound joints without any defects were produced by keeping the copper material in the retreating side instead and with moderate tool pin offset of 2mm to the copper and 4mm in the aluminum. Copper at advancing side leads to improper material mixing i.e. in that case aluminum material flows to the copper but copper doesn't. And larger tool pin offset and lesser plunge depths leads to the defects like voids and tunnel holes.

From the above experimental work it was also noticed that FSW Tools with Right helix thread tool and Left helix thread are perfectly suited for the welding of dissimilar Cu-Aluminum alloys. From the results of tensile test and hardness test it was perceived that RHT tools provided superior than weld quality that of LHT tools. Unique improvement in the

hardness at nugget zone was observed due to the formation of hard intermetallic phases. During tool stirring and traversing, the softened Al alloy reacted strongly with copper pieces spread throughout the nugget zone, which resulted in the formation of the Al–Cu intermetallic compounds $CuAl_2$

6.3 Investigation of FSW on dissimilar alluminium alloys

6.3.1 Introduction

The present section focusses on the parametric analysis on friction stir welding of dissimilar alluminium alloys i.e. AA5083-AA1100 using different tool geometries. A multi-response optimization problem was developed to perceive optimal process parameters for friction stir welding of dissimilar alluminium alloys to achieve the better mechanical properties. Taguchi's L16 orthogonal array design and the signal-to-noise ratio (S/N ratio) concept was selected to acquire the objective functions to optimize with in the experimental data. The objective functions were chosen with respect to process parameters of tool rotational speed, welding speed, tool shoulder diameter, and tool pin type (keeping all other parameters constant). The tools with various shoulder sizes used in this study is shown in Figure 6.15. The Taguchi's approach was followed by the Grey relational analysis was successfully applied to solve this multi-response optimization problem. The ANOVA method was used to evaluate the overall output of the various factor considered and the optimal result was been confirmed with an additional experiment. This present study specifies the application viability of the Grey-Taguchi method for the continuous enhancement of the weld quality in the manufacturing sector. Various process parameters used for welding these dissimilar alluminium alloys are shown in Table 6.3

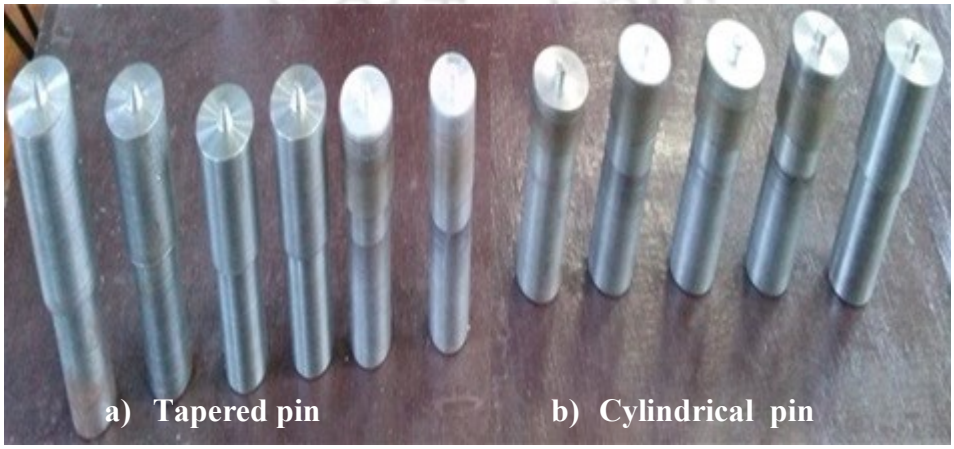

Figure 6.15 Fabricated FSW tools

Table 6.3 Process parameters and their limits

Parameters	Notation	Unit	Levels of Factors			
			1	2	3	4
Tool Rotational Speed	TRS	rpm	600	815	1000	1500
Welding Speed	WS	mm/sec	36	63	98	132
Tool Shoulder diameter	SD	mm	24	26	28	30
Tool Pin Type	TP	--	CYL		TC	

Taguchi's Design of experiments (DOE) were performed using the above said process parameters. Mixed level design was selected i.e. 4 levels for three parameters and 2 levels for one parameter shown in Table 6.3. Sixteen number experiments were conducted using the following approach shown in the Table 6.4.

Table 6.4 Taguchi's L16 orthogonal array design

S.No	TRS	WS	SD	TP
1	600	36	24	CYL
2	600	63	26	CYL
3	600	98	28	TC
4	600	132	30	TC
5	815	36	26	TC
6	815	63	24	TC
7	815	98	30	CYL
8	815	132	28	CYL
9	1100	36	28	CYL
10	1100	63	30	CYL
11	1100	98	24	TC
12	1100	132	26	TC
13	1500	36	30	TC
14	1500	63	28	TC
15	1500	98	26	CYL
16	1500	132	24	CYL

Based on the Table 6.4, the experiments were performed and the tensile testing was done to evaluate mechanical properties of welded samples. The test samples for tensile testing were taken from the middle portions of the weld perpendicular to the weld line by using the metal jig saw. The specimens were machined by milling machine according to the ASTM E-8

standard. Figure 6.16 shows the tested tensile samples which were broken away to the welding zone i.e. between heat affected zone and base material of AA1100. Table 6.5 shows the tensile properties of two un-welded base metals. Table 6.6 represents the experimental data for 16 welded samples. The peak temperature mentioned in the Table 6.6 was taken 15mm away to the weld centre line.

Table 6.5 Mechanical properties of AA1100 and AA5083

Material	Yield Strength (MPa)	Ultimate Tensile Strength (MPa)	Elongation (%)
Base Material (AA1100 H-16)	138	155	6
Base Material (AA5083)	170	235	16

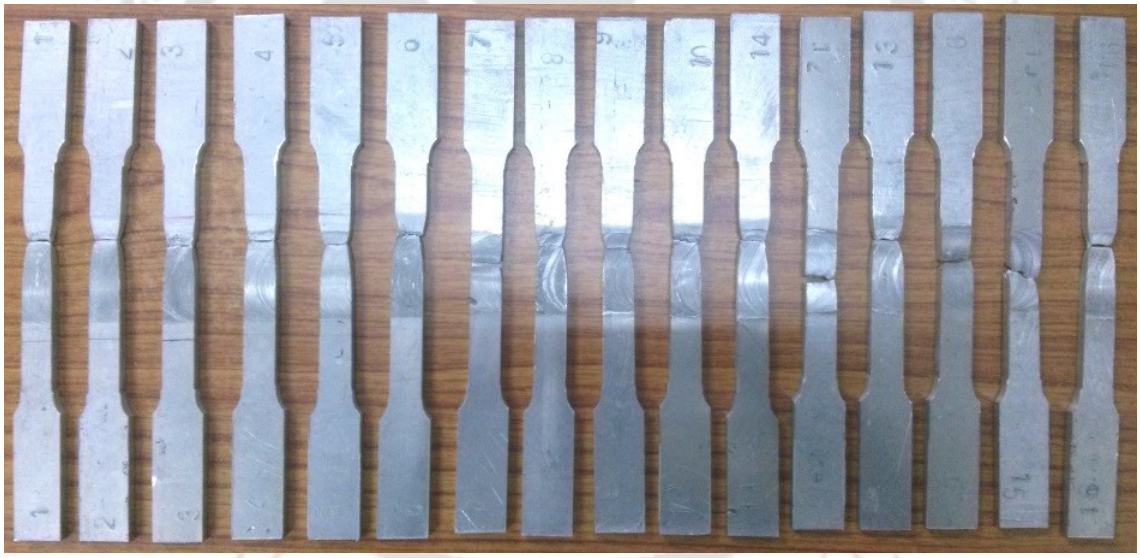

Figure 6.16 Tensile test samples

Table 6.6 Experimental data

S.No	Yield Strength (MPa)	Ultimate Tensile Strength (MPa)	Elongation (%)	Peak Temp (^{0}C)
1	107.5	127.2	14.1	322.5
2	118	140.1	14.5	321.8
3	116.8	138.8	15.2	332.1
4	113.5	139.6	14.7	324.3
5	118.7	150.2	15.1	334.6
6	120.1	157.5	16.2	322.8

7	115.9	142.9	15.3	333.5
8	119.8	139.8	14.8	328.9
9	121.3	140.8	14.2	341.1
10	119.8	145.2	15.4	341.8
11	122.1	150.4	16.2	333.5
12	117.2	141.5	14.2	324.1
13	115.4	144.1	15.4	346.2
14	118.8	139.9	14.8	338.7
15	116.2	143.2	14.3	330.8
16	109.9	138.5	13.9	328.4

6.3.2 Optimisation of FSW on AA1100-AA5083

After completion of experimental studies the results were used to find the optimal process parameters using Grey-Taguchi optimisation method. This procedure helps to examine the output data and to predict the optimal results. The S/N ratio is the ratio of the mean (signal) to the standard deviation (noise). The standard S/N ratios generally used are as: Nominal is best (NB), lower the better (LB) and higher the better (HB). The optimal setting is the parameter combination, which has the highest S/N ratio. The detailed steps and results obtained from the analysis were discussed below.

Initial step in the grey relational analysis is the normalisation of output data which is called grey relational generation (GRG) i.e. all the measured experimental output characteristics should be normalized ranging from zero to one. In GRG, the normalised Yield Strength, Ultimate Tensile Strength, % Elongation, Peak Temperature corresponding to Larger-the-better criterion can be expressed as shown in equation (6.1)

$$x_i(k) = \frac{\max y_i(k) - y_i(k)}{\max y_i(k) - min\, y_i(k)} \qquad 6.1$$

Where x_i (k) is the value after the Grey relational generation, min y_i (k) is the smallest value of y_i (k) for the k_{th} response, and max y_i (k) is the largest value of y_i (k) for the k_{th} response. The normalized output data after Grey relational generation are tabulated in Table 6.17.

Table 6.7 Normalisation of output data (Grey relational generation)

S.No	Yield Strength	Ultimate Tensile Strength	Elongation	Peak Temp
1	0	0	0.086957	0.028688525
2	0.719178082	0.425742574	0.26087	0
3	0.636986301	0.382838284	0.565217	0.422131148
4	0.410958904	0.409240924	0.347826	0.102459016
5	0.767123288	0.759075908	0.521739	0.524590164
6	0.863013699	1	1	0.040983607
7	0.575342466	0.518151815	0.608696	0.479508197
8	0.842465753	0.415841584	0.391304	0.290983607
9	0.945205479	0.448844884	0.130435	0.790983607
10	0.842465753	0.594059406	0.652174	0.819672131
11	1	0.765676568	1	0.479508197
12	0.664383562	0.471947195	0.130435	0.094262295
13	0.54109589	0.557755776	0.652174	1
14	0.773972603	0.419141914	0.391304	0.692622951
15	0.595890411	0.528052805	0.173913	0.368852459
16	0.164383562	0.372937294	0	0.270491803

Where $\Delta_{0i} = \| x_0(k) - x_i(k) \|$ = difference of absolute value $x_0(k) and\, x_i(k)$; Ψ is the distinguishing coefficient $0 \leq \Psi \leq 1$; $\Delta_{min} = \forall j^{min} \in i \forall k^{min} \| x_0(k) - x_j(k) \|$ = the smallest value of Δ_{0i}, and $\Delta_{max} = \forall j^{max} \in i \forall k^{max} \| x_0(k) - x_j(k) \|$ =largest value of Δ_{0i}. The average of all grey relational coefficients corresponding to the selected responses gives the grey relational grade. This method renovates the multi response problem in to a single response optimisation problem.

Table 6.8 Evaluation of $\Delta 0_i$ for each of the responses

Sl. No	Yield Strength	Ultimate Tensile Strength	Elongation	Peak Temp
1	1	1	0.913043	0.971311
2	0.280822	0.574257	0.73913	1
3	0.363014	0.617162	0.434783	0.577869
4	0.589041	0.590759	0.652174	0.897541
5	0.232877	0.240924	0.478261	0.47541
6	0.136986	0	0	0.959016
7	0.424658	0.481848	0.391304	0.520492
8	0.157534	0.584158	0.608696	0.709016
9	0.054795	0.551155	0.869565	0.209016
10	0.157534	0.405941	0.347826	0.180328
11	0	0.234323	0	0.520492
12	0.335616	0.528053	0.869565	0.905738
13	0.458904	0.442244	0.347826	0
14	0.226027	0.580858	0.608696	0.307377

15	0.40411	0.471947	0.826087	0.631148
16	0.835616	0.627063	1	0.729508

Next to normalisation of experimental data, Grey relational coefficient (GRC) is calculated which represents the correlation between the desired and actual experimental output data. The GRC can be calculated using the equation as shown in equation (6.2).

$$\xi_i\,(k) = \frac{\Delta_{min} + \Psi\Delta_{max}}{\Delta_{0i}(k) + \Psi\Delta_{max}} \qquad 6.2$$

By averaging the grey relational coefficient, the grey relational grade (ω) was calculated using the following equation (6.3).

$$\Omega_i = \frac{1}{n}\sum_{k=1}^{n}\xi_i\,(k) \qquad 6.3$$

Where n= no of process responses. The utmost value of grey relational grade gives the best process sequence.

Table 6.9 Grey relational coefficient of each performance characteristics where the value for Ψ = 0.5 was taken in order to give equal priority.

Table 6.9 Grey relational coefficients of each performance characteristics

Sl. No	Yield Strength	Ultimate Tensile Strength	Elongation	Peak Temp
1	0.333333	0.333333	0.353846	0.339833
2	0.640351	0.465438	0.403509	0.333333
3	0.579365	0.447563	0.534884	0.463878
4	0.459119	0.458396	0.433962	0.357771
5	0.682243	0.674833	0.511111	0.512605
6	0.784946	1	1	0.342697
7	0.540741	0.509244	0.560976	0.48996
8	0.760417	0.461187	0.45098	0.413559
9	0.901235	0.475667	0.365079	0.705202
10	0.760417	0.551913	0.589744	0.73494
11	1	0.680899	1	0.48996
12	0.598361	0.486356	0.365079	0.355685
13	0.521429	0.530648	0.589744	1
14	0.688679	0.462595	0.45098	0.619289
15	0.55303	0.514431	0.377049	0.442029
16	0.374359	0.443631	0.333333	0.406667

Table 6.10 represents the Grey relational grade. The maximum value in the grey relational grade represents the optimal experiment which contains the optimum output data. The maximum obtained value in the grey relational grade is 0.825529 for the experiment no 6.

Therefore the optimal process parameters obtained for the maximum grey relational grade are TRS: 815 rpm, WS: 63mm/min, TD: 24 mm, TP: TC.

Table 6.10 Grey relational grades

Experiment No	Grey relational grade
1	0.338736
2	0.461765
3	0.494558
4	0.43378
5	0.61191
6	0.825529
7	0.52213
8	0.509159
9	0.584709
10	0.637951
11	0.771345
12	0.458494
13	0.634437
14	0.536888
15	0.480053
16	0.400412

Figure 6.17 represents the main effect plots for overall grey relational grade. Table 6.11 represents the analysis of variance using adjusted SS for tests.

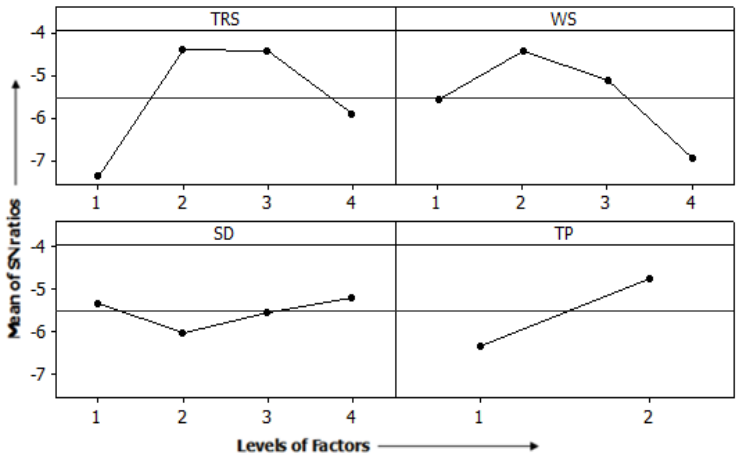

Figure 6.17 Main effect plots for overall Grey relational grade

Table 6.11 Analysis of variance using adjusted SS for tests

Parameter	% Contribution
TRS	37.53131586
WS	22.90532
SD	5.738259
Tool pin type	17.20682
Residual Error	16.61828
Total	100

From the Table 6.11 it is clear that the most influencing process parameters with in the considered overall parameters are tool rotational speed (TRS) is about 37.5% and welding speed (WS) is about 23%. As there is huge difference in the physical properties of the chosen materials, the residual error obtained about 16%.

From the Figure 6.17, it is evident that the compared to all other set of parameters the parameters of experiment no 6 (i.e. TRS: 815 rpm, WS: 63mm/min, TD: 24 mm, TP: TC) gives the optimal results hence the fractograph of welded samples of experiment no 6 is shown in Figure 6.18.

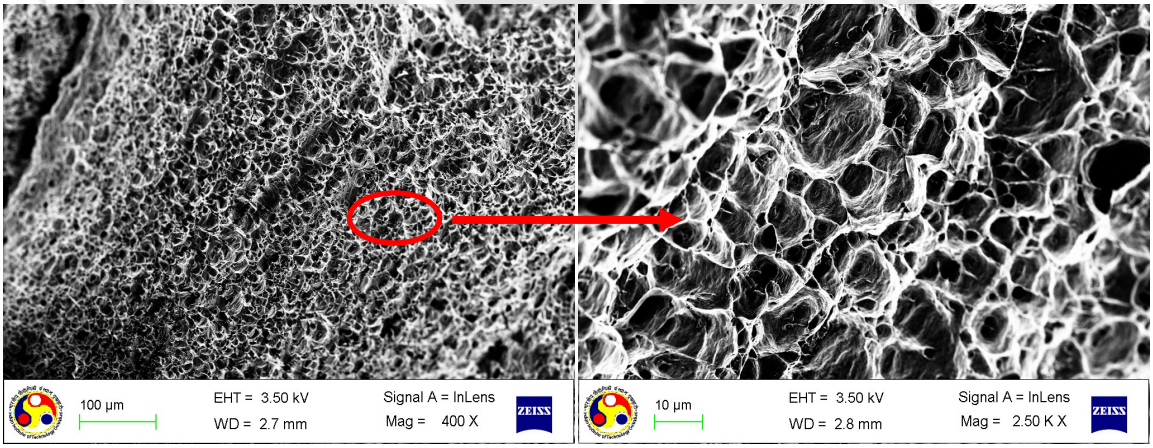

Figure 6.18 FESEM analysis of fractograph of FSW samples no 6.
a) Mag 400X b) Mag 2.5kX

The fracture surface of the FSW sample no 6 was studied using field emission scanning electron microscope (FESEM) at 400X and 2500X. The fractured surface of the samples appears to have dimples around the nodule and it is uniform as well. The presence of dimples

occurred due to the formation of micro-voids and coalescence phenomena, when specimen is under uniaxial tensile loading. The presence of dimples characterise the ductile fracture.

6.3.3 Summary

It was observed from experimental investigations that the welding process parameters and tool geometries have significant effect on weld quality of dissimilar alluminium alloys. The comprehensive methodology of Taguchi optimization technique combined with the Grey relational analysis has been successfully applied and reported for evaluating optimal process parametric combination of friction stir welding on dissimilar aluminum alloys. Establishment of correlations between the most significant parameters and the mechanical properties and heat output of the FSW process using grey taguchi technique is feasible. Minimised numbers of experimental runs have been performed using the most effective taguchi optimisation technique. The most important criteria in dissimilar metal FSW joints are that the joint strength should not be lesser than the weakest of the combination.

The maximum value in the grey relational grade represents the optimal experiment which contains the optimum output data. The maximum obtained value in the grey relational grade is 0.825529 for the experiment no 6. Therefore the optimal process parameters obtained for the maximum grey relational grade are TRS: 815 rpm, WS: 63mm/min, TD: 24 mm, TP: TC. Quality assessment of FSW joints by the tensile behaviour reveals that the tapered cylindrical pin tool perfectly suits for the successful welding of two dissimilar combination of alluminium (i.e. AA1100 to AA5083). From the Table 6.11 it is also seen that the most influencing process parameter is tool rotational speed and welding traverse speed which has the impact of 37.5% and 23%.

Chapter 7

Summary and Conclusions

7.1 Summary

In this thesis, numerical analysis and experimental investigations of Friction Stir Welding on both similar and dissimilar alloys have been carried out. Numerical modelling considering all the physical phenomena is an extremely tough task. However, with the help of suitable assumptions and few other methodologies developed by the previous researchers have made this process simulation possible. The developed FE model has an ability to address issues like temperature distributions in similar and dissimilar FSW. Experimental data related to temperature distributions are important to verify the results obtained from the modelling.

The present simulation study was performed based on the finite element method (FEM) in which distributed moving heat source based three-dimensional modelling has been adopted. Numerical modelling of FSW process benefits by eliminating the failures occurred in the experimental work. In this present investigation an attempt was made to demonstrate that the numerical analysis and experimental investigations can be a complementary to each other and at the same time numerical analysis can be implemented independently depending on the physical and mechanical properties of the materials to be joined. Although a good amount of published literature available on experimental study of FSW process, but there is a lack of modelling approaches with experimental validations which is applicable for both similar and dissimilar material combinations.

This thesis also focused on the experimental investigations on effect of tool geometries and process parameters on the weld quality of similar and dissimilar joints. FSW of similar materials was conducted on 6mm thick alluminium alloys to find out the optimal tool pin geometry for producing defect free welds. This study was further extended to investigate the same tool geometries is feasible enough to weld thicker alluminium plates. Then the work shifted to FSW of dissimilar materials which consists of joining dissimilar material combinations (i.e. Cu-Al and AA1100 and AA5083). The conclusions made from the above work have been given below.

7.2 Conclusions

The important conclusions from the present work can be précised as:

- The developed 3-Dimensional FE model for transient thermal analysis on FSW was successfully conducted and compared with the experimental analysis and validated with the published literature. This model stands flexible to analyze FSW for any kind of material.
- The 3-Dimensional FE model for friction stir welding of similar alluminium alloys have been developed based on the following assumptions:
  a) The material is isotropic
  b) All the material properties are temperature dependent
  c) Linear Newtonian convection cooling was considered on all the surfaces.
- The most influencing operating parameters of FSW (i.e. tool geometries, tool rotational speed, traverse speed, and plunge depth) were rigorously analyzed by using FE simulation, experimental investigation, and multi objective optimization approaches.
- The optimum tool shoulder size and pin geometries for obtaining the required temperature of FSW on AA1100 was performed and the obtained numerical results were fairly evaluated and they were matched with the experimental results with in the variation of 8%.
- In concern of several practical hurdles in the FSW process (i.e. tool wear, tool breakage and tool manufacturing difficulty), the best tool pin geometries were investigated both numerically and experimentally to achieve the better weld quality and it was observed that the trapezoidal pin tool and tapered pin tool performs well compared to other standard tool geometries.
- The overall mechanical response depends on the ratio of tool rpm to tool traverse speed. A correlation was done between tool rpm and traverse speed for obtaining the maximum ductility as well as load bearing capcity of 6mm thick alluminium alloys. It was found that to achieve friction stir welded joints having maximum ductility as well as load bearing capacity a suitable ratio of tool rpm to tool traverse speed between around 95 to 100 rad/mm should be considered to decide on the weld parameters.
- For welding of thick alluminium plates the most significant parameter which decides the weld quality was found to be the dwell time. An optimum dwell time was analyzed by experimental study for achieving the essential temperature on FSW weld quality. The

effect of dwell time was checked by mechanical and microstructural properties and found that at very low and high dwell time the ductility of welded joints significantly reduced. It was also seen that the tools with trapezoidal pin and tapered cylindrical pin profiles produces the acceptable welds for welding thick alluminium alloys, the same result was observed for lesser thick plates also.

- For welding of dissimilar material particularly high strength to low strength alloys, the above said tools doesn't gives good welds. It was found that for welding of Cu-Al dissimilar combination, the right helix threaded tools with clockwise tool rotations generates sound welds. The material mixing was homogeneous and this was revealed by the mechanical properties study, microstructural investigations and EDX analysis of welded joints.
- It was noticed that for welding of dissimilar material combinations, (i.e. AA1100-AA5083 and Cu-Al) clamping the harder material at advancing side with slight tool offset towards softer material side leads to homogeneous material mixing and produced good welds.
- The results of the present investigations are very encouraging. The numerical and experimental methodology developed in this work can be gainfully applied in the similar and dissimilar FSW in practical application.

7.3 Scope for future work

The computational procedure developed in the present work enables to acquire the thermal history of friction stir welding process. The numerical methodology of present work can assist to investigate the heat losses during the FSW through both the backing plates and work piece holding devices.

It is also important to understand the material flow phenomena during the tool stirring and traversing actions. Hence, involvement on this research area may help to gain advancement to this process.

The present numerical and experimental analysis can be extended for friction stir welding of high melting point alloys (viz. ferrous based alloys).

This process can be extended to hybrid FSW process like plasma arc assisted FSW or Laser assisted welding especially for high melting point materials (e.g. Low carbon steel, stainless steel).

References

1. Houldcroft PT (1986) Welding process developments and future trends. Materials and Design 7(4): 162–169.
2. Messler RW. (1999) Fusion Welding Processes, in Principles of Welding: Processes, Physics, Chemistry, and Metallurgy, Wiley-VCH Verlag GmbH, Weinheim, Germany. doi: 10.1002/9783527617487.ch3
3. Kallee SW (2010) Industrial applications of friction stir welding, Friction stir welding from basics to applications. Book chapter, wood head publishing limited, ISBN: 978-1-84569-450-0, Ps 118-163.
4. Mishra RS, Ma ZY (2005) Friction stir welding and processing-review. Materials Science and Engineering R 50: 1–78.
5. Tomohiko G, Hiroaki S, Daisuke T, Hideaki S, Takeshi Y, Hidenori H (2005) Highly reliable tank structure of H-IIB launch vehicle. Mitsubishi Heavy Industries Ltd, Technical Review 42: 5.
6. Smith CB (2000) Robotic Friction Stir Welding of Tailor Welded Blanks. Report #1536, Tower Automotive Internal Report.
7. Okamoto K, Hunt F, Hirano S (2005) Friction Stir Welding of Magnesium for Automotive Applications. SAE Technical Paper 2005-01-0730.
8. Thomas WM, Nicholas ED, Needham JC, Murch MG, Temple-Smith P and Dawes CJ (1995) Improvements relating to friction welding. TWI, Patent No: EP0615480.
9. Rajakumar S, Muralidharan C, Balasubramanian V (2010) Optimization of the Friction Stir Welding process and tool parameters to attain a maximum tensile strength of AA7075-T6 aluminium alloy. Proc. IMechE, Part B, Journal of Engineering Manufacture 224(B8): 1175-1191.
10. Su JQ, Nelson TW, Mishra R, Mahoney M (2003) Microstructural investigation of friction stir welded 7050-T651 aluminium. Acta Materialia 51(3): 713-729.
11. Dawes CJ, Thomas WM (1999) Development of improved tool designs for friction stir welding of aluminium. Proceedings of the 1st International Friction stir welding symposium, Oaks, CA, USA, June 14-16.
12. Lakshminarayan AK, Balasubramanian V (2008) Process parameters optimization for friction stir welding of RDE-40 aluminium alloy using Taguchi technique. Transactions of Nonferrous Metals Society of China 18: 548-554.
13. Saeid T, Abdollah-zadeh A, Assadi H, Ghaini FM (2008) Effect of friction stir welding speed on the microstructure and mechanical properties of a duplex stainless steel. Materials Science and Engineering A 496: 262–268.

14. Cam G, Gucluer S, Cakan A, Serindag HT (2008) Mechanical properties of friction stir butt-welded Al-5086 H32 plate. Journal of Achievements in Materials and Manufacturing Engineering 30(2): 151-156.
15. Lorrain O, Favier V, Zahrouni H, Lawrjaniec D (2010) Understanding the material flow path of friction stir welding process using unthreaded tools. Journal of Materials Processing Technology 210: 603–609.
16. Guerra M, Schmidt C, McClure JC, Murr LE, Nunes AC (2003) Flow patterns during friction stir welding. Materials Characterization 49: 95–101.
17. Lienert TJ, Stellwag WL, Grimmett BB, Warke RW (2003) Friction Stir Welding Studies on Mild Steel. Welding Journal: January 1S-9S.
18. Sato YS, Nelson TW, Sterling CJ (2005) Recrystallization in type 304L stainless steel during friction stirring. Acta Materialia 53: 637–645.
19. Charit I, Mishra RS (2005) Low temperature super plasticity in a friction-stir-processed ultrafine grained Al–Zn–Mg–Sc alloy. Acta Materialia 53: 4211–4223.
20. Barcellona A, Buffa G, Fratini L, Palmeri D (2006) On microstructural phenomena occurring in friction stir welding of aluminium alloys. Journal of Materials Processing Technology 177: 340–343.
21. Soundararajan V, Valant M, Kovacevic R, An overview of R&D work in friction stir welding at SMU. Association of Metallurgical Engineers of Serbia, Review paper, AMES (UDC: 669.141.243.046.516=20): 275-295.
22. Thomas WM, Nicholas ED, Smith SD, Das SK, Kaufman JG, Lienert TJ. Eds. (2001) Aluminum 2001 Proceedings of the TMS 2001 Aluminum Automotive and Joining Sessions, TMS, p. 213.
23. Thomas WM, Johnson KI, Wiesner CS (2003) Friction Stir Welding – Recent Developments in Tool and Process Technologies. Advanced Engineering Materials 5: 485–490.
24. Yuqing M, Liming K, Fencheng L, Qiang L, Chunping H, Li X (2014) Effect of tool pin eccentricity on microstructure and mechanical properties in friction stir welded 7075 aluminum alloy thick plate. Materials & Design Volume 62: 334–343.
25. Rabby Md ER, Reynolds AP (2014) Effect of tool pin thread forms on friction stir weldability of different aluminum alloys. Procedia Engineering 90: 637 – 642.
26. Biswas P, Kumar DA, Mandal NR (2012) Friction stir welding of aluminum alloy with varying tool geometry and process parameters. Proc. IMechE Part-B, Journal of Engineering Manufacture 226(4): 641-648.
27. Mohanty HK, Mahapatra MM, Kumar P, Biswas P, Mandal NR (2012) Study on the effect of tool profiles on temperature distribution and material flow characteristics in friction stir welding. Proc. IMechE Part-B, Journal of Engineering Manufacture 226(9): 1527-1535.

28. Mohanty HK, Mahapatra MM, Biswas P, Mandal NR (2012) Modelling the effects of tool shoulder and probe profile geometries on friction stirred aluminium welds using Response Surface Methodology. Journal of Marine Science and Applications. 11(4): 493-503.
29. Biswas P, Mandal NR, (2011) Effect of Tool Geometries on Thermal History of FSW of AA1100. Welding Journal 90: 129S-135S.
30. Mohanty HK, Mahapatra MM, Biswas P, Mandal NR (2013) Predicting the effects of tool geometries on friction stirred aluminum welds using artificial neural networks and fuzzy logic techniques. International Journal of Manufacturing Research 8(3): 296-312.
31. Biswas P, Mandal NR (2009) Experimental Study on Friction Stir Welding of Marine grade Aluminum Alloy. Journal of Ship Production 25(1): 1–6.
32. Sayer S, Ceyhun V (2008) Influence of pin structure on microstructure and mechanical properties of friction stir welded 6063 (Al Mg Si 0.5) Aluminum alloy. Materials Testing 50(5): 259-263.
33. Yeni C (2008) Effect of post-weld aging on the mechanical and microstructural properties of friction stir welded aluminum alloy 7075. Archives of Materials Science and Engineering 34(2): 105-109.
34. Leal RM, Leitao C, Loureiro A, Rodrigues DM, Vilac P (2008) Material flow in heterogeneous friction stir welding of thin aluminium sheets: Effect of shoulder geometry. Materials Science and Engineering 498: 384–391.
35. Sato YS, Urata M, Kokawa H (2002) Parameters controlling microstructure and hardness during friction-stir welding of precipitation-hardenable aluminum alloy 6063. Metallurgical and Materials Transactions 33(A): 625–635.
36. Lee WB, Yeon YM, Jung SB (2003) Evaluation of the microstructure and mechanical properties of friction stir welded 6005 aluminum alloy. Materials Science and Technology 19(11): 1513-1518.
37. Simar A, Brechet Y, Meester B, Denquin A, Pardoen T (2008) Microstructure, local and global mechanical properties of friction stir welds in aluminium alloy 6005A-T6. Material Science and Engineering A 486 (1–2): 85–95.
38. Peel MJ, Steuwer A, Withers PJ (2006a) Dissimilar friction stir welds in AA5083–AA6082. Part II: process parameter effects on microstructure. Metallurgical and Materials Transactions 37(A): 2195–2206.
39. Lim S, Kim S, Lee CG, Kim SJ (2004) Tensile behaviour of friction-stir-welded Al 6061-T651. Metallurgical and Materials Transactions 35(A): 2829–2835.
40. Peel MJ, Steuwer A, Withers PJ, Dickerson T, Shi Q, Shercliff H (2006b) Dissimilar friction stir welds in AA5083–AA6082. Part I: process parameter effects on thermal history and weld properties. Metallurgical and Materials Transactions 37(A): 2183–2193.

41. Ren SR, Ma ZY, Chen LQ (2007) Effect of welding parameters on tensile properties and fracture behaviour of friction stir welded Al–Mg–Si alloy. Scripta Materialia 56: 69–72.
42. Longhurst WR, Strauss AM, Cook GE, Cox CD, Hendricks CE, Gibson BT, Dawant YS (2010) Investigation of Force-controlled Friction Stir welding for manufacturing and automation. Proc IMechE, Part B, Journal of Engineering Manufacture 224(6): 937-949.
43. Soundararajan V, Atharifar H, Kovacevic R (2006) Monitoring and processing the Acoustic Emission Signals from Friction Stir Welding. Proc IMechE, Part B, Journal of Engineering Manufacture 220(10): 1673-1685.
44. Aota K, Ikeuchi K (2010) Friction stir welding of aluminium lap joint by tool without probe. Welding International 24(3): 197-205.
45. Shtrikman MM, Pinskii AV, Kashchuk NM (2012) Friction welding of T-joints in sheet structures of aluminium alloys. Welding International 26(4): 292-296.
46. Kumar K, Kailas SV, Srivatsan TS (2011) The Role of Tool Design in Influencing the Mechanism for the Formation of Friction Stir Welds in Aluminum Alloy 7020. Materials and Manufacturing Processes 26(7): 915-921.
47. Cavaliere P, Santis AD, Panella F, Squillace A (2009) Effect of welding parameters on mechanical and microstructural properties of dissimilar AA6082–AA2024 joints produced by friction stir welding. Materials and Design 30: 609–616.
48. Taban E, Kaluc E (2007) Comparison between microstructure characteristics and joint performance of 5086-H32 aluminium alloy welded by MIG, TIG and friction stir welding processes. Metallic materials 45(5): 241–248
49. Peel M, Steuwer A, Preuss M, Withers PJ (2003) Microstructure, mechanical properties and residual stresses as a function of welding speed in aluminium AA5083 friction stir welds. Acta Materialia 51: 4791–4801.
50. 50Lee WB, Yeon YM, Jung SB (2003) The improvement of mechanical properties of friction-stir-welded A356 Al alloy. Materials Science and Engineering A 355: 154-159.
51. Murr LE, Li Y, Flores RD, Trillo E, McClure JC (1998) Intercalation vortices and related microstructural features in the friction-stir welding of dissimilar metals. Mater Research and Innovation 2(3): 150-163.
52. Benavides S, Li Y, Murr LE, Brown D, McClure JC (1999) Low-Temperature Friction-stir Welding of 2024 Aluminum. Scripta Materialia 41(8): 809-815.
53. Li Y, Murr LE, McClure JC (1999) Flow visualization and residual microstructures associated with the friction-stir welding of 2024 aluminum to 6061 aluminum. Material Science and Engineering A 271: 213–223.
54. Ma ZY, Mishra RS, Mahoney MW (2002) Superplastic deformation behaviour of friction stir processed 7075Al alloy. Acta Materialia 50: 4419-4430.

55. Mahoney MW, Rhodes CG, Flintoff JG, Spurling RA, Bingel WH (1998) Metallurgical and Materials Transactions A 29(A): 1955-1964.
56. Tang W, Guo X, McClure JC, Murr LE (1998) Heat input and temperature distribution in friction stir welding. Journal of Material Processing Manufacturing Science 7:163–172.
57. Kwon YJ, Saito N, Shigematsu I, (2002) Friction stir process as a new manufacturing technique of ultrafine-grained aluminum alloy. Journal of Material Science Letters 21: 1473-1476.
58. Ma ZY, Mishra RS, Mahoney MW (2003) Friction Stir Welding and Processing II, Jata KV, Mahoney MW, Mishra RS, Semiatin SL, Lienert T, Ed., TMS, San Diego: 221–230.
59. Rhodes CG, Mahoney MW, Bingel WH, Spurling RA, Bampton CC (1997) Effects of friction stir welding on microstructure of 7075 Alluminium. Scripta Materialia 36: 69-75.
60. Liu G, Murr LE, Niou CS, McClure JC, Vega FR (1997) Microstructural Aspects of the Friction-Stir Welding of 6061 -T6 Aluminum. Scripta Materialia 37(3): 355-361.
61. Sato YS, Kokawa H, Enmoto M, Jogan S (1999) Microstructural evaluation of 6063 Aluminum during friction-stir welding. Metallurgical and Materials Transactions A 30(9): 2429-286.
62. Heinz B, Skrotzki B (2002) Characterization of friction stir aluminum alloy 6013. Metallurgical and Materials Transactions B 33(6): 489-498.
63. Jata KV, Sankaran KK, Ruschau JJ (2000) Friction stir welding effects on microstructure and fatigue of alluminium alloy 7050-T7451.Metallurgical and Materials Transactions A 31 (9): 2181-2192.
64. James M, Mahoney M (1999) In: Proceedings of the First International Symposium on Friction Stir Welding, Thousand Oaks, CA, USA, June 14–16, 1999.
65. Zhao YH, Reynolds AP, (2000) Visualisation of material flow in autogenous friction stir welds. Science and Technology of Welding and Joining 5(2): 120–124.
66. Yong Y, Da-tong Z, Cheng Q, Wen Z (2010) Dissimilar friction stir welding between 5052 aluminum alloy and AZ31 magnesium alloy. Transactions of Nonferrous Metals Society of China 20: 619−623.
67. Saeid T, Abdollah-zadeh A, Sazgari B (2010) Weldability and mechanical properties of dissimilar aluminum–copper lap joints made by friction stir welding. Journal of Alloys and Compounds 490: 652–655
68. Xue P, Xiao BL, Wang D, Ma ZY (2011) Achieving high property friction stir welded aluminium/copper lap joint at low heat input. Science and Technology of Welding and Joining 16(8): 657-667.
69. Miara D, Pietras A (2013) Friction stir welding of aluminium casting alloys. Welding International 27(12): 907-914.
70. Gachi S, Boubenider F, Belahcene F (2011) Residual stress, microstructure and microhardness measurements in AA7075-T6 FSW welded sheets. Non-destructive Testing and Evaluation 26(1) 1-11.

71. Lakshminarayanan AK, Balasubramanian V (2011) Comparison of Electron Beam and Friction Stir Weldments of Modified 12 wt% Ferritic Stainless Steel. Materials and Manufacturing Processes 26(6): 868-877

72. Topic I, Hoppel HW, Goken M (2007) Friction stir welding of accumulative roll-bonded commercial-purity aluminium AA1050 and aluminium alloy AA6016. Materials Science and Engineering A 503: 163-166.

73. Tehyo M, Muangjunburee P, Chuchom S (2011) Friction stir welding of dissimilar joint between semi-solid metal 356 and AA6061-T651 by computerized numerical control machine. Songklanakarin journal of science and technology 33(4): 441-448.

74. Chao YJ, Wang Y, Miller KW (2001) Effect of friction stir welding on dynamic properties of AA2024-t3 and AA7075-t7351. Welding research supplement 196-200.

75. Moreira PMGP, Santos T, Tavares SMO, Trummer VR, Vilaca P, de Castro PMST (2009) Mechanical and metallurgical characterization of friction stir welding joints of AA6061-T6 with AA6082-T6. Materials and Design 30:180–187.

76. Koilraj M, Sundareswaran V, Vijayan S, Koteswararao SR (2012) Friction stir welding of dissimilar aluminum alloys AA2219 to AA5083 – Optimization of process parameters using Taguchi technique. Materials and Design, 42: 1-7.

77. Zadpoor AA, Sinke J, Benedictus R (2010) Global and Local Mechanical Properties and Microstructure of Friction Stir Welds with Dissimilar Materials and/or Thicknesses. Metallurgical and Materials Transactions A 41(13)3365-3378.

78. Hantrais EC, Ehrtsrom JC, Nardin C (2010) Friction stir welding dissimilar alloys for tailoring properties of aerospace parts. Science and Technology of Welding and Joining 15(8): 69-705.

79. Da Silva AAM, Arruti E, Janeiro G, Aldanondo E, Alvarez P, Echeverria A, (2011) Material flow and mechanical behaviour of dissimilar AA2024-T3 and AA7075-T6 aluminium alloys friction stir welds. Materials and Design 32(4): 2021–2027.

80. Galvao I, Oliveira JC, Loureiro A, Rodrigues DM (2012) Formation and distribution of brittle structures in friction stir welding of aluminium and copper: Influence of shoulder geometry. Intermetallics 22: 122-128.

81. Xia-wei L, Da-tong Z, Cheng Q, Wen Z (2012) Microstructure and mechanical properties of dissimilar pure copper/1350 aluminum alloy butt joints by friction stir welding. Transactions of Nonferrous Metals Society of China 22: 1298-1306.

82. Wei Y, Li J, Xiong J, Huang F, Zhang F, Raza SH, (2012) Joining aluminum to titanium alloy by friction stir lap welding with cutting pin. Materials characterization 71: 1-5

83. Shojaeefard MH, Akbari M, Tahani M and Farhani F, (2013) Sensitivity Analysis of the Artificial Neural Network Outputs in Friction Stir Lap Joining of Aluminum to Brass. Hindawi Publishing Corporation Advances in Materials Science and Engineering 574914:1- 7.

84. Shtrikman MM, Polovtsev VA, Shillo GV, Makarov NV, Sabantsev AN (2004) Friction welding sheet structures made of 1201 and AMg6 aluminium alloys. Welding International 18(9): 742-747.

85. Okamura H, K Aota K (2004) Joining of dissimilar materials with friction stir welding. Welding International 18(11): 852-860.

86. Seidel TU, Reynolds AP (2001) Visualization of the Material Flow in AA2195 Friction-Stir Welds Using a Marker Insert Technique. Metallurgy and Material science and Transactions A, 32: 2879–2884.

87. Guerra M, Schmidt C, McClure JC, Murr LE, Nunes AC Jr (2003) Flow Pat-terns during Friction Stir Welding. Materials Characterization 49: 95–101.

88. London B, Mahoney M, Bingel W, Calabrese M, Bossi RH, Waldron D (2003) Material Flow in Friction Stir Monitored with Al-SiC and Al-W Composite Markers. Proceedings Symposium on FSW and Processing II, Jata KW, Ma-honey MW, Mishra RS, Semiatin SL, and Lienert T, Ed., TMS, (2003), p 3–12.

89. Amancio S, Sheikhi S, Santos JD, Bolfarini C, (2008) Preliminary study on the microstructure and mechanical properties of dissimilar friction stir welds in aircraft aluminium alloys 2024-T351 and 6056-T4. Journal of Materials Processing Technology 206(1-3) 132-142.

90. Thaiping C, Wei-Bang L (2008) A prime study on FSW joint of dissimilar metals. Proceedings of the XI International Congress and Exposition, Orlando, Florida, USA 2008.

91. Bisadi H, Tavakoli A, Sangsaraki TM, Sangsaraki TK, (2013) The influences of rotational and welding speeds on microstructures and mechanical properties of friction stir welded Al5083 and commercially pure copper sheets lap joints. Materials and Design 43: 80–88.

92. Beygi R, Kazeminezhad M, Kokabi AH, (2012) Butt joining of Al−Cu bilayer sheet through friction stir welding. Transactions of Nonferrous Materials Society China 22: 2925−2929.

93. Galvao I, Leal RM, Rodrigues DM, Loureiro A, (2013) Influence of tool shoulder geometry on properties of friction stir welds in thin copper sheets", Journal of Materials Processing Technology 213: 129–135.

94. Kim HJ, Lee JY, Paik KW, (2003) Effects of Cu/Al intermetallic compound (IMC) on copper wire and aluminum pad bondability. Transactions on Components packaging and manufacturing Technology, 26(2): 367-374.

95. Rajan K, Wallach ER (1980) A transmission electron microscopy study of intermetallic formation in aluminum-copper thin film couples. Journal of Crystal Growth 49(2): 297-302.

96. Movahedi M, Kokabi AH, Seyed Reihani SMS, Najafi H (2012) Effect of tool travel and rotation speeds on weld zone defects and joint strength of aluminium steel lap joints made by friction stir welding. Science and Technology of Welding and Joining (17)2: 162-167.

97. Barlas Z, Ozsarac U (2012) Effects of FSW Parameters on Joint Properties of AlMg3 Alloy. Welding Journal January 91: 16 –22.

98. Kahl S, Osikowicz W (2013) Composite Aluminum-Copper Sheet Material by Friction Stir Welding and Cold Rolling. Journal of Materials Engineering and Performance 22:2176–2184.

99. Assidi M, Fourment L, Guerdoux S, Nelson T (2010) Friction model for friction stir welding process simulation:Calibrations from welding experiments. International Journal of Machine Tools & Manufacture 50(2): 143–155.

100. Kim D, Badarinarayan H, Kim JH, Kim C, Okamoto K, Wagoner RH, Chung K (2010) Numerical simulation of friction stir butt welding process for AA5083-H18 sheets. European Journal of Mechanics A/Solids, 29(2): 204-215.

101. Feulvarch E, Rouxb JC, Bergheau JM (2013) A simple and robust moving mesh technique for the finite element simulation of Friction Stir Welding. Journal of Computational and Applied Mathematics 246: 269-277.

102. Song M, Kovacevic R (2003) Thermal modeling of friction stir welding in a moving coordinate system and its validation. International Journal of Machine Tools & Manufacture 43(6): 605–615.

103. Chen CM, Kovacevic R (2003) Finite element modeling of friction stir welding-thermal and thermomechanical analysis. International Journal of Machine Tools & Manufacture 43(13): 1319–1326.

104. Buffa G, Ducato A, Fratini L (2011) Numerical procedure for residual stresses prediction in friction stir welding. Finite Elements in Analysis and Design 47(4): 470-476.

105. Trimble D, Monaghan J, O'Donnell GE (2012) Force generation during friction stir welding of AA2024-T3. CIRP Annals - Manufacturing Technology 61(1): 9-12.

106. Chiumenti M, Cervera M, Agelet de Saracibar C, Dialami N (2013) Numerical modeling of friction stir welding processes. Computer Methods in Applied Mechanics and Engineering 254:353-369.

107. Dialami N, Chiumenti M, Cervera M, Agelet de Saracibar C (2013) An apropos kinematic framework for the numerical modeling of friction stir welding. Computers and Structures 117: 48–57.

108. Gemme F, Verreman Y, Dubourg L, Jahazi M (2010) Numerical analysis of the dwell phase in friction stir welding and comparison with experimental data. Materials Science and Engineering A 527: 4152–4160.

109. Vilaca P, Quintino L, Dos Santos JF (2005) iSTIR—Analytical thermal model for friction stir welding. Journal of Materials Processing Technology 169 (3): 452–465.

110. Zhang HW, Zhang Z, Chen JT (2007) 3D modeling of material flow in friction stir welding under different process parameters. Journal of Materials Processing Technology183(1): 62–70.

111. Jacquin D, De Meester B, Simar A, Deloison D, Montheillet F, Desrayaud C (2011) A simple Eulerian thermomechanical modeling of friction stir welding. Journal of Materials Processing Technology 211(1): 57-65.

112. Heurtier P, Jones MJ, Desrayaud C, Montheillet F, Allehaux D, Driver J (2006) Mechanical and thermal modeling of friction stir welding. Journal of Materials Processing Technology 171(3): 348–357.
113. Soundararajan V, Zekovic S, Kovacevic R (2005) Thermo-mechanical model with adaptive boundary conditions for friction stir welding of Al 6061. International Journal of Machine Tools & Manufacture 45(14): 1577–1587.
114. Geiger M, Micari F, Merklein M, Fratini L, Contorno D, Giera A, Staud D (2008) Friction Stir Knead Welding of steel aluminium butt joints. International Journal of Machine Tools & Manufacture 48(5): 515–521, 2008.
115. Hamilton C, Sommers A, Dymek S (2009) A thermal model of friction sti rwelding applied to Sc-modified Al–Zn–Mg–Cu alloy extrusions. International Journal of Machine Tool & Manufacture 49: 230–238, 2009.
116. Vilaca P, Quintino L, Dos Santos JF, Zettler R, Sheikhi S (2007) Quality assessment of friction stir welding joints via an analytical thermal model, Istir. Materials Science and Engineering 445: 501–508.
117. http://www.matweb.com.
118. http://www.crucibleservice.com.
119. Hamilton C, Dymek S, Sommers A (2008) A thermal model of friction stir welding in aluminum alloys. International Journal of Machine Tools & Manufacture 48(10): 1120–1130.
120. Aval HJ, Serajzadeh S, Kokabi AH (2011) Evolution of microstructures and mechanical properties in similar and dissimilar friction stir welding of AA5086 and AA6061. Materials Science and Engineering A528(28): 8071– 8083.
121. Zhu XK, Chao YJ (2004) Numerical simulation of transient temperature and residual stresses in friction stir welding of 304L stainless steel. Journal of Materials Processing Technology 146(2): 263–272.
122. Heurtier P, Jones MJ, Desrayaud C, Driver JH, Montheillet F, Allehaux D (2006) Mechanical and thermal modelling of Friction Stir Welding. Journal of Materials Processing Technology 171(3): 348–357.
123. Mandal S, Williamson K (2006) A thermomechanical hot channel approach for friction stir welding. Journal of Materials Processing Technology 174(1-3): 190-194.
124. Williamson KM, Salam TA (2006) A moving boundary formulation for recursive plastic heat release during friction stir welding. Journal of Materials Processing Technology 180(1): 49-52.
125. Buffa G, Fratini L, Shivpuri R (2007) CDRX modelling in friction stir welding of AA7075-T6 aluminum alloy: Analytical approaches. Journal of Materials Processing Technology 191(1-3): 356–359.
126. Buffa G, Fratini L (2005) CDRX modeling in friction stir welding of aluminum. Journal of Materials Processing Technology 45(10):1188–1194.

127. Cerri E, Evangelista E, Forcellese A, McQueen H (1995) Comparative hot workability of 7012 and 7075 alloys after different pretreatments. Material Science and Engineering A 197(2): 181–198.
128. Zhang Z, Zhang HW (2009) Numerical studies on controlling of process parameters in friction stir welding. Journal of materials processing technology 209(1): 241–270.
129. Hirasawa S, Badarinarayan H, Okamoto K, Tomimura T, Kawanami T (2010) Analysis of effect of tool geometry on plastic flow during friction stir spot welding using particle method. Journal of Materials Processing Technology 210(11): 1455–1463.
130. Hilgert J, Schmidt HNB, Dos Santos JF, Huber N (2011) Thermal models for bobbin tool friction stir welding. Journal of Materials Processing Technology 211(2): 197–204.
131. Hattel JH, Nielsen KL, Tutum CC (2012) The effect of post-welding conditions in friction stir welds: From weld simulation to ductile failure. European Journal of Mechanics A/Solids 33: 67-74.
132. Hong-wu Z, Zhao Z, Jun B, Lei Z, Jin-tao C (2006) Effect of viscosity on material behavior in friction stir welding process. Transactions of Nonferrous Metals Society of China 16: 1045-1052.
133. Ponthot JP (1998) An extension of the mdid return algorithm to Bccount for ratedependent effects in fictional contact and visco-plasticity. Journal of Materials Processing Technology 80: 628-634.
134. Chuan-song WU, Wen-bin Z, Lei S, Mao-ai C (2012) Visualization and simulation of plastic material flow in friction stir welding of 2024 aluminium alloy plates. Transactions of Nonferrous Metals Society of China 22(6): 1445-1451.
135. Mendez PF, Tello KE, Lienert TJ (2010) Scaling of coupled heat transfer and plastic deformation around the pin in friction stir welding. Acta Materialia 58(18): 6012–6026.
136. Schmidt HB, Hattel JH (2008) Thermal modelling of friction stir welding. Scripta Materialia 58(5): 332–337.
137. Boldsaikhan E, Corwin EM, Logar AM, Arbegast WJ (2011) The use of neural network and discrete Fourier transform for real-time evaluation of friction stir welding. Applied Soft Computing 11(8): 4839–4846.
138. Lawrjaniec D, Abisror A, Decker C, Kocak M, Dos Santos J, Gardiner S (2004) Digital simulation of the friction stir welding process, Welding International, 18(10): 798-802.
139. Deloison D, Darcourt C, Abisror A, Decker C, Journet B (2004) Recent Advances in Welding Simulation of Aeronautical Components. Revue Europeenne des Elements 13(3-4): 377-389.
140. Arora A, DebRoy T, Bhadeshia HKDH (2011) Back-of-the-envelope calculations in friction stir welding – Velocities, peak temperature, torque, and hardness. Acta Materialia 59(5): 2020–2028.

141. Sinclair PC, Longhurst WR, Cox CD, Lammlein DH, Strauss AM, Cook GE (2010) Heated Friction Stir Welding: An Experimental and Theoretical Investigation into How Preheating Influences Process Forces. Materials and Manufacturing Processes 25(11): 1283-1291.
142. Kumbhar NT, Bhanumurthy K (2012) Friction Stir Welding of Al 5052 with Al 6061 Alloys. Journal of Metallurgy 2012: 1- 7.
143. Park JC, Kim SJ (2010) The effect of traveling and rotation speeds on mechanical properties during friction stir welding of dissimilar Al alloys. Defect and Diffusion Forum 297-301: 590–595.
144. Gerlich A, Su P, Yamamoto M, North TH (2008) Material flow and intermixing during dissimilar friction stir welding. Science and Technology of Welding and Joining 13(3): 254-264.
145. Bahemmat P, Haghpanahi M, Besharati MK, Ahsanizadeh S, Rezaei H (2010) Study on mechanical, micro and macro structural characteristics of dissimilar friction stir welding of AA6061-T6 and AA7075-T6. Journal of Engineering Manufacture 224: 1854-1865.
146. Mroczka K, Wojcicka A, Adam Pietras A (2013) Characteristics of Dissimilar FSW Welds of Aluminum Alloys 2017A and 7075 on the Basis of Multiple Layer Research. Journal of Materials Engineering and Performance 22(9):2698–2705.
147. Chao YJ, Qi, X (1998) Thermal and Thermo-Mechanical Modeling of Friction Stir Welding of Aluminum Alloy 6061-T6. Journal of Materials Processing & Manufacturing Science 7: 215–233.
148. Michael Bauccio (1993) ASM Metals Reference Book, 3rd Edition, page 250-254.
149. ASTM E1382-97 (2010) Standard Test Methods for Determining Average Grain Size Using Semiautomatic and Automatic Image Analysis, ASTM International, West Conshohocken, PA, 2010.
150. Pankaj Biswas and N R Mandal (2011) Effect of Tool Geometries on Thermal History of FSW of AA1100. Welding Journal, July 2011: 129S-135S.
151. Chao YJ, Qi X, Tang W (2003) Heat Transfer in Friction Stir Welding-Experimental and Numerical Studies. Transactions of the ASME 125: 138-145.
152. Khatibi, G., Zimprich, P., Betzwar-Kotas, A., Lederer, M. and Weiss, B. (2006) Temperature Dependent Elastic and Thermal Properties of Thin Copper Foils, in Copper: Better Properties for Innovative Products (ed J.-M. Welter), Wiley-VCH Verlag GmbH & Co. KGaA, Weinheim, Germany. doi: 10.1002/9783527610327.ch35.

Author's Resume

Born in 1983 at Rajahmundry, Andhra Pradesh. India. Obtained Bachelor's degree in Mechanical Engineering from BVCE College, JNTUK, Andhra Pradesh in 2007. Then passed M.Tech in Advanced Manufacturing Systems from Jawaharlal Nehru Technological University, Hyderabad in 2010. Joined the Doctoral Research Programme in the Department of Mechanical Engineering, Indian Institute of Technology Guwahati in January 2010 as an Institute Research Scholar. The author's interest lies in the field of computational weld mechanics, numerical methods and experimental work. His publications are as follows:

(A) International Journals:

1. Pankaj Biswas, **Anil Kumar D**, Mandal NR, M. M. Mahapatra (2011) Study on the Effect of Welding Sequence in Fabrication of Large Stiffened Plate Panels. Journal of Marine Science and Applications 10: 429-436.
2. Biswas Pankaj, **Anil Kumar D**, Mandal NR (2012) Friction stir welding of aluminum alloy with varying tool geometry and process parameters. Proc. IMechE Part-B, Journal of Engineering Manufacture 226(4):641-648.
3. **Anil Kumar Deepati**, Pankaj Biswas (2013) A study on friction stir welding of 12mm thick aluminum alloy plates. Journal of Marine Science and Applications 12: 493-499.
4. **Anil Kumar Deepati**, Arun Kumar Kadian, Pankaj Biswas (2014) Numerical and experimental study on influence of tool plunging force and shoulder size on thermal history of friction stir welding. International Journal of Manufacturing Research 10(1): 64-86. (*In press*)
5. **Anil Kumar Deepati**, Himanshu Chaturvedi and Pankaj Biswas (2014) Experimental investigation of mechanical properties on friction stir welding of dissimilar aluminum alloys. International Journal of Current Engineering and Technology. Special issue; pp. 2277 – 4106
6. **Anil Kumar Deepati**, Pankaj Biswas (2014) Effect of process parameters on progression of weld quality in FSW of aluminum and copper alloy plates. International Journal of Advanced Manufacturing Technology. (*revised paper submitted*)
7. **Anil Kumar Deepati**, and Pankaj Biswas (2014). Numerical and experimental thermal studies on friction stir welding of alluminium and copper alloys. Journal of Materials Engineering and Performance. (*revised paper submitted*)

8. **Anil Kumar Deepati** and Pankaj Biswas (2014). Parametric analysis of friction stir welding of dissimilar aluminum alloys using Grey-taguchi optimisation method. Proc. IMechE Part-B, Journal of Engineering Manufacture 648. (*Under review*)

(B) Conference Proceedings:

9. **Anil Kumar Deepati**, Arun Kadian, Leena Nemade, and Pankaj Biswas (2012). Effect of tool shoulder diameter on thermal history of FSW of aluminium alloy. 21st International Symposium on Processing and Fabrication of Advanced Materials PFAMXXI, Guwahati, India. Vol -2, 12-2012
10. **Anil Kumar Deepati**, Pankaj Biswas, Arun Kadian, and Leena Nemade (2013). 3D-Finite element modelling and the effect of backing plate on thermal history of FSW AA5083. National Conference on Advances in Welding Technology, NERIST, Itanagar, India, pp. 49–56.
11. **Anil Kumar Deepati**, Leena Nemade and Pankaj Biswas (2014). 3-D FE transient thermal analysis of dissimilar alluminium and copper alloys by FSW process. International Institute of Welding – International Welding Congress 2014 (IC 2014), New Delhi, India, Pp. 353-359.
12. **Anil Kumar Deepati**, Pankaj Biswas (2014). Numerical analysis of FSW on dissimilar (Cu/Al) metals. Technical poster presentation, Department of Mechanical Engineering, IITGuwahati, February 17-18, 2014.